

---

Electronic Thesis and Dissertation Repository

---

8-25-2020 2:00 PM

## Fast spiking GABAergic interneurons in the dorsolateral prefrontal cortex of non-human primate: Comparison study to mice and human, with focus on subthreshold intrinsic properties

Michelle Stephanie Jimenez-Sosa, *The University of Western Ontario*

Supervisor: Martinez Trujillo J., *The University of Western Ontario*

Co-Supervisor: Inoue W., *The University of Western Ontario*

A thesis submitted in partial fulfillment of the requirements for the Master of Science degree in Neuroscience

© Michelle Stephanie Jimenez-Sosa 2020

Follow this and additional works at: <https://ir.lib.uwo.ca/etd>

---

### Recommended Citation

Jimenez-Sosa, Michelle Stephanie, "Fast spiking GABAergic interneurons in the dorsolateral prefrontal cortex of non-human primate: Comparison study to mice and human, with focus on subthreshold intrinsic properties" (2020). *Electronic Thesis and Dissertation Repository*. 7228.  
<https://ir.lib.uwo.ca/etd/7228>

This Dissertation/Thesis is brought to you for free and open access by Scholarship@Western. It has been accepted for inclusion in Electronic Thesis and Dissertation Repository by an authorized administrator of Scholarship@Western. For more information, please contact [wlsadmin@uwo.ca](mailto:wlsadmin@uwo.ca).

## **Abstract**

Fast spiking (FS) parvalbumin expressing cells are one of the three major subpopulations of GABAergic interneurons. They generally show a consistent set of electrophysiological features across brain areas and species: short and narrow action potentials and capability of high frequency firing. These features are believed to be crucial for fast inhibition and generation of network oscillations associated with various cognitive phenomena. However, it is unclear whether other intrinsic properties of FS interneurons vary across species and/or brain areas. This study maps out the subthreshold intrinsic properties of FS neurons of mouse, macaque and human. Features are derived from intracellular recordings of acute slices from two different databases (© 2018 Allen Brain Atlas: Allen Cell Type Database and NHP database from the Martinez Trujillo Laboratory). To classify FS interneurons in primates we developed a model based on parvalbumin specific mouse lines. Our results showed significant differences in almost all considered features. Primate neurons were more alike, having higher excitability and sag amplitude; however, between primates macaque cells reached higher values which may be due to differences in sampled brain region.

## **Keywords**

Fast-spiking interneurons, parvalbumin neurons, electrophysiology, cross species comparison, subthreshold properties.

## Summary for lay audience

Our brain is made up of multiple neuron types. The fast spiking cell is a neuron type that has very distinct electrical activity. This electrical activity could be recorded to analyze the properties of the cell. Recordings from fast spiking cells show characteristic thin and short electrical pulses called “spikes” that could reach high spiking frequencies in comparison to other cell types. Fast spiking cells have shown to play a role in mental abilities in primates (monkeys and humans) for example decision making, and attention. Even though commonalities in the electrical features of fast spiking cells have been shown to be present in different species, it is unclear whether what properties of FS neurons might vary across species. In order to understand the differences and similarities of these neurons across species we compare the electrical properties during negative current injections. Our results showed significant differences across species in almost all considered features. The primate neurons were more alike being easily stimulated to get to spikes, however, monkey cells reached higher values which may be explained by differences in the brain areas that we sampled.

## Co-Authorship Statement

<b>Contribution to this thesis</b>	
Biopsy surgeries to obtain brain samples from non-human primate	JM, MR, BC, BM, DB, RL
Preparation of solutions for biopsy surgeries	MJ
Preparation of brain slices	WI, JS, SMe, SMa, MJ
Electrophysiological recordings from non-human primate cells including preparation of materials for experiments	JS,SMe,MW,SMa,MJ
Quality control of intracellular recordings	EK, MF
MATLAB script for extraction of features	EK, MF, MJ
Staining, imaging and histological evaluation of NHP neurons	MJ
Data analysis and interpretation	MJ
Revision to scientific content of manuscript	MP, JM, WI, MF
Grammatical revision	SV,RL,BC,MR,EK
Supervision of the project	JM, WI

Michelle Jimenez  
(Candidate)

Michael Poulter (PI)

Julio Martinez (PI)

Wataru Inoue (PI)

Michael Feyerabend

Eric Kuebler

Sam Mestern

Julia Sunstrum

Sara Matovic

Meagan Wiederman

Megan Roussy

Ben Corrigan

Borna Mahmoudian

Diego Buitrago-Piza

Rogelio Luna

Susheel Vijayraghavan

## **Dedication**

**This study is dedicated to my family**

**Mis padres Juan Jimenez y Josefa de Jimenez**

Por su incondicional amor y por siempre creer en mi

**A mi querido novio Michael Feyerabend**

Quien con cariño me acompañó en los días buenos y en los más cansados, pero siempre me dio motivos para sonreír

**A mi hermana Eddy Jimenez, mi hermano Juan Jimenez y mi cuñado Raúl González**

Por ser mi inspiración y contante motivación, ayudándome y proveyendo en todo momento.

Todos ustedes han sido una pieza fundamental de este anhelado sueño.

## Acknowledgements

In a very special way I would like to express my gratitude to my advisors Dr. Julio Martinez-Trujillo, Dr. Michael Poulter (†) and Dr. Wataru Inoue who trusted in me and gave me the opportunity to accomplish this thesis project under their supervision. Thank you for your guidance, advice and for providing all the necessary resources for the development of this study. To Michael Feyerabend for his advice and encouraging support though the analysis and conceptual part of this project. To Eric Kuebler who in addition of collaborating in the data analysis was always willing to give his time and advice. To everybody who collaborated in the acquisition of the data or tissue extraction: Sam Mestern, Sara Matovic, Julia Sunstrum, Meagan Wiederman, Chakravarthi Narla, Megan Roussy, Ben Corrigan, Borna Mahmoudian, Diego Buitrago-Piza, Susheel Vijayraghavan, Rogelio Luna, Nika Khajehdehi, William Assis, Joshua Poulin, Kim Thomaes, Rhonda Kersten, and Chinmay Patel. To Dr. Jochen Staiger and Pavel Truschow from the University of Gottingen for instructed me in the wonderful art of the neuronal reconstruction. To Susan Simpson and Lara Staecker who in a kindly and diligence way support me in the administrative matters of the program. To Kevin Barr, Michelle Everest and Jackson Blonde for their kindly support in the lab and imaging facilities. And to Jaymin Jeong and Sally Esmail for being friendly and helping colleges.

# Table of contents

Abstract.....	ii
Keywords.....	ii
Summary for lay audience .....	iii
Co-Authorship Statement .....	iv
Dedication .....	iii
Acknowledgements.....	iv
Table of contents .....	v
List of Tables.....	viii
List of figures.....	viii
List of appendices .....	ix
1. Introduction.....	1
1.1. Neuronal diversity in the cortical network.....	1
1.2. Excitatory neurons vs inhibitory interneurons.....	1
1.3. Interneurons classification: morphological and electrophysiological features, taxonomy in rodents.....	2
1.4. Introduction to the fast spiking interneuron.....	5
1.5. FS interneuron morphology.....	6
1.6. FS interneurons electrophysiological features.....	7
1.7. Function of the FS PV+ interneurons in the PFC .....	7
1.8. FS interneurons across species.....	8
2. Aim of the thesis .....	10
3. Material and methods.....	10

3.1. Mouse and human dataset.....	10
3.2. NHP dataset .....	11
3.3. Electrophysiological quality control .....	20
3.4. Statistical analysis .....	20
4. Results.....	21
4.1. Descriptive statistics of used datasets.....	21
4.1.1. Composition of the databases .....	21
4.1.2. General distribution of waveform parameters across species.....	26
4.1.3. Distribution of key spike train features.....	32
4.1.4. Distribution of subthreshold properties .....	34
4.2. Using mouse PV+ cells for cross-species classification of cortical FS cells.....	37
4.2.1. Linear discriminant analysis classifier .....	37
4.2.2. Normalization of the across species.....	40
4.2.3. Training and testing samples.....	40
4.2.3. Classifier performance in various cell type-specific reporter lines.....	41
4.3. Description of putative cortical FS cells in primates .....	49
4.3.1. Dendritic type and layer distribution of human pFS cells .....	49
4.3.2. Dendritic type and layer distribution of NHP pFS cells .....	50
4.3.3. Communalities and differences in firing pattern and morphological phenotype .....	51
4.4. Comparing FS subthreshold properties across species .....	56
4.4.1. Descriptive statistics of subthreshold properties of FS cells .....	56
4.5. Revealing cell type and species dependent effects by comparing FS with excitatory cells.....	59
5. Discussion.....	65



5.1. Summary of results.....	65
5.2. Methodological considerations .....	67
6. Conclusion.....	71
7. References.....	73
8. Appendix .....	79

## List of Tables

- Table 1. Mouse transgenic lines
- Table 2. Descriptive statistics from mayor electrophysiological parameters
- Table 3. Subthreshold properties of FS cells across species
- Table 4. Two-way ANOVA and descriptive statistics comparing FS and Exc cells across species.

## List of figures

- Figure 1. Overview of the two major cell population in the cerebral cortex
- Figure 2. Taxonomy overview of murine neocortical GABAergic Interneurons
- Figure 3. Schematic representation of electrophysiological parameters
- Figure 4. Dendritic type and layer distribution of mouse database
- Figure 5. Dendritic type and layer distribution of human database
- Figure 6. Dendritic type and layer distribution of NHP database
- Figure 7. Distribution of waveform parameters across species (1)
- Figure 8. Distribution of waveform parameters across species (2)
- Figure 9. Distribution of spike train features across species
- Figure 10. Distribution of subthreshold parameters across species
- Figure 11. Correlations between subthreshold and suprathreshold parameters of mouse cells
- Figure 12. Suprathreshold parameters used to classify FS cells
- Figure 13. Comparison between PV+ and pFS cells in the mouse database
- Figure 14. Prevalence of various transgenic reporter lines in the total mouse dataset and their contribution to the pFS population
- Figure 15. Intrinsic properties of Basket and Chandelier PV+ cells in the mouse database

- Figure 16. Non FS specific transgenic lines containing cells with strong FS phenotype
- Figure 17. Classification of pFS primate neurons
- Figure 18. Intrinsic biophysical properties of human cells
- Figure 19. Intrinsic biophysical properties of NHP cells
- Figure 20. Morphological characterization of human cells
- Figure 21. Morphological characterization of NHP cells
- Figure 22. Subthreshold properties of PV+ and pFS neurons across species
- Figure 23. Comparison of subthreshold properties of FS and Exc cells across species.

## **List of appendices**

- Appendix A. Methodology comparison between species

# 1. Introduction

## 1.1. Neuronal diversity in the cortical network

A 100 billion neurons are contained in the human brain (Herculano-Houzel 2009) and the extraordinary diversity of the cells make possible the multiple functions of our brains. This diversity goes from morphological features to less visible properties, such as different membrane channel components. Neurons not only differ in shape and size, but also they fire in many different tempos and patterns: some constantly fire with a high speed, while others prefer to keep silent or sporadically burst on a stuttering way.

## 1.2. Excitatory neurons vs inhibitory interneurons

In a simplified view, the neuronal network is mainly composed by excitatory and inhibitory neurons. The excitatory cells (Exc), also called pyramidal cells (PCs), represent the ~80 to 85% of the neuronal population (see **Figure 1**). They are projecting neurons that contain the neurotransmitter glutamate and can be morphologically distinguish by its typical triangular soma, from which a long apical dendrite and basal dendrites come out of. They also have protrusions along their dendritic arbor known as spines. In contrast, the inhibitory interneurons are a diverse population of cells marked by different electrophysiological and morphological phenotypes. They characteristically have none or much fewer spines along the dendrites, and therefore are referred as aspiny or sparsely spiny cells. Their axon synapses with neurons of the local circuitry and utilize  $\gamma$ -aminobutyric acid (GABA) as neurotransmitter. Despite being in minority, inhibitory interneurons are key regulators of activity levels of the pyramidal neurons. They partake in all cortical processing and their dysfunction is thought to contribute to numerous neuropsychiatric disorders (Di Cristo and Chattopadhyaya 2012; Gao and Penzes 2015; Hua Hu, Gan, and Jonas 2014).

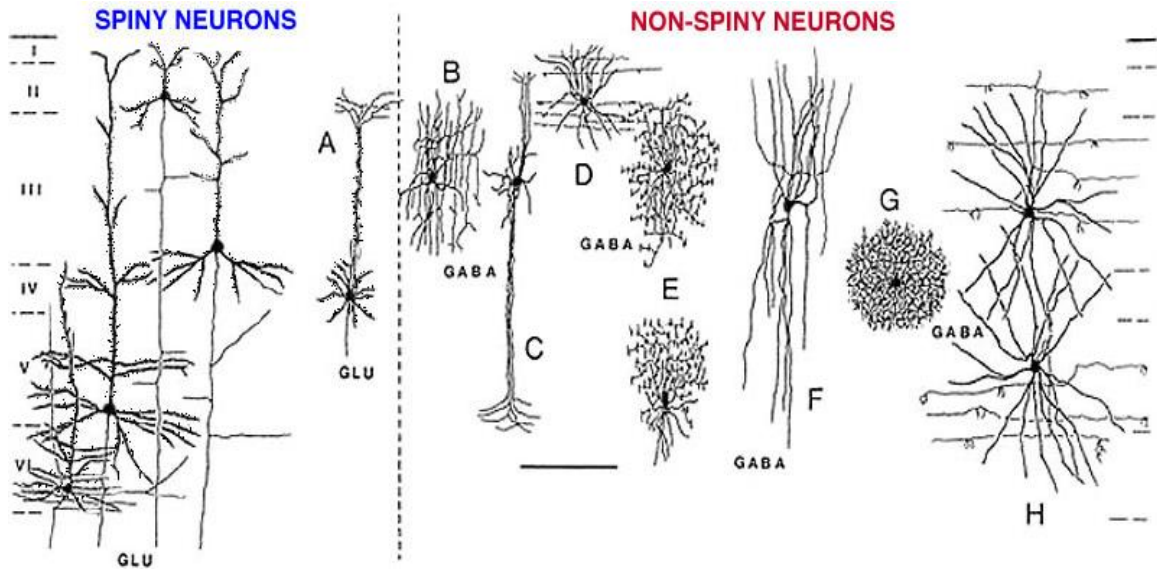


**Figure 1. Overview of the two major cell population in the cerebral cortex.** Cells on the left are characterized by densely packed protrusion on their dendritic tree, which are also known as spines. Cells on the right of the dashed vertical line, on the other hand, have a smooth dendrite and are hence called non-spiny or aspiny. This distinction gets further weight by the fact that both populations utilize two different neurotransmitter: cells on the left use glutamate (GLU) which excites postsynaptic neocortical cells, whereas cells on the right use GABA, which has the opposite effect. Most excitatory cells look comparatively similar, marked by a rectangular somatodendritic configuration with an ascending apical dendrite. This morphology is known as pyramidal cell (A). Aspiny neurons on the other hand show a stronger diversity that comprises many different morphological types: (B) cell with local axon arcades (C) double bouquet cell (D, H) basket cell (E) chandelier cells (F) bitufted cell; adapted from Jones, 1986 (Jones and Hendry 1986).

### **1.3. Interneurons classification: morphological and electrophysiological features, taxonomy in rodents**

Since the pioneering work of Golgi and Ramon y Cajal, neuroscientists have tried to make sense of the diversity of neocortical GABAergic interneurons by classifying them into

distinct subpopulations. Traditionally this endeavor focused on the anatomy of individual neurons. Observations of their axonal arborizations revealed that there are major differences in postsynaptic targeting between different types of interneurons (see **Figure 2** as overview). Despite morphology being a clear hallmark of interneurons diversity, current taxonomy and identification schemes rely on a multi-modal approach including intrinsic biophysical properties (Ascoli et al. 2008; Gouwens et al. 2018). Furthermore, GABAergic interneurons are known to possess a remarkable diversity in genetic and neurochemical markers (Hendry et al. 1989; Tasic et al. 2018). Hence, over the last decades a plethora of different genetic and immunohistochemical markers that target different subpopulations or blends of subpopulations have been described (Hendry et al. 1984). However, the functional relevance of most of these markers (like neuropeptides, various receptors, etc.) is unknown and there are considerable differences across species. Bona-fide cell types show a distinct profile in all these different domains with tight associations between specific phenotypes.

New developments in genetic engineering within the last 20 years have led to enormous progress in the field of interneuron diversity and made the house mouse (*Mus musculus*) to the principal model system. Particularly noteworthy in this context are the studies that have taken the developmental perspective (Lim et al. 2018). Unlike excitatory cells, which are born in the subventricular zone in the proximity of their final location, neocortical GABAergic interneurons are born in the ventral telencephalon and migrate dorsally into the cortex (Wonders and Anderson 2006). The spectrum of GABAergic diversity can be divided into three major non-overlapping subpopulations, which originate from different locations in the brain and are named according the selective expression of certain marker proteins (Rudy et al. 2011). Two of these populations, the somatostatin (SST) and parvalbumin (PV) expressing cells, are derived from the medial ganglionic eminence (MGE), whereas the third group, expressing the ionotropic serotonin receptor 3A (5-HT<sub>3a</sub>R), is born in the caudal ganglionic eminence (CGE) (Miyoshi et al. 2007, 2010). This population matures later in development and shows a remarkable amount of in-group diversity and is predominantly found in superficial cortical layers. SST and PV cells, on the other hand, are comparatively homogenous groups. Since they are both generated at the same location, the exact fate determination is still unclear. However, the majority of SST

cells are reported to be generated a little earlier than PV cells (J. S. Hu et al. 2017). This genetic program fits nicely with the inside out development of excitatory cells with SST cells being very abundant in infragranular layers which are generated first.

In recent years, the characterization of new and rarer cell types has been made possible by the generation of transgenic lines based on conditional recombination like the Cre-lox system (Madisen et al. 2015; Taniguchi 2014). These driver lines lead to a specific expression of fluorescent reporter proteins and can also be combined in a Boolean manner, allowing a better characterization of interneurons and creation of new insights in diversity, connectivity and function of known subpopulations (Fenno et al. 2014; He et al. 2016; Paul et al. 2017). However, the ability to target interneurons in this manner is not available in primates and neuronal types are less characterized and not as well defined (Kuang, Wang, and Tsien 2009; Aleksey V. Zaitsev, Povysheva, Gonzalez-Burgos, et al. 2009). Consequently it is unclear, which insights from mouse can be directly applied to the human or NHP.

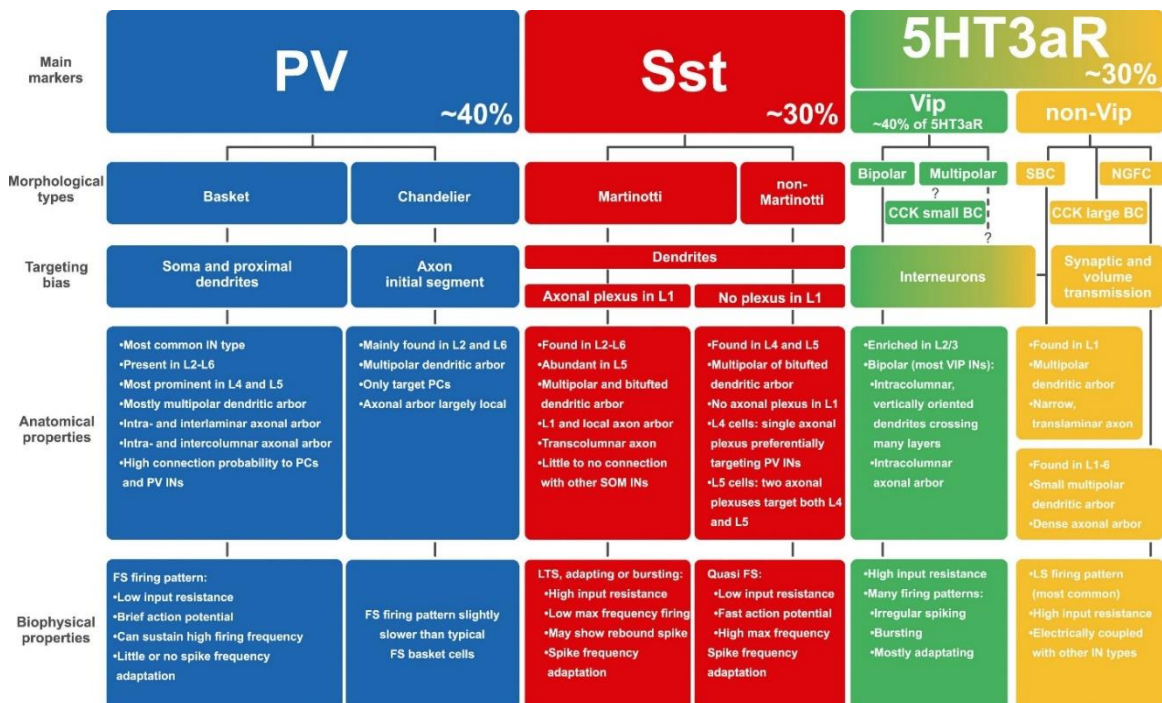


**Figure 2. Taxonomy overview of murine neocortical GABAergic Interneurons.**

There are three major non-overlapping subpopulations, which can be further differentiated. Each group shows a distinct set of anatomical and biophysical properties that cluster them together. Prevalence of each class are taken from the primary somatosensory cortex. PV cells are characterized by the fast spiking (FS) phenotype and the basket or chandelier morphology. SST cells on the other hand are in majority the Martinotti cells (MCs) being associated with either low threshold spiking (LTS), adapting or bursting. However, there is also the non-MC morphology, which is described as quasi FS. 5-HT<sub>3a</sub>R-expressing cells are very heterogeneous and can be further subdivided according to expression of the marker vasoactive-intestinal polypeptide (Vip). Several morphologies have been associated with this population: The single bouquet cell (SBC), the neurogliaform cell (NGFC) and the small and large non-FS basket cells (BC), which are also known to express cholecystokinin (CCK). Figure adopted from Tremblay et al., 2016 (Tremblay, Lee, and Rudy 2016).

#### **1.4. Introduction to the fast spiking interneuron**

The focus of this study are fast spiking (FS) parvalbumin (PV) expressing neurons, which are the most studied among the interneurons. They are not only the most prevalent GABAergic cell, but are also the most distinct to excitatory cells in their intrinsic biophysical features. Consequently, they have been described in the neocortex as early as 1969 by Mountcastle et al. as “thin” spiking neurons (Mountcastle et al. 1969). From their first description they were suspected to be interneurons, but it took the development of the ex-vivo preparation and intracellular labeling to confirm that neocortical FS cells are indeed interneurons (McCormick et al. 1985). Then, in the first multimodal study of its kind, Kawaguchi et al. showed in 1987 that FS basket cells in the hippocampus express the calcium binding protein (CBP) PV (Kawaguchi et al. 1987). The relationship between the FS phenotype and expression of PV is so robust across species and brain areas, that they are often used interchangeably.



## 1.5. FS interneuron morphology

The FS PV<sup>+</sup> neurons show at least two morphologically distinct classes. The chandelier (ChCs) and the basket cells (BCs) (Buhl, Stezhka, and Somogyi 1994; Hendryt and Jonest 2000). The axons of BCs target the soma and proximal dendrites of pyramidal neurons. If several cells are stained, they appear to form basket-like arrangements which surround the unlabeled soma of their postsynaptic partner. The ChCs, on the other hand, take their name from a high prevalence of axon segments reminiscent of the candlesticks of a chandelier. The underlying mechanism of this phenomena is the targeting of the initial segment of the axon of principal neurons, which project towards the white matter and leads to the formation of short vertical clusters of boutons (Hua Hu, Gan, and Jonas 2014; A. V. Zaitsev et al. 2012). Generally, the axon of the FS PV<sup>+</sup> neurons show extensive arborization in comparison to other interneurons, with a cumulative axonal length of 20-24 mm in the frontal cortex, allowing the FS PV<sup>+</sup> cell the generation of massively divergent inhibitory output. The targeting areas of these interneurons suggest a powerful inhibition from these cells, made by the innervation of large number of cells near the site of the action potential initiation. The FS PV<sup>+</sup> interneurons have multiple dendrites that often cross layers, and permits the interneurons to received input from different pathways, such as feedback and feedforward pathways. The cumulative dendritic length of a single FS PV<sup>+</sup> cell ranges from 3.1 to 9 mm. The long dendrites allow these neurons to sample input from a large population of pyramidal cells. They receive convergent excitatory input from pyramidal neurons and inhibitory input primary from other FS PV<sup>+</sup> neurons (Hua Hu, Gan, and Jonas 2014; Karube, Kubota, and Kawaguchi 2004). A study developed in L2 PV<sup>+</sup> interneurons from mouse cortex reported that characteristically asymmetric and predominantly polarized projection towards L1 of the dendritic branches with preference for vertically orientation in ChCs whereas BCs appeared with an isotropic dendritic configuration (Woodruff et al. 2011) suggesting different sources of afferent input for ChCs and BCs. In neuronal models the size of the dendritic arbors have also been proposed to strongly modulate the shape of the AP onset at the axon initial segment. Neurons with larger dendritic surface area shows accelerated APs, implying an improvement in their encoding capabilities (Eyal et al. 2014). In addition, intrinsic electrophysiological properties have been proposed to be useful predictors of the morphology of PV<sup>+</sup> interneurons in mouse cortex (Woodruff et al. 2011).

However, little is known about the somatodendritic configuration and differences across cortical layers from PV+ interneurons between mice, NHP and human.

## **1.6. FS interneurons electrophysiological features**

The PV+ BCs and ChCs both have the same “fast spiking” phenotype with a high frequency firing rate and short width action potential. The intrinsic properties of these cells have shown a remarkable array of molecular and cellular specializations to ensure a fast, reliable, strong and temporally precise inhibition on their target cells (Tremblay, Lee, and Rudy 2016). For example, the delay between the peak of an action potential in a BC soma and the unitary inhibitory postsynaptic current evoked on a PC is on the average of 0.7 ms at ~31 °C. And the delay between the initiation of the stimulus and the beginning of a PV+ cell response also called latency is less than 1 ms showing the incredible speed of PV neurons in comparison to pyramidal neurons and other interneuron types (Pouille and Scanziani 2001; Rossignol et al. 2013). The FS PV+ interneurons have been found to present a short membrane time constant and a low membrane resistance that is usually compensated by receiving large excitatory synaptic inputs (Nadezhda V. Povysheva et al. 2013). The weakly excitable dendrites from the PV+ cells allows them to sample activity in their surrounding network, whereas the highly excitable axon contributes to the fast propagation of digital signal to a large number of target cells (Goldberg et al. 2005; Hua Hu and Jonas 2014). These characteristics allow PV+ cells to not only be useful in basic microcircuit functions, such as feedforward and feedback inhibition or gamma-frequency oscillations, but also in complex network operations, including expansion of dynamic activity range, pattern separation, phase procession, and gain modulation in sensory responses (Jensen, Kaiser, and Lachaux 2007; Leutgeb et al. 2007; Wonders and Anderson 2006).

## **1.7. Function of the FS PV+ interneurons in the PFC**

The FS PV+ interneurons have a prominent role in the prefrontal cortex (PFC) (Ferguson and Gao 2018). They contribute to the feedback and feedforward inhibition and are critically involved in the generation of network oscillations that are crucial for cognition

and behavior (Bissonette et al. 2014). They can convert an excitatory input signal into an inhibitory output signal within a millisecond (Hua Hu, Gan, and Jonas 2014). In the NHP dorsolateral prefrontal cortex (DLPFC) the FS interneurons play a prominent role in working memory, which is the temporarily active maintenance and manipulation of information important for reasoning, decision-making and behavior.(Dehorter et al. 2015) It has been shown that morphological and molecular alterations in the DLPFC PV neurons are implicated in the deficit of working memory in schizophrenia and autism spectrum disorder pathology (J. F. Enwright et al. 2018; John F. Enwright et al. 2016). These alterations include reduced levels of PV protein as well as PV mRNA, especially in layers 3 and 4, which coincidentally participate in the generation of the synchronized activity that occurs during working memory produced through reciprocal microcircuit connections between excitatory PCs and PV interneurons (Fung et al. 2010; Glausier et al. 2015; Hashimoto et al. 2003). NHP and rodent in vivo electrophysiological studies have indicated that the sustained delay activity recorded in the PFC is involved in working memory. However, many differences are notable between species, starting with the not comparable anatomical PFC regions between mice and primates. Behavioral flexibility is more prominent in NHP than in rodents, and in humans than in NHP, which may be a manifestation of the PFC function (Bienvenu et al. 2012; Castner, Goldman-rakic, and Williams 2004; Emmenegger et al. 2018; Gouwens et al. 2018; Staiger et al. 2016; Tsutsui et al. 2016). The intrinsic properties of the PFC FS neurons is a crucial piece to understand the cognitive abilities present in different species (Friedman and Goldman-Rakic 1994; Miller, Erickson, and Desimone 2018; A. V. Zaitsev et al. 2012). Studies suggest that cell specialization depends on the nature and unique spatial distribution of ion channels in the total area of the neuronal surface (soma, dendrites and axon).

## **1.8. FS interneurons across species**

Rodents have been extensively used to study the cerebral cortex and its neuronal population, however, anatomical and functional differences across species also suggest differences in neuronal properties (A. V. Zaitsev et al. 2005). The layer organization of the neurons has shown to change with the expansion of the cortex. For example, while monkey and human prefrontal regions contain a sharply laminated granular and agranular cortex

that allows for the distinction between areas such as orbitofrontal cortex, anterior cingulate cortex, and DLPFC; in rodent, the PFC is exclusively agranular, making these distinctions impossible, especially the DLPFC (Ongur and Price 2000; Watson and Platt 2012). Moreover, in contrast to rodent and NHP in which L2-3 limit is not totally defined, human L2-3 in neocortex are easily distinguishable from one another and further sublaminae distinctions within L3 can be made based upon the size and organization of the neurons (Kalmbach et al. 2018). Cellular components have also shown to be different between species. In the NHP cortex, calretinin is the most abundant CBP, while in the rodent; the PV+ neurons are the predominant. In addition, a high degree of colocalization of CBPs is present in rodent, but not in the NHP PFC (A. V. Zaitsev et al. 2005).

A previous study revealed differences in the electrophysiological membrane properties of putative PV+ cells from NHP and rat PFC (Nadezhda V. Povysheva et al. 2013). They found total 7 inter-species differences in electrophysiological parameters: A substantially higher firing frequency (81 vs 65 Hz) and input resistance (286 vs 174 M $\Omega$ ) in NHP than in rat, whereas the rheobase was lower in NHP (57 vs 115 pA). The action potential threshold was more negative in monkey than in rat (-42 vs -36 mV) and the sag and medium afterhyperpolarization amplitude (mAHP) were more pronounced in NHP (20 vs 5% sag and 6 vs 2.4mV mAHP, respectively). When comparing the PV+ chandelier cells (ChCs) and basket cells (BC), they surprisingly found an interaction effect between species and cell type. In which ChCs in rat presented longer latency before firing the first action potential (AP) than the monkey and the opposite latency effect across species observed on BCs (Nadezhda V. Povysheva et al. 2013). These intrinsic electrophysiological differences across species may contribute to the differences in the spiking behavior of FS interneurons observed in vivo during performance of working memory tasks in NHP and rat (Constantinidis and Goldman-Rakic 2002; Jung et al. 1998). In NHP, PFC putative FS interneurons are reported to fire at a frequency of 40–60 Hz during the delay period of oculomotor delayed response task, whereas in rat PFC, FS units fire with a lower frequency of 12 Hz during delayed spatial alternation task. All these data suggest differences across species in the cortical organization and functional specialization of neuronal intrinsic properties associated with higher cognitive functions and cortical expansion with the rodent located in the lower end of the phylogenetic spectrum with respect to NHP and Human

(Constantinidis and Goldman-Rakic 2002; Jung et al. 1998; Wilson, Scalaide, and Goldman-Rakic 1994; Woodruff et al. 2011).

How exactly PV-FS interneurons are participating in various phenomena of cortical processing (conscious sensation, working memory, etc.) is an open issue. We do not know how strongly they directly participate in computations compared to matching any increase in excitatory tonus. Extracellular in-vivo recordings in different areas and species can help us to find the common principle in their activity. However, to better understand extracellular activity of single fast or narrow spiking units in the cortical circuitry, we need to have a good understanding of their intrinsic properties.

## **2. Aim of the thesis**

The aim of this thesis is to characterize the subthreshold intrinsic properties of DLPFC FS neurons in the NHP and compare to mouse and human. For this we want to develop an objective method to identify FS neurons in the primates due to the lack of transgenic reporter lines in these species.

Our hypothesis is that the subthreshold intrinsic properties from NHP FS neurons are more similar to human than mouse.

## **3. Material and methods**

### **3.1. Mouse and human dataset**

The mouse (n=1920) and human cells (n=413) used in this study were obtained from the publicly available online resource provided by the Allen Institute; The Allen Cell type Database (© 2018 Allen Brain Atlas: Allen Cell Type Database). The downloaded data include: electrophysiological recordings, three-dimensional reconstructions of morphology, information of the soma localization in cortical layers and reported status from

transgenic lines of the neurons. The detailed electrophysiological and morphological methodology is explained in the electrophysiology and morphology overview technical whitepapers available from: <https://celltypes.brain-map.org/>. The most important methodological differences between the Allen Institute mouse and human database as well as the NHP primate database are summarized in *appendix 1* of this thesis.

### **3.2. NHP dataset**

The non-human primate neurons (n=105) were obtained from the DLPFC, areas 8a, 9, and 46 from 6 adult cynomolgus monkeys (*Macaca fascicularis*, 4-11 years old) and 2 rhesus monkeys (*Macaca mulatta*, 7 and 10 years old). All animals were treated according to the guidelines from the Canadian Council on Animal Care and Ontario authorities complying with the 3Rs guiding principles for animal experimentation. All procedures were performed under the approval of the Animal Care Committee (ACC) at Western University. The data was obtained using whole cell patch clamp recordings and morphological characterization of biocytin labeled neurons (Hamill et al. 1981). Features extracted were: dendritic type and cortical layer localization of the soma. The detailed methodology is described below.

- Tissue acquisition

In this study, animals were euthanized for tissue extraction. They were previously used in different experiments that did not compromise our interests. The biopsies were made via surgery under general anesthesia with isoflurane. Monkeys were placed in a stereotaxic instrument (KOPF-1430) and a craniotomy was performed over the DLPFC in one hemisphere. After opening the dura mater areas 8a, 9 and 46 were identified using the principal and arcuate sulcus of the cortex as reference markers. The exposed tissue was immediately infused with 500ml of *slicing solution* (description below in the section: Reagent preparation) at 4°C. A sample of about 1x1 cm was obtained using a customized biopsy tool. The biopsy sample was immersed in ice-cold *slicing solution* straight away, which had been previously saturated with carboxygen (95 % O<sub>2</sub>/5 % CO<sub>2</sub>). Then, it was transported from the surgery room to the neurophysiology laboratory, which is located at

less than 5 minutes from the operating room. The biopsy samples and slicing solution were always contained at 4°C. After controlling bleeding with saline solution and sterile sponge (GELFOAM, Pfizer Inc.), the biopsy was repeated in the contralateral hemisphere if the animal was stable or alternatively the animal was euthanized.

- Preparation of brain slice

Multiple slices of 300 µm thickness were prepared on a Leica 1200S vibratome. During the slicing the sample was immersed in ice-cold *slicing solution* and then settled for recovery in 30°C *slicing solution* during 15 minutes. The slices were cut perpendicular to the pial surface ensuring the presence of white matter and pia in all samples. Finally, the slices were relocated into holding chambers filled with *HEPES solution* (description below in the section: Reagent preparation) at room temperature. Here, they were stored for at least one hour before recording.

- Electrophysiological recordings

Whole cell patch-clamp recordings were obtained from one cell per slice. Each slice was placed in the recording chamber and hold in place with platinum anchors. The sample was bathed in artificial cerebrospinal fluid (*aCSF*, description below in the section: Reagent preparation) at  $34 \pm 1^\circ\text{C}$  to approximate physiological conditions and the level of oxygen was maintained with 95% O<sub>2</sub> 5% CO<sub>2</sub> gas in the specimen reservoir as well as the recording chamber through the perfusion system. The bath temperature was continuously monitored and recorded with every data trace. Neurons were observed under 40X magnification via a Dodt gradient contrast (DGC) system and visualized on an analog monitor through an infrared camera (Dage-MTI IR-1000) (Dodt et al. 1998). At the end of each recording, the patched cell was visualized under fluorescence microscopy to verify its placement in the slice.

Recordings were made using a MultiClamp 700B amplifier (Axon Instruments), operating in bridge-balance mode, filtered on line at 10 kHz, digitized with an Axon Digidata 1440A

and acquired on a personal computer at sampling rate of 20 kHz using pClamp software (Axon). During whole cell patch-clamp recordings, borosilicate glass pipettes (glass thickness 0.64mm) with fire polished tips (2.0-4.0 M $\Omega$  resistance) and filled with internal solution (description below in the section: Reagent preparation) were used. The neurons were target at all cortical layers with preference to interneurons, which were identified based on their small soma size, with round or oval shape and the absence of an apical dendrite.(5) However, a population of pyramidal cells were also patched for this study. The recordings were performed after reaching a stable seal resistance of at least 1G $\Omega$ . The electrophysiological stimulus consisted in a one-second current pulse injection with a series of depolarizing and hyperpolarizing steps of gradually increasing amplitude that went from -110pA to rheobase + 270pA, in 20pA increments. Each experiment lasted up to 17hrs as dictated by the survival of the slices. During the recording time, the neurons were filled with biocytin (0.5%) added to the internal solution through the recording pipette for subsequent morphological visualization. The calculation of intrinsic biophysical properties are described later in the section Electrophysiological data analysis.

- Reagent preparation

Four solutions were used during the tissue acquisition, slice preparation and recording. The *HEPES solution*, *aCSF* and *internal solution* were made fresh (<3hrs) for every recording day. The *slicing solution* stock was prepared every 2 months.

*Slicing solution*: This solution was used during biopsy acquisition, transportation, and tissue slicing. It was composed of: choline chloride, 110 mM; potassium chloride, 2.5 mM; sodium dihydrogen phosphate, 1.2 mM; sodium bicarbonate, 25 mM; Sodium Pyruvate, 2.4 mM; Ascorbate, 1.3 mM; Dextrose, 20 mM. The calcium chloride, 0.5 mM; and magnesium chloride, 7mM; were added to the solution on the recording day (6,7). Osmolarity was verified to be between 300-305 mOSM and pH was adjusted to 7.3-7.4 using NaOH or HCL. The *slicing solution* was saturated with 95 % O<sub>2</sub>, 5 % CO<sub>2</sub> prior used.



*HEPES solution*: Used for tissue maintenance prior to recording and contains: sodium chloride, 92mM; potassium chloride, 2.5 mM; sodium dihydrogen phosphate, 1.2 mM; sodium bicarbonate, 2.4 mM; sodium Pyruvate, 3 mM; ascorbate, 5 mM; thiourea, 2mM; HEPES, 20mM; dextrose, 25 mM. magnesium chloride, 2mM; calcium chloride, 2mM. Osmolarity was verified to be between 300-350 mOSM and pH was adjusted to 7.3-7.4 using NaOH or HCL. The *HEPES solution* was saturated with 95 % O<sub>2</sub>, 5 % CO<sub>2</sub> prior used.

*aCSF*: Used for bathing the slices during the electrophysiological recording session and contains: sodium chloride, 126 mM; potassium chloride, 2.5 mM; sodium dihydrogen phosphate, 1.2 mM; sodium bicarbonate, 26 mM; calcium chloride, 2 mM; magnesium chloride, 2 mM; Dextrose, 10 mM. Osmolarity was verified to be 300-305 mOSM/kg and pH was adjusted to 7.3-7.4 using NaOH or HCL. To block fast glutamatergic and GABAergic synaptic transmission, 2 mM of Kynurenic and 100 uM of picrotoxin were added, respectively. The *aCSF* was constantly saturated with 95 % O<sub>2</sub>, 5 % CO<sub>2</sub>.

*Internal solution with biocytin*: The recording electrodes were filled with an internal solution containing potassium gluconate, 116 mM; potassium chloride, 8mM; sodium gluconate, 12mM; HEPES, 10.0 mM; potassium ethylene glycol-bis (2-aminoethylether)-N,N,N',N'-tetraacetic acid, 1.0 mM; calcium chloride, 0.24 mM; magnesium chloride, 2 mM; guanosine 5'-triphosphate sodium salt hydrate, 0.3 mM; adenosine 5'-triphosphate potassium salt, 4 mM; and biocytin (innvitrogen B1592), 0.5-1%. Osmolality was verified to be between 290-295 mOsm/kg. To confirm the placement of the neuron in the slice after removing the pipette at the end of the recording, 0.2 mM of Alexa fluor 488 (Invitrogen A11001) was added to the internal solution. pH was adjusted to 7.2-7.4 using KOH.

- Histological processing

After the physiological characterization, the slices were fixated and stored in Lana's Fixative solution (4% paraformaldehyde, 20% picric acid) at 4°C during 1-4 months. All

neurons were stained with DAPI for cortical layer delimitation and by anti-biocyntin-streptavidin 488. Free floating sections were washed two times in 1x Phosphate Buffer saline (PBS) + 2% Triton X for 10 minutes before incubation in blocking solution (0.05% Triton X + 0.5% bovine serum albumin in 1x PBS) at room temperature for one hour. Then, the slices were incubated overnight with a goat anti-biotin antibody (dilution 1:100, Sigma, USA, cat.nr. B3640) at 4°C.

The following day, two 5-minute washes with 1x PBS were performed before diluting the streptavidin-Alexa 488 (dilution 1:1000, Invitrogen, USA, cat.nr. S32354) in blocking solution, added to each well and incubated for 1hr at room temperature. The tray was covered from this step forward to prevent photo bleaching. Then, two 5-minute washes in 1x PBS and a 5-minute wash in 1x PBS + 1:1000 DAPI (4',6-diamidino-2-phenylindole) were performed, followed by a final 1xPBS wash. The tissue was treated with 1% Sudan Black dissolved in 70% ethanol for 1 minute, washed with ethanol 70% two times for 2 minutes and rehydrated in 1xPBS 2 times for 5 minutes before mounting using Aqua-Poly Mount mounting media which enhances and retains fluorescent stains.

- Image acquisition, dendritic type and layer localization of the neuron

Mounted sections were imaged using 3 different parameters for different purposes: For preliminary visualization of morphology and layer localization, epifluorescence images were acquired using an Olympus BX51 fluorescence microscope equipped with a Teledyne Photometrics CoolSNAP camera (6.45 x 6.45 microns pixel size) with 10x air, 20x air and 60x oil immersion objective for spines identification. The images were obtained using DAPI channel (to delineate cortical layers) and GFP channel (for biocytin-filled neuron visualization). These overview images were taken with 10x or 20x air objectives depending on the size of the neuron.

- Three-dimensional reconstruction

Some cells were three-dimensional reconstructed using the 63x high-resolution z-stack images using Neurolucida 2019 software (v.1.3 MBF Bioscience, Williston, VT USA). The reconstructions were trace manually and store in .DAT.

- Electrophysiological data analysis

Patch clamp recordings were obtained via Clampfit in the abf format. Data from the Allen Brain Institute were provided in the NWB format (Teeters et al. 2015). All recordings were analyzed by custom MATLAB scripts, primarily written by Eric Kuebler. The electrical features were extracted from voltage responses to long hyperpolarizing and depolarizing somatic current injections. Automatic computation of waveform parameters was done in the following way: Every event in which the voltage trace reaches a higher  $dV/dt$  than 20 mV/ms and was followed by a slope of 0 during stimulation was considered a suprathreshold event. From each continuous suprathreshold segment a peak amplitude was determined. From there, the slope of the rising phase could be evaluated as the first derivative, going backward from peak to reaching zero or near zero. According to this the following features were calculated (See **Figure 3**):

- Waveform parameters (features from the first evoked AP):

**Threshold (mV):** Point before the peak where the  $dV/dt$  was 5% of the maximum  $dV/dt$ . If the absolute value of the slope was lower than 2.9 mV/ms, the threshold was determined at this value.

**Peak (mV):** Maximum value of the membrane potential during the AP.

**Through (mV):** Minimum value of the membrane potential in the interval between the peak and the time of the next action potential.

**Peak up stroke (dV/dt):** The minimum value of  $dV/dt$  between the action potential threshold and the action potential peak.

**Peak down stroke (dV/dt):** The minimum value of  $dV/dt$  between the action potential peak and the action potential trough.

**AP half width (ms):** Time interval between both points in the voltage trace on either side of the peak calculated at the half height of the AP. The half-height was defined as the midpoint of the voltage difference between the threshold and peak.

**AP height (mV):** Defined as the difference between the action potential threshold and peak.

- Spike train features:

**Firing rate (Hz):** Calculated per sweep. As the spike counts across the 1 second stimulus interval.

**Maximum firing rate (Hz):** The maximum firing rate calculated for each cell.

**Inter-spike interval (ISI, ms):** calculated between spikes as the distance between the peak of an action potential and the peak of following action potential.

**Median instantaneous frequency (Mdn instant freq, Hz):** 1 divided by the median ISI of all sweeps of a neuron.

**Adaptation index:** It is the rate at which firing speeds up or slows down during a stimulus. It was calculated from a moderate current stimulation determined as the closest to 1.5 times the rheobase sweep. The Adaptation index was calculated with the following formula:  $\frac{1}{N-1} \sum_{n=1}^{N-1} \frac{ISI_{n+1} - ISI_n}{ISI_{n+1} + ISI_n}$  with N being the number of ISIs in the analyzed sweep.

- Subthreshold properties

**Steady state:** Calculated for each sweep. For this parameter we measure the mean and standard deviation for several 50 ms time windows within the last 300ms of the current stimulus. The shift between considered time windows was 5 ms. From all the obtained values, the steady state was determined as the mean membrane potential of the 50ms section with the smallest standard deviation. If the standard deviation was higher than 0.2 mV, the sweep did not have an acceptable steady state.

**Sag:** Measured from the voltage difference between the minimum membrane potential and steady state. It was calculated from the -90 current stimulus sweep of the cell if available, if not, it was obtained from the -110 sweep, and if none of the previous sweeps were available then the -70 sweep was used.

**Sag ratio:** Determined from the same sweep as the sag. This parameter was defined as the ratio of peak deflection divided by the steady state. It has minimum value of 1 in case of no sag.

***Resting membrane potential (RMP, mV):*** pre-stimulus membrane potential from the sweep where the sag was calculated. This sweep was chosen for a more sensible correlation with the sag ratio.

***Input resistance (Rin, MΩ):*** Slope of the linear fit to the voltage change from RMP to steady state in response to current stimulus across sweeps. The fit included also the point of origin (0, 0).

***Rheobase:*** The minimum current amplitude that evoked an action potential.

***Time constant:*** The time required for the membrane voltage to reach the 63% of the minimum membrane potential upon current injection. Tau is calculated as the average from each value obtained by hyperpolarizing sweeps (below -100 pA) of the long square.

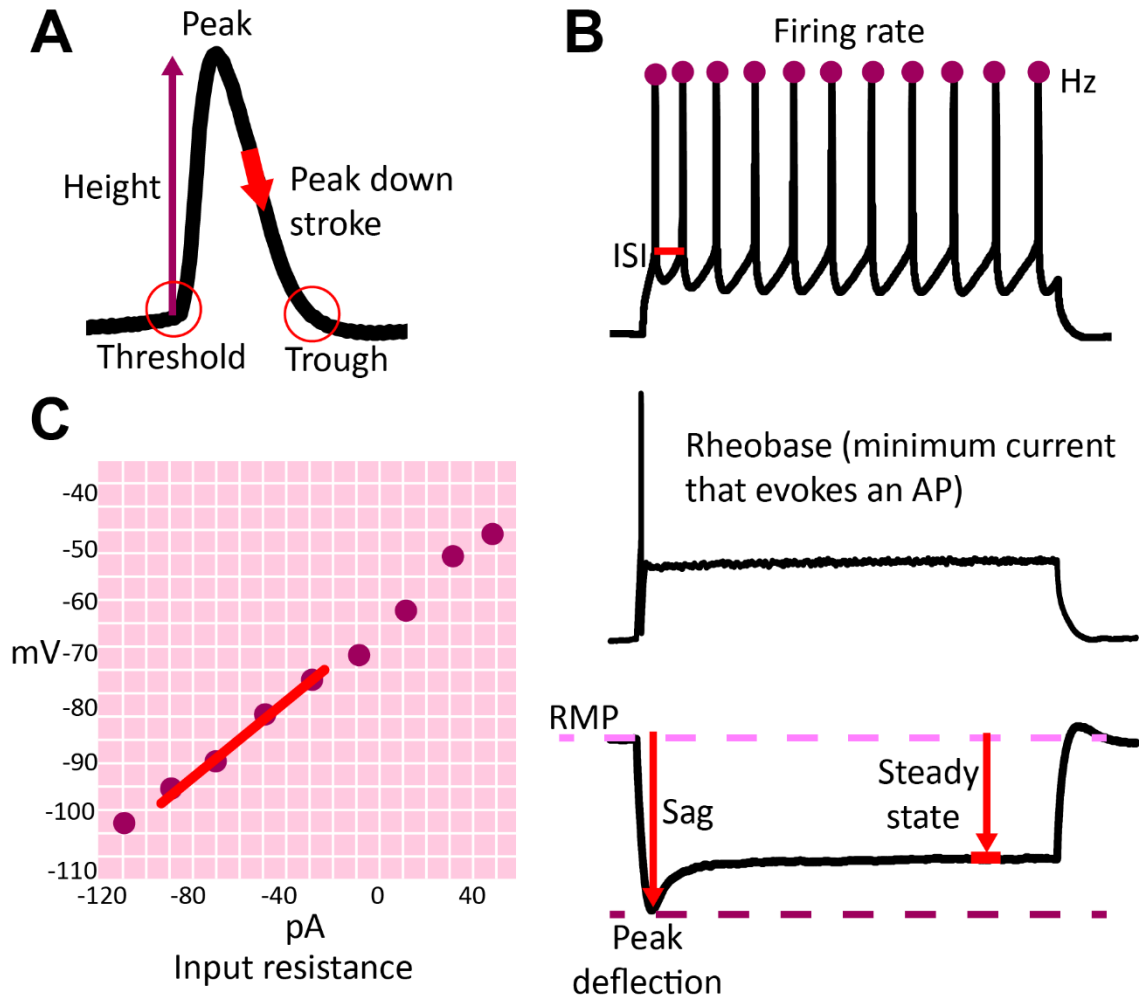


**Figure 3. Schematic representation of electrophysiological parameters.** **A** shows peak, threshold, trough, height, and peak down stroke of an action potential (AP). **B.** Shows the relationship between the cell membrane voltage and current injected. The slope of the linear fit (light red line) determines the input resistance. **C.** Examples of suprathreshold traces. In the high current stimulation on top, the peaks of all action potentials are marked in dark red and the first inter-spike interval (ISI) in light red. The amount of APs during the stimulus durations (1 second) is the firing rate of the sweep. The hyperpolarizing current stimulus on the bottom shows the resting membrane potential of the sweep (RMP, pink dashed line), the peak deflection (dark red dashed line), sag, and steady state (red arrows). The trace located in the middle shows a rheobase sweep which is the sweep with the minimum current injection that has an action potential.

### **3.3. Electrophysiological quality control**

All electrophysiological recordings from the Allen cell type database and NHP included in this study passed three levels of quality control (QC): cell, sweep and spike QC. At the cell level the following criteria must be met: The electrode must be zeroed before recording, a Giga-seal ( $>1.0 \text{ G}\Omega$ ) must have been reached prior to brake in. The initial access resistance must be  $< 20\text{M}\Omega$  and the recordings must have enough information to calculate input resistance  $R_{in}$  (measure of change in the membrane voltage to current stimulus) and Rheobase (the lowest amplitude required to generate a spike). Within a sweep the minimum pre-stimulus RMP must be  $> -50\text{mV}$ , Long term RMS estimated for both pre- and post-stimulus time window must be  $<0.75$ . Between all sweeps of a cell the mean pre-stimulus voltage and standard deviation were measured, if the standard deviation was less than 0.7, the cell passed this QC. If it were greater than 0.7 but less than 3 all sweeps with  $>1.75$  standard deviations plus/minus the mean, and if they were  $> 3$  the cell was removed. For the spike QC, action potentials that had the following characteristics were not evaluated : threshold to peak height  $< 35\text{mV}$  or  $45 \text{ mV}$ , respectively (the latter criterium applies to spikes with a width of above 0.8 ms),  $>1.5$  milliseconds between threshold and peak, peak to trough height  $< 30\text{mV}$ , peak to through height  $< 30\%$  of the spike rheobase and threshold  $> -27.5\text{mV}$ .

### **3.4. Statistical analysis**

One-way analysis of variance (ANOVA) was used for group comparisons between FS neurons across species. Tukey's honestly significant difference criterion was used as a post hoc test. To examine cell type-specific (FS vs Exc cells) and species-specific (mouse, NHP, human) differences in membrane properties, two-way ANOVAs were performed with subsequent Bonferroni-corrected multiple comparison. Statistical tests were performed using Matlab R2019a. Values are presented as means  $\pm$  standard deviation.

## 4. Results

### 4.1. Descriptive statistics of used datasets

In this study we used two different datasets containing electrophysiological recordings and morphological characterization (dendritic type, layer localization and cell morphology) of cortical neurons: The publically available dataset for mouse and human from the Allen Institute (© 2018 Allen Brain Atlas: Allen Cell Type Database), and our own NHP dataset. The data was used to conduct common parameter comparisons across species (waveform, spike train and subthreshold parameters).

#### 4.1.1. Composition of the databases

- Mouse dataset

From the 1920 mouse neurons from the Allen Institute cell type database, 1895 cells passed our quality control and were included for analysis. Most of these neurons stem from visual cortical areas (96.5%), while cells from auditory, retrosplenial, and primary somatosensory areas are the remaining 3.5%. These cells in comparison to primate neurons were patched under fluorescence microscopy. If the recorded cell expressed a fluorescent protein (1779 of 1920 cases) it is labeled as reporter status positive. The sample contains cells that belong to 37 different transgenic lines. Most lines are specific for excitatory or inhibitory cells but some of them are positive to both type of cells. (See table 1.1) Reporter lines for parvalbumin expressing cells (*Pvalb-Cre*, *Pvalb-CreERT2*, *Pvalb-FlpO/Vipr2-Cre* lines, and *Chrna2-Cre/Pvalb-Dre*, simplified nomenclature for readability) constitute the 12.6% of the mouse cells. Lines such as *Slc32a1-FlpO/Vipr2-Cre* and *Nkx2-1-CreERT2* which are the most appropriate lines to target chandelier cells have 4.1% (8). *Vipr2-Cre* and *Vipr2-Cre-neo* lines also target chandelier neurons to a smallest extent since their promoter leads to their expression in excitatory cells as well. They are expressed in 1.5% of the neurons. Other important lines are the *Htr3a-Cre* and *Sst-Cre* for Htr3a and SST cells. These cell groups together with the PV are known to be the most abundant and not overlapping subpopulations of interneurons in the mouse neocortex. In this study they were expressed in 8.2 and 6.8% of the cells respectively. *Vip-Cre* was present in the 5.0% of the cells and



*Chat-Cre* in 3.7%. These are transgenic lines for VIP cells (a sub-population of neurons present in the *Htr3a* group). Although *Chat-Cre* is also expressed in other inhibitory interneurons. *Gad2-Cre* is a pan-interneuron line.

<i>Excitatory lines</i>	<i>Inhibitory lines</i>	<i>Mixed lines</i>
Rorb-IRES2-Cre (7.3%)	Pvalb-IRES-Cre (12.0%)	Ndnf-IRES2-dgCre (5.1%)
Scnn1a-Tg3-Cre (4.7%)	Htr3a-Cre_NO152 (8.2%)	Chrna2-Cre_OE25 (3.7%)
Nr5a1-Cre (4.5%)	Sst-IRES-Cre (6.8%)	Oxtr-T2A-Cre (2.5%)
Rbp4-Cre_KL100 (4.5%)	Vip-IRES-Cre (5.0%)	Nos1-CreERT2 Sst-IRES-FlpO (2.3%)
Cux2-CreERT2 (4.3%)	Chat-IRES-Cre-neo (3.7%)	Vipr2-IRES2-Cre (1.5%)
Ntsr1-Cre_GN220 (3.0%)	Nkx2-1-CreERT2 (2.5%)	Nos1-CreERT2 (1.2%)
Ctgf-T2A-dgCre (2.8%)	Slc32a1-T2A-FlpO Vipr2-IRES2-Cre (1.6%)	Vipr2-IRES2-Cre-neo (0.05%)
Scnn1a-Tg2-Cre (2.3%)	Gad2-IRES-Cre (1.0%)	
Tlx3-Cre_PL56 (2.3%)	Htr3a-Cre_NO152 Pvalb-T2A-Dre (0.7%)	
Sim1-Cre_KJ18 (1.7%)	Chrna2-Cre_OE25 Pvalb-T2A-Dre (0.4%)	
Esr2-IRES2-Cre (1.4%)	Pvalb-T2A-CreERT2 (0.1%)	
Glt25d2-Cre_NF107 (0.6%)	Pvalb-T2A-FlpO Vipr2-IRES2-Cre (0.1%)	
Slc17a6-IRES-Cre (0.1%)	Gng7-Cre_KH71 (0.05%)	
Esr2-IRES2-Cre PhiC31-neo (0.1%)		
Penk-IRES2-Cre-neo (0.3%)		
Esr2-IRES2-Cre-neo PhiC31-neo (0.05%)		
Esr2-IRES2-Cre-neo (0.05%)		

*Table 1: Mouse transgenic lines used in the Allen brain cell type data base. Transgenic lines in the mouse dataset. The reporter lines are classified according to their cell type specificity for excitatory, inhibitory or a mix of both cell types. The relative frequency of cells with positive reporter status for each transgenic line is shown in parenthesis. The reporter lines are ranked according to their prevalence in the database. The more prevalent transgenic lines mark PV, Htr3a and SST inhibitory interneurons, however the vast majority of the database is by excitatory cells that are marked by many different reporter lines.*

The dendritic type in the mouse cells show a similar frequency of spiny and aspiny neurons. 46.7% of the cells have a spiny dendritic type, 47.8% are aspiny and 5.5% are sparsely spiny. Most of the cells were located in L2/3, L4 and L5, followed by L6a, and a smaller amount in L6b and L1. The distribution of different dendritic types also vary across layers. L1 contains only aspiny neurons. The proportion of aspiny neurons and other dendritic types are higher in L2/3, while the biggest proportion of spiny cells is present in L4. L5 show an almost balanced distribution between cells with spiny and other dendritic types. In L6a and L6b the biggest proportion was given by spiny neurons. Sparsely spiny cells were only found in L2/3, L5 and L6a, with the largest amount located in L5 (See **Figure 4**).

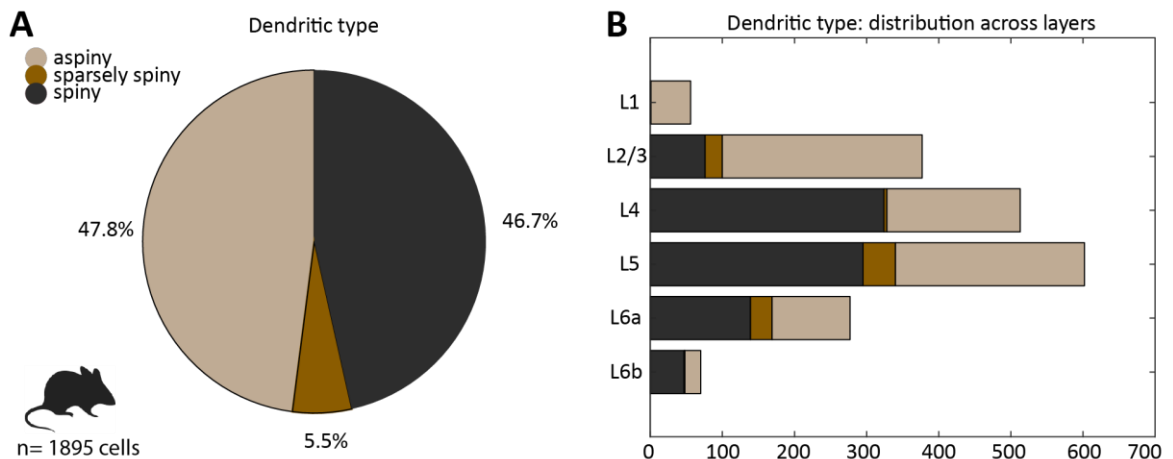


**Figure 4. Dendritic type and layer distribution of mouse database.**

**A.** Prevalence of dendritic types in the mouse dataset (n=1895 cells). 47.8% of the neurons have an aspiny dendritic type (shown in khaki), 46.7% are spiny (shown in black) and only 5.5% of them are sparsely spiny (shown in brown). **B.** Distribution of neurons and dendritic types across cortical layers. The layers with higher numbers of cells are L5, L4, and L2/3. L1 and L2/3 have higher prevalence of aspiny neurons while the spiny cells are the majority of the cells in all other layers. Sparsely spiny neurons are located in L2/3, L5, and L6a.

- Human dataset

From the 413 human cells in the Allen Institute cell type database, 393 cells passed our quality control and were included for analysis. Most of these neurons (82.7%) stem from the temporal lobe, 13.5% from frontal lobe (No DLPFC), and 3.8% from the angular gyrus. 78% of the cells have a spiny dendritic type, 19% are aspiny and 3% are sparsely spiny. The distribution of dendritic types varies across layers. Most cells were located in L3, followed by L5/6 and L4, with fewer in L2 and L1. The proportion of spiny neurons to other dendritic types is higher in all cortical layers with exception of L1. L1 contains only aspiny and sparsely spiny neurons. The largest amount of aspiny cells are present in L3; however, this layer is the only one that does not contain any sparsely spiny cells (See **Figure 5**).

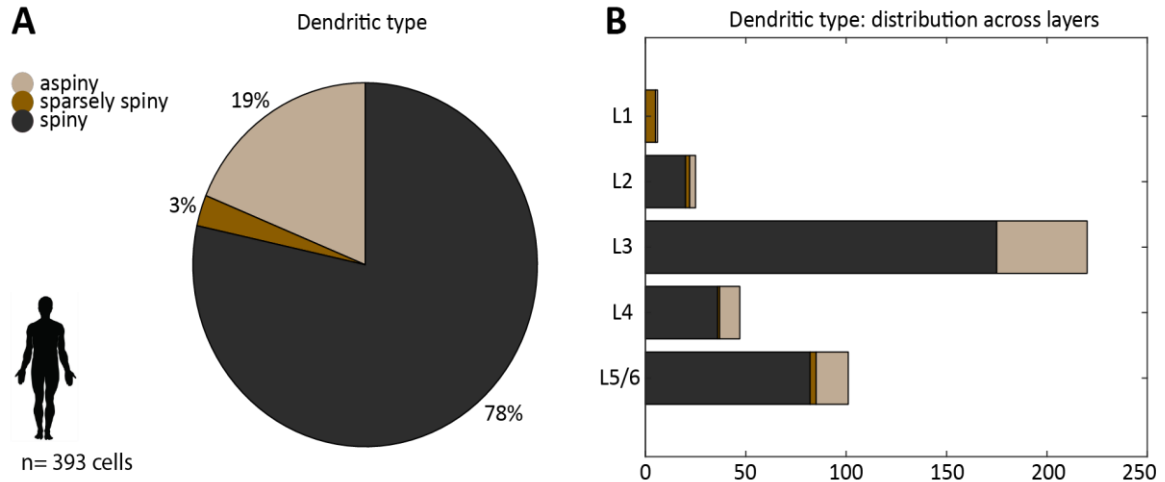


**Figure 5. Dendritic type and layer distribution of human database.**

**A.** Pie chart showing the prevalence of dendritic types in the human dataset (n= 393 cells). Most of the human cells (78%) have a spiny dendritic type (shown in black) while 19% are aspiny (shown in khaki) and 3% sparsely spiny (shown in brown). **B.** Distribution of neurons across cortical layers. The dendritic type of neurons is shown in different colors. The layers with the largest amount of cells are L3 and L5/6. Spiny cells are the more prevalent neurons in all layers. The highest amount of aspiny cells are located in L3, followed by L5/6 and L4. Sparsely spiny neurons are primarily located in L1, although some of them are found in L2 and L5/6.

- NHP dataset

The NHP database consisted of 105 cells. These cells stem from the DLPFC of macaques. We obtained a successful biocytin filling and histological staining of 44 cells for layer and/or dendritic type analysis. Most of the cells (61.4) show an aspiny dendritic type and 38.6% were spiny. For the NHP, the sparsely spiny and aspiny cells were classified in the same dendritic type group (aspiny). The largest amount of cells were located in L3, followed by L5/6, L4 and L2; no cells from L1 were found. The proportion of dendritic types varies across layers. L2 and L4 have the same proportion of spiny and aspiny cells, whereas L3 and L5/6 have a higher proportion of aspiny neurons in comparison to spiny. Most of the aspiny cells were located in L3 (See **Figure 6**).

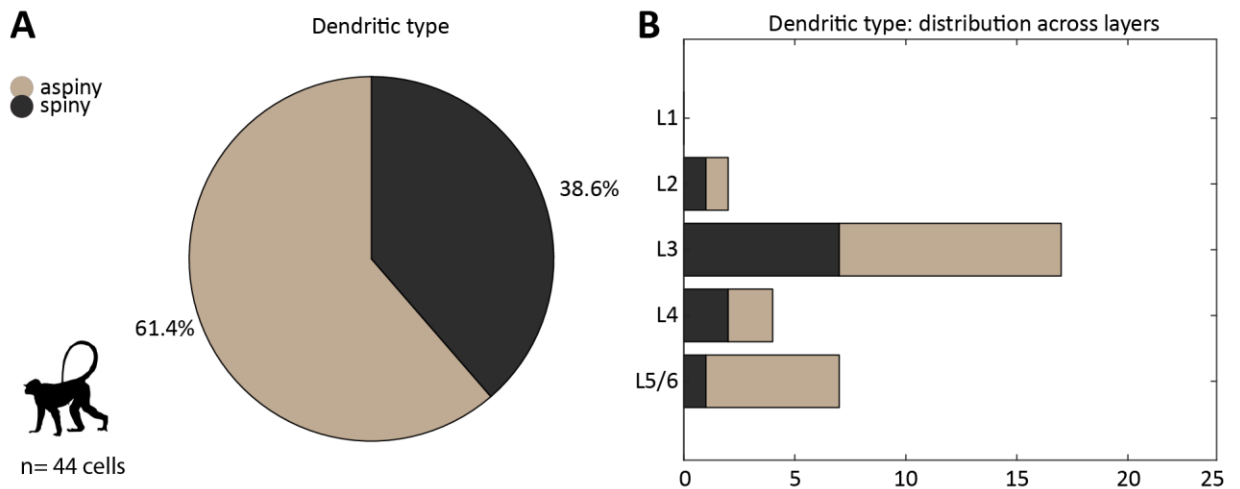


**Figure 6. Dendritic type and layer distribution of NHP database.** **A.** Pie chart showing the prevalence of dendritic types in the NHP dataset (n= 44 cells). Most of the NHP cells (61.4%) have an aspiny dendritic type (shown in khaki) while 38.6% were spiny (shown in black) **B.** Distribution of neurons across cortical layers. Dendritic type is shown in different colors. L3 and L5/6 had the largest number of cells. The largest amount of aspiny cells is located in L3, followed by L5/6. L4 and L2 have the same proportion of spiny and aspiny cells.

#### 4.1.2. General distribution of waveform parameters across species

For most features the different distributions across species show a consistent pattern that probably relates to major differences in sampling. The data sets with a high fraction of interneurons also show a higher variability: the inter-quartile range in many features (like threshold, RMP) is wider in mouse and NHP, which might be due to a higher diversity of intrinsic properties of cortical GABAergic interneurons. A long that line, the human data show median values that suggest a majority of regular spiking excitatory cells in which medians of AP height and peak are considerably higher than the two other aforementioned groups, whereas inter-spike intervals are longer and show a higher adaptation. However, some features of NHP cells stand out from the expected pattern. Most prominent here is the peak up stroke, which seems to be on half the level of mouse. Other strong disparities

between the data sets can be found in the subthreshold parameters Rin and sag ratio. In the following section, the distributions and basic metrics are discussed for each intrinsic biophysical parameter (See **table 2**):

	<b>Mouse (n= 1895)</b>	<b>Human (n= 393)</b>	<b>NHP (n= 105)</b>
	<b>Median(IQR)</b>	<b>Median(IQR)</b>	<b>Median(IQR)</b>
<b>Waveform Parameters</b>			
Threshold (mV)	-37.9 (6.3)	-39.4 (4.7)	-42.4 (6.7)
Peak (mV)	31.8 (16.6)	42.9 (9.8)	29.0 (15.6)
Through (mV)	-54.2 (6.3)	-53.4 (6.8)	-56.7 (7.8)
Peak up stroke (dV/dt)	294.6 (105.7)	276.2 (61.2)	143.1 (39.2)
Peak down stroke (dV/dt)	-106.7 (54.5)	-93.3 (29.2)	-87.8 (50.4)
AP half width (ms)	0.7 (0.4)	0.8 (0.2)	0.8 (0.4)
AP height (mV)	69.9 (17.6)	82.4 (11.3)	71.8 (17.9)
<b>Spike train features</b>			
Max. firing rate (Hz)	25 (18)	16 (25)	28 (78)
Mdn instant freq (Hz)	23.1 (14.8)	17.5 (26)	48.9 (76.4)
Adaptation index	0.017 (0.033)	0.060 (0.107)	0.016 (0.052)
<b>Subthreshold properties</b>			
RMP (mV)	-72.5 (7.5)	-70.1 (5.9)	-67.3 (9.4)
Rin (M $\Omega$ )	163.2 (93.8)	111.9 (104.0)	226.4 (157.5)
Tau (ms)	15.6 (12.1)	23.0 (12.9)	20.4 (9.9)
Rheobase (pA)	90 (80)	130 (140)	70 (62)
Sag ratio	1.007 (0.008)	1.014 (0.017)	1.049 (0.062)

## Table 2. Descriptive statistics from mayor electrophysiological parameters

Comparison table of median and interquartile range (IQR) of the distributions of waveform, spike train features and subthreshold properties from the total cell population of mouse (n= 1895 cells), human (n= 393 cells) and non-human primate (NHP, n= 105 cells). Abbreviations: AP, Action potential; Max, maximum; Mdn, median; RMP, resting membrane potential; Rin, input resistance; Tau, time constant.

### ○ AP Threshold

In the mouse, the threshold values show a skewed left distribution with a median of -37.9mV and inter quartile range (IQR) of 6.3mV. The peak is located at the 13th bin [-38.9: -37.5]. The human data is close to a symmetrical distribution with a median of -39.4mV and IQR of 4.7mV. The peak is located at the 13th bin [-39.3: -37.9]. In NHP instead, the values are more hyperpolarized, having a right skewed distribution with a median of -42.4mV and IQR of 6.7mV. The peak plateau is located at the 10th and 11th bin [-45.5: -42.1] (See **Figure 7**).

### ○ AP Peak

The AP peak have a skewed distribution to the left in the mouse with a median of 31.8mV and an IQR of 16.6mV. The peak is at the 14th bin [35: 38]. In the human, the distribution shows a similar trend than the observed in mouse, however, the transition toward the tail on the left is more abrupt. The median is 42.9mV with an IQR of 9.8mV. The distribution peak is located at the 16th bin [46.5: 49.2]. The NHP data suggest a symmetrical distribution with a median of 29.0mV and IQR of 15.6mV. The peak is located at the 11th bin [29: 31.9] (See **Figure 7**).

### ○ AP Through

In mouse, the AP through values show a skewed left distribution with a median of -54.2mV and IQR of 6.3mV. The peak is located at the 13th bin [-55.12: -53.3]. The human distribution shows a more complex pattern. At least two peaks can be distinguished: the first peak at the 12th bin [-54.7: -53.2] and a peak plateau at the 15th bin [-50.2: -48.7]. The

median from this distribution is  $-53.4\text{mV}$  with an IQR of  $6.8\text{mV}$ . The median of the NHP distribution is  $-56.7\text{mV}$  with an IQR of  $7.8\text{mV}$ . The peak is located at the 11th bin  $[-56.6:-55.2]$ , but the low cell counts per bin makes an interpretation difficult (See **Figure 7**).

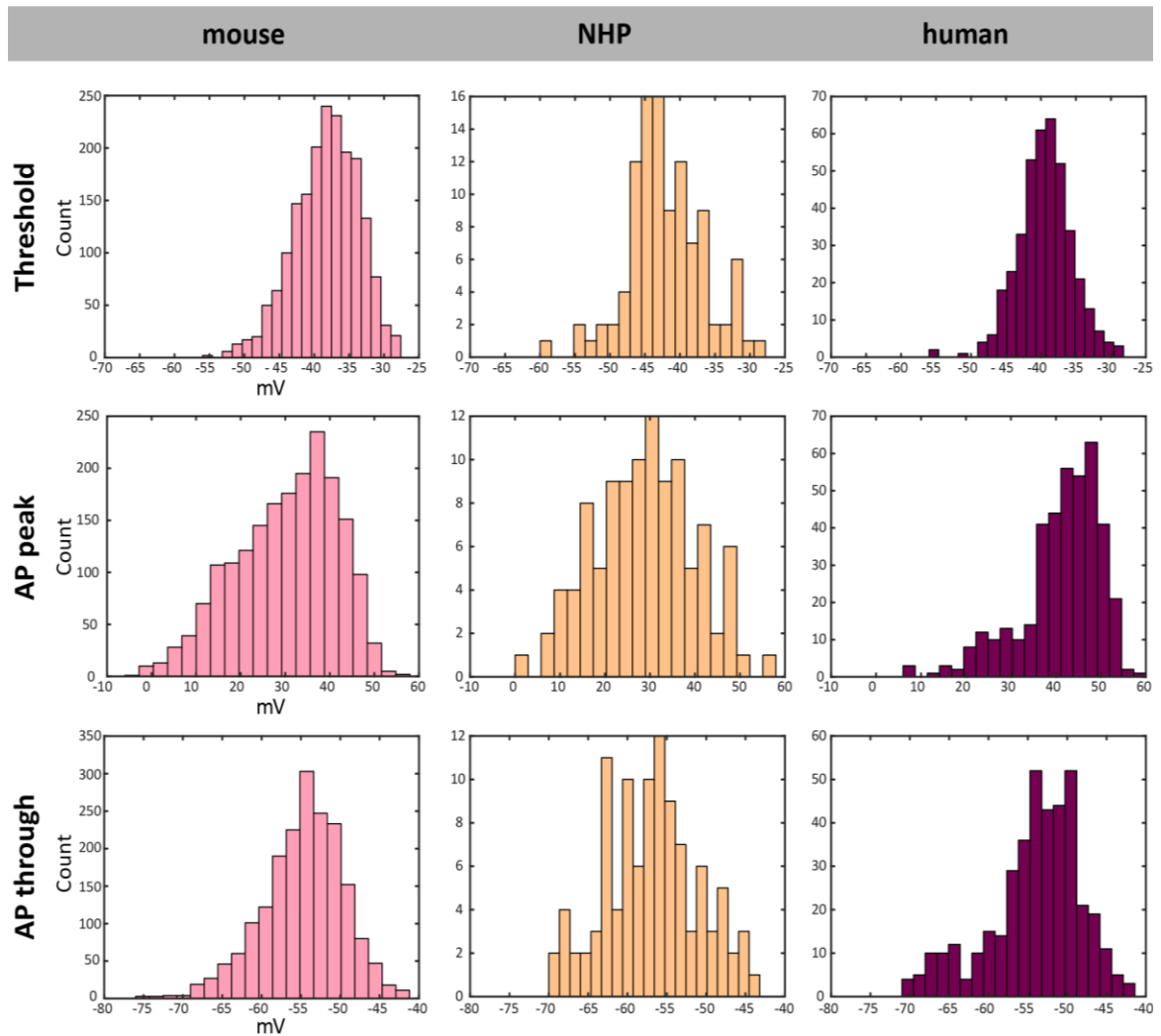


**Figure 7. Distribution of waveform parameters across species (1)**  
 Distribution of threshold, action potential (AP) peak and AP through in the total cell population of mouse in pink ( $n= 1895$  cells), NHP in yellow ( $n= 105$  cells) and human in cherry red ( $n= 393$  cells).



- AP peak up stroke

In mouse, the AP peak up stroke values show a right skewed distribution with a median of 294.7 and IQR of 105.7. The peak is located at the 6th bin [250: 282]. In the human the distribution is skewed to the left. It has a median of 276.2 with an IQR of 61.2. The peak is located at the 11th bin [270: 285]. In the NHP, the distribution is also skewed to the left. It has a median of 143.1 and an IQR of 39.2. The peak is located at the 12th bin [132.6: 1472.2]. The total range of the distributions varies greatly across species (See **Figure 8**).

- AP peak down stroke

The AP peak down stroke data show similar skewed distributions to the left in all species. The mouse values have a median of -111.6 and an IQR of 85.4 with the peak located at the 23th bin [-105.2: -88.4]. In the human, the left tail of the distribution is longer than other species. It has a median of -93.3 with an IQR of 29.2 with the peak located at the 18th bin [-92.9: -76.6]. The NHP left tail of the distribution happens more abruptly. It has a median of -87.8 and IQR of 50.4 and the peak located at the 12th bin [-70.5: -64] (See **Figure 8**).

- AP half width

The distribution of the half width threshold to peak in the mouse is clearly bimodal. The smaller peak is located at the 2nd bin [0.29: 0.35], and the biggest one at the 11th bin [0.71: 0.77]. The median is 0.66ms with an IQR of 0.36ms. This pattern suggests the presence of at least two subpopulations. This bimodal distribution is also found in human but not in NHP, in which the sample size and cell count per bin does not allow inferences about the nature of the distribution. The median obtained from the human distribution is 0.82ms with an IQR of 0.2ms with the higher peak located at the 10th bin [0.79: 0.86]. In the NHP the median is 0.85ms with an IQR of 0.4ms and the peak is located at the 11th bin [0.95:1.01] (See **Figure 8**).

- AP height

The AP height show a skewed distribution to the left in mouse and human but a more symmetrically distribution in the NHP. The mouse median is 69.9mV with an IQR of 17.6mV. The peak is located at the 12th bin [70.4: 73.8]. The human median is 82.4mV with an IQR of 11.3mV. The peak is located at the 16th bin [84: 87.2]. In the NHP the

median is 71.8mV with an IQR of 17.9mV and the peak is located at the 10th [69: 72] and 11th [72: 75] (See **Figure 8**).

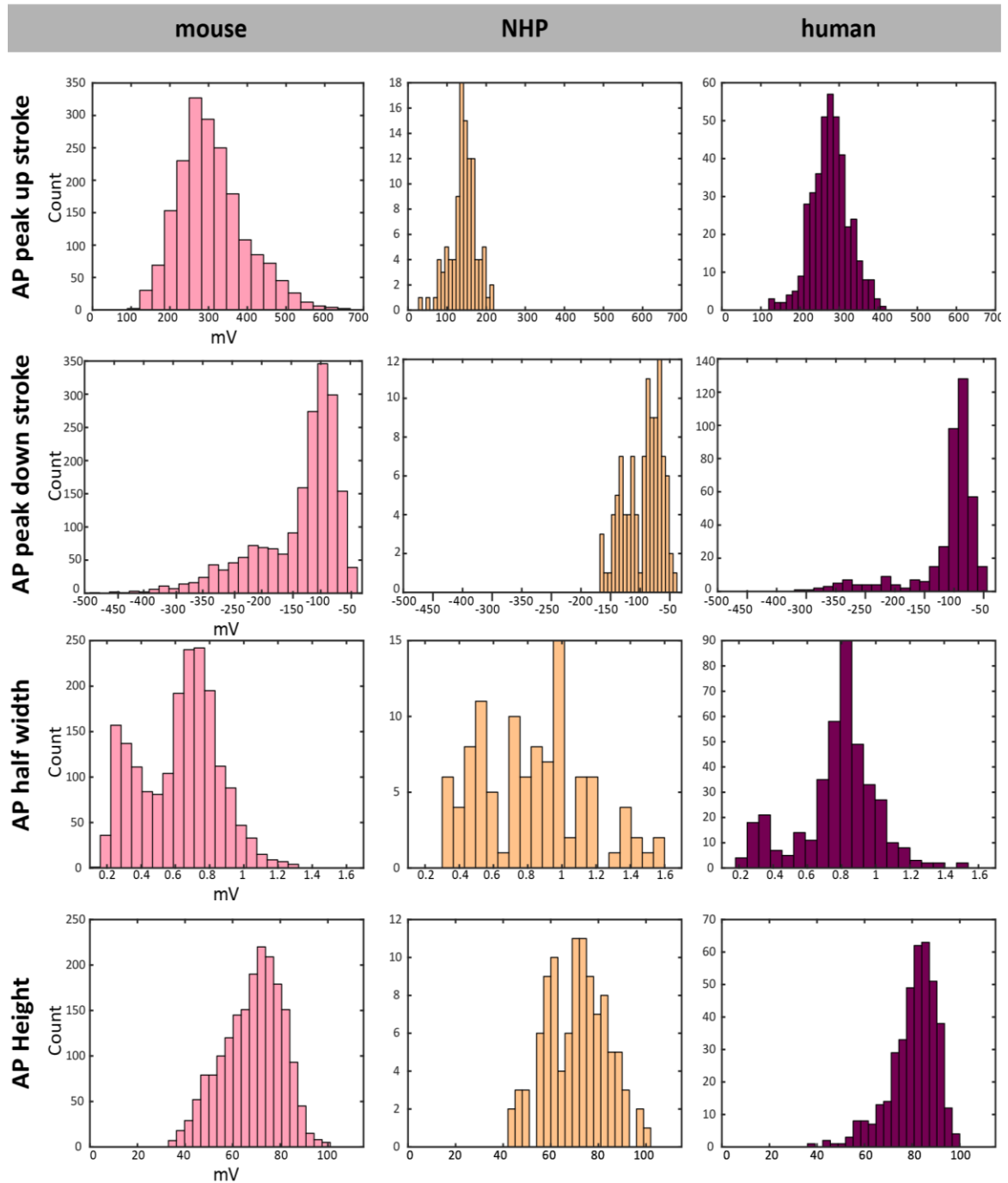


**Figure 8. Distribution of waveform parameters across species (2)**

Distribution of action potential (AP) peak up stroke, peak down stroke, half width and height in the total cell population of mouse in pink (n= 1895 cells), NHP in yellow (n= 105 cells) and human in cherry red (n= 393 cells).

#### 4.1.3. Distribution of key spike train features

- Maximum firing rate

The maximum firing rate values show a right skewed distribution in all species, but the total distribution range changes considerably between them. In the mouse the median of the distribution is 25Hz with an IQR of 18Hz. The peak was located at the 3th [17.0: 25.5]. The human data have a median of 16Hz and an IQR of 25Hz. The peak is located at the 1st bin [0: 6.2]. In the NHP, the median is 28Hz with an IQR of 78Hz and the peak is located at the 1st bin [0: 10.5]. In primates, the location of the peaks at the initial segment of the distributions suggests a high proportion of non persistent firing cells in the databases (See **Figure 9**).

- Median instantaneous frequency

The mdn instant freq values show a right skewed distribution in all species, but differ in the total range of the distributions. In the mouse, the median of the distribution is 23.1Hz with an IQR of 14.8Hz. The peak was located at the 3th bin [16.4: 24.6]. The human data have a median of 17.5Hz and an IQR of 26Hz. The peak is located at the 1st bin [0: 12.3]. In the NHP the median is 48.9Hz with an IQR of 76.4Hz and the peak is located at the 2nd bin [10.2: 20.4] (See **Figure 9**).

- Adaptation index

The distribution of the adaptation index is skewed to the right in all species. Meaning that adaptation is more prevalent than acceleration. The median in the mouse is 0.017 with an IQR of 0.033 and the peak located at the 9th bin [-0.006: 0.012]. In human the median is 0.060 with an IQR of 0.107, the peak is located at the 3rd bin [0.02: 0.06]. The median in the NHP data is 0.016 with an IQR of 0.052. The peak is located at the 5th bin [-0.02:

0.005]. It stands out that human cells have higher adaptation than NHP and mouse (See **Figure 9**).

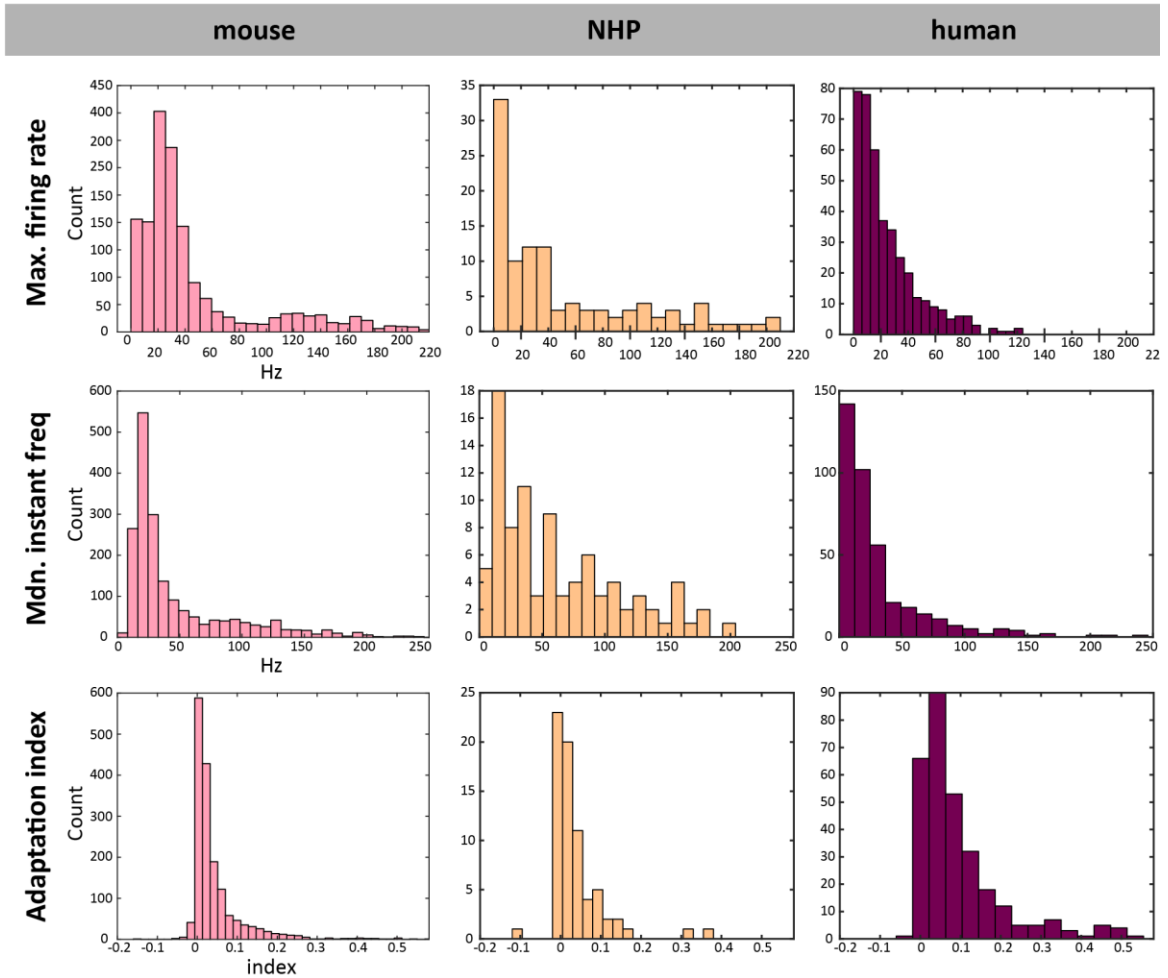


**Figure 9. Distribution of spike train features across species**

Distribution of the maximum firing rate, median instantaneous frequency (mdn instant freq) and adaptation index in the total cell population of mouse in pink (n= 1895 cells), NHP in yellow (n= 105 cells) and human in cherry red (n= 393 cells).

#### 4.1.4. Distribution of subthreshold properties

- Resting membrane potential

The RMP values show an irregular but close to symmetrical distribution in all species. In mouse the median is  $-72.5\text{mV}$  with an IQR of  $7.5\text{mV}$  with the peak located at the 8th bin  $[-75.13: -73.72]$ . In human the median is  $-70.1\text{mV}$  with an IQR of  $5.9\text{mV}$ , and the peak located at the 11th bin  $[-70.4: -69.1]$ . The median in the NHP is  $-67.3\text{mV}$  with an IQR of  $9.4\text{mV}$ . The peak is located at the 14th bin  $[-64.0: -63.3]$ . The NHP, besides having the smaller cell count in comparison to other species also shows a larger range of values in both tails of the distribution (See **Figure 10**).

- Input resistance

The  $R_{in}$  values show a right skewed distribution in all species. In NHP, a larger proportion of cells have higher  $R_{in}$  values. The median for mouse is  $163.2\text{M}\Omega$  with an IQR of  $93.8\text{M}\Omega$ . The peak is located at the 6th bin  $[155: 182]$ . In the human, the median is  $111.9\text{M}\Omega$  with an IQR of  $104.0\text{M}\Omega$ . The peak is located at the 2th bin  $[48: 76]$ . In the NHP, the median is  $226.4\text{M}\Omega$  with an IQR of  $157.5\text{M}\Omega$  and the peak located at the 5th  $[156: 180]$  and 8th bins  $[228: 252]$  (See **Figure 10**).

- Time constant

The Tau values show a skewed right distribution in all species. In the mouse, the median is  $15.6\text{ms}$  with an IQR of  $12.1\text{ms}$ . The peak is located at the 2th bin  $[6.7: 10.3]$ . In the human, the median is  $23.0\text{ms}$  with an IQR of  $12.9\text{ms}$ . The peak is located at the 5th bin  $[16.4: 19.5]$ . The median for NHP is  $20.4\text{ms}$  with an IQR of  $9.9\text{ms}$  and the peak located at the 5th bin  $[16: 18.5]$  (See **Figure 10**).

- Rheobase

The rheobase values show a right skewed distribution in all species but in human in which the neurons reach higher values. The median in mouse is  $90\text{pA}$  with an IQR of  $80\text{pA}$ . The peak is located at the 2th  $[40: 80]$ . In the human the median is  $130\text{pA}$  with an IQR of  $140\text{pA}$ . The peak is located at the 3rd bin  $[66: 99]$ . In the NHP the median is  $70\text{pA}$  with an IQR of  $62\text{pA}$ . The peak is at the 4th bin  $[58: 74]$  (See **Figure 10**).

- Sag ratio

The sag ratio values show a right skewed distribution in all species. The mouse data show much smaller sag ratio values than primates with median of 1.007 and an IQR of 0.008. The peak is located at the 1st bin [1: 1.01]. In the human, the median is 1.014 with an IQR of 1.049 with an IQR of 0.062. The peak is located at the 2nd bin [1.02: 1.03] (See **Figure 10**).

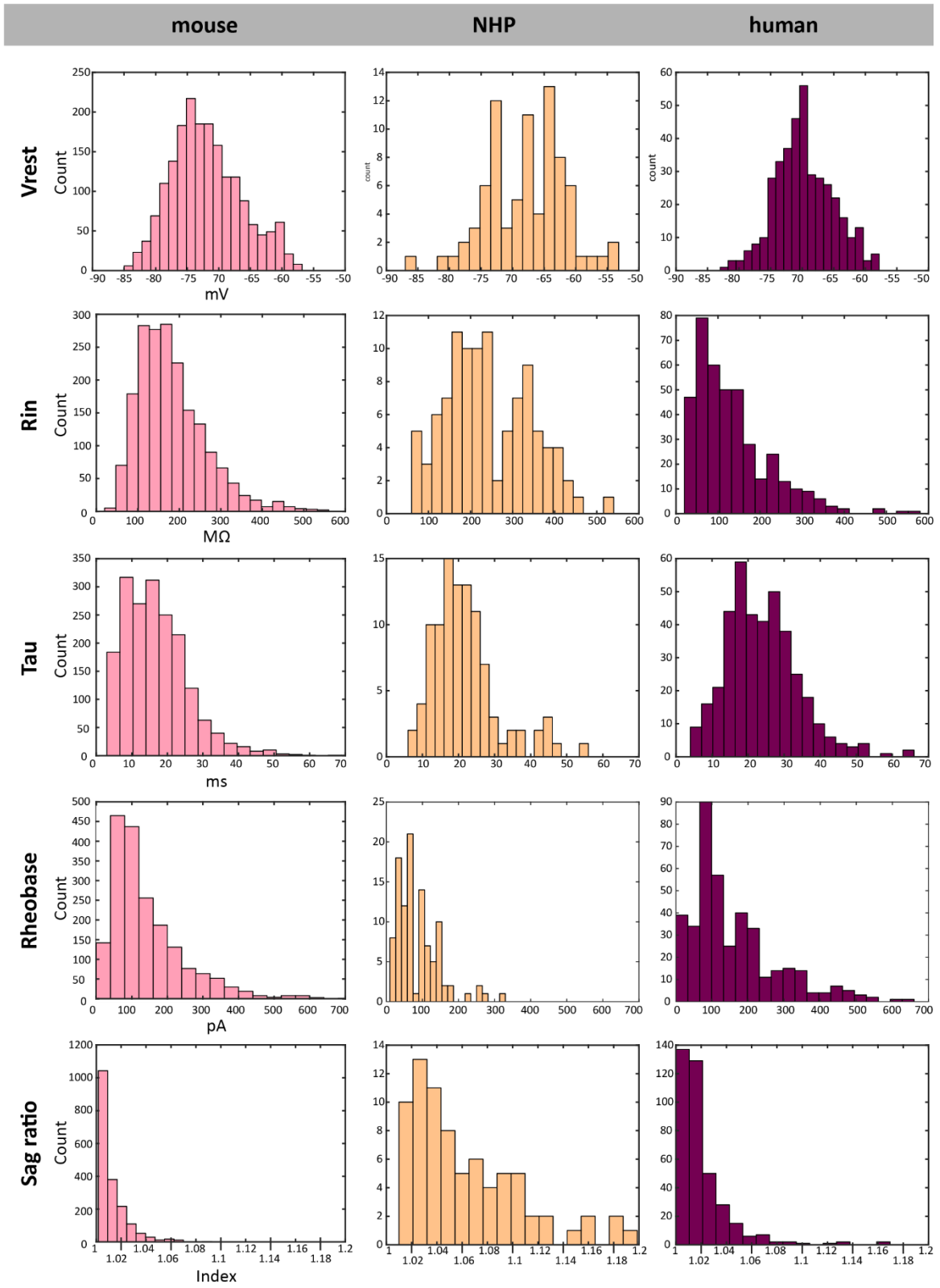


**Figure 10. Distribution of subthreshold parameters across species.** Distribution of resting membrane potential (RMP), input resistance ( $R_{in}$ ), time constant ( $\tau$ ), Rheobase and sag ratio in the total cell population of mouse in pink ( $n=1895$  cells), NHP in yellow ( $n=105$  cells) and human in cherry red ( $n=393$  cells).

## 4.2. Using mouse PV+ cells for cross-species classification of cortical FS cells

Since the focus of this study is on FS neurons, we used the large dataset from transgenic mice containing genetic labelled cells to generate a model that could identify and classify FS neurons in primates which do not have any genetic marker.

### 4.2.1. Linear discriminant analysis classifier

- Selection of predictive parameters

In order to identify fast spiking neurons in the human and non-human primate we developed a linear discriminant analysis classifier using features from the mouse FS PV-cre cells. For the selection of the predictor variables, we limited our candidate pool to suprathreshold features, to leave room for comparing the subthreshold domain of FS neurons. Note that the overall correlation between the subthreshold and suprathreshold parameters is much lower outside than within their domains (See **Figure 11**).

Most cell types (including the FS cells) have a stereotypical electrophysiological profile that links certain suprathreshold features with subthreshold ones. Interestingly, this fact does not seem to considerably raise the correlation level across domains: a finding that suggests two underlying non-overlapping sets of conductances dictated by different ion selectivities, gating and channel dynamics. The key assumption for the following analysis is that there is little direct interaction between predictors of the classifier and the ultimate variables of interest.



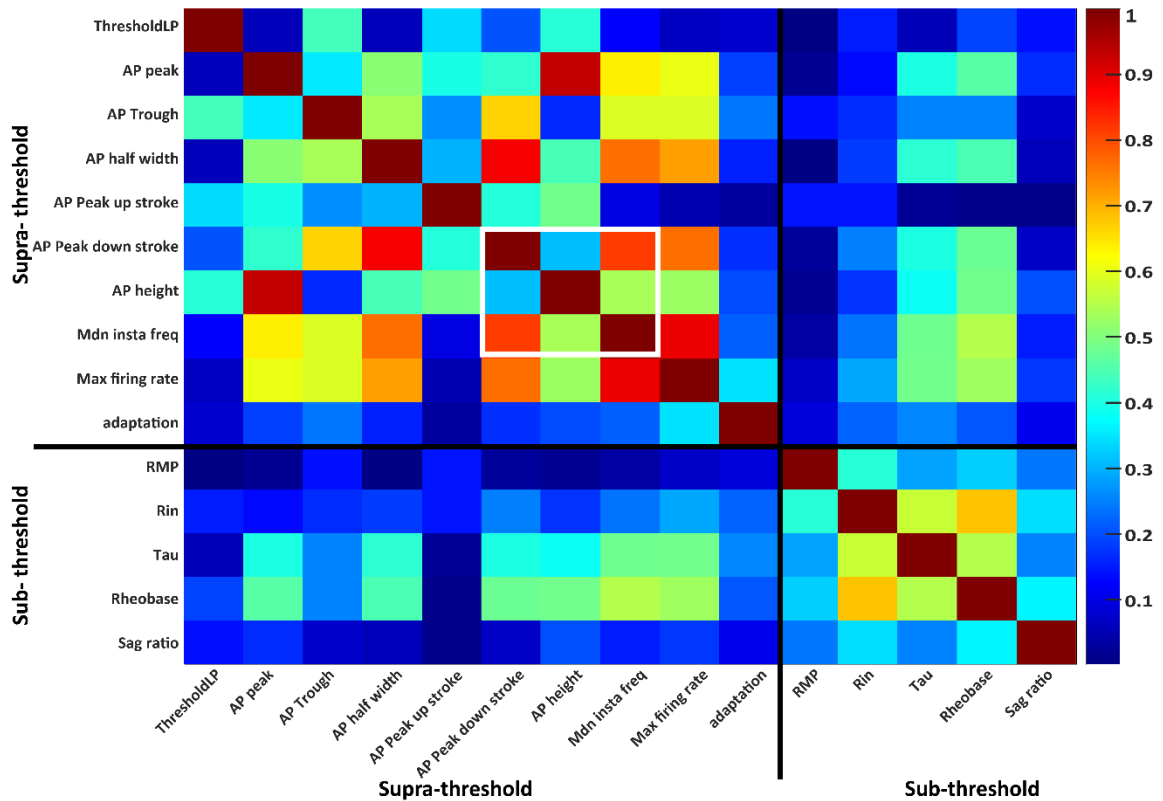


**Figure 11: Correlations between murine sub- and suprathreshold parameters**

Heat map representing color coded correlations (Pearson correlations) between each analyzed parameter (waveform parameters, spike train features and subthreshold properties) compared to any other parameter in the mouse dataset (n= 1895). Black lines separate the subthreshold and suprathreshold variables. The white square indicates the correlations between the selected parameters used for training the FS classifier.

From all suprathreshold parameters we then limited the number of predictor variables in the model to three; this decision was based on the following: firstly, to ensure a robust and comparable performance across species by limiting complexity and avoiding overfitting. Secondly, we assumed that the very distinct FS phenotype is mainly determined by the fast and strong voltage-gated K<sup>+</sup> based conductance (mainly mediated by the Kv3 channel family (4)), that can be captured with a limited number of variables. And thirdly, a three dimensional parameter space is easy to understand and visually monitor.

To maximize the potential information contained in the predictors, we selected two variables that potentially relate to different components of the AP and show minimal correlation with each other (see white box in correlation matrix in **Figure 11**). The AP height (measured from threshold to peak) was used to represent the rising phase of the spike waveform while the peak down stroke represented the repolarizing phase. The third selected parameter is the mdn. instant freq that relates to the cell's firing pattern. These three parameters are evidently different between PV-cre and non PV cells (See **Figure 12**). PV-cre FS cells shows the characteristically short (smaller height) and thin AP (faster repolarization [peak down stroke], as well as higher mdn. instant freq caused by the high frequency firing.

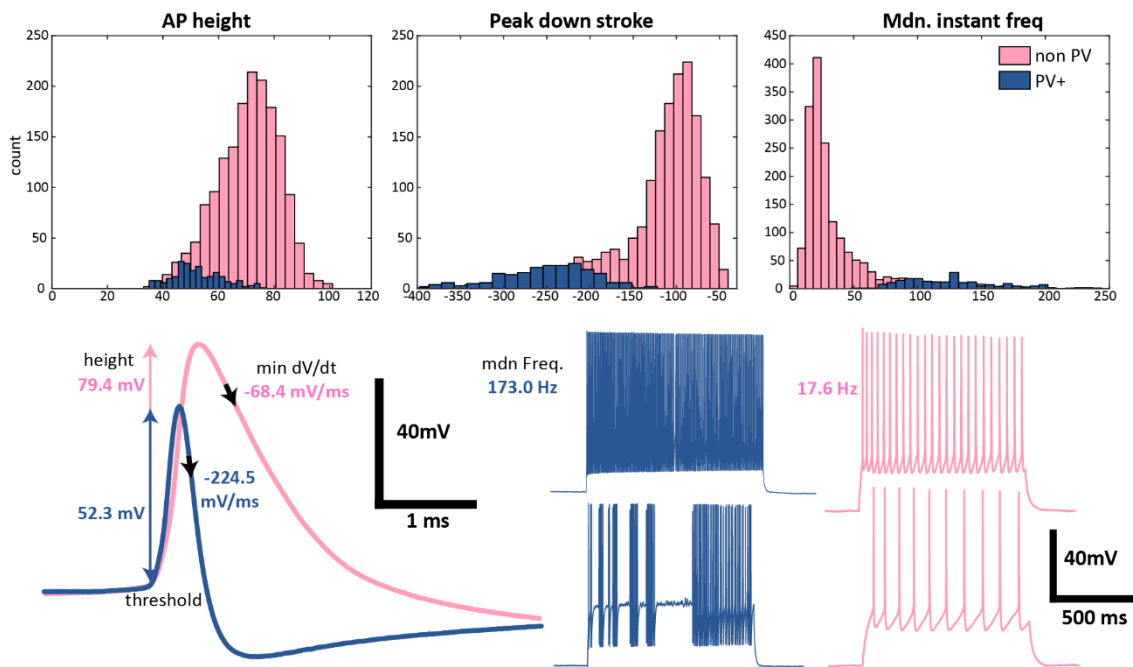


**Figure 12: Suprathreshold parameters used to classify FS cells.**

A. Comparison of distributions of AP height, peak down stroke and median instantaneous frequency (mdn instant freq) of parvalbumin positive cells (PV+) shown in blue, and cells from different transgenic lines (non PV) shown in pink. B. Spike train examples from a PV+ and a non PV cells. Even though both cells have a high maximum firing rate the mdn instant freq shows big differences between the cells. C. Higher magnification from a single action potential shows evident differences between PV+ and non PV neurons. The PV+ FS cell shows the characteristically short (smaller height) and thin AP (faster repolarization [peak down

#### 4.2.2. Normalization of the across species

All parameter values used for training and testing the classifier were normalized for each specie. In order to ensure a similar dispersion in the parameter space, the distribution of values were trimmed at different percentiles depending on the sample size. The mouse data set, being the largest with  $n = 1895$  (after QC), was trimmed at the 0.001 and 0.999 percentile, whereas percentile borders were narrowed with decrease in sample size (human: 0.005/0.995 percentile,  $n= 399$ ; NHP: 0.02/ 0.98 percentile,  $n= 105$ ). Normalization was performed using the following formula:

$$X' = \frac{X - X_{p1}}{X_{p2} - X_{p1}}$$

#### 4.2.3. Training and testing samples

As ground truth we used a stratified data set of mouse transgenic lines for PV, SST, Htr3a and Exc cell types; The four non overlapping cells populations in the cortex. These four groups cover the entire spectrum of the known cell type diversity in the visual cortex (9). For the PV group ( $n= 216$ ), we used all FS PV-Cre reporter positive cells. In order to take into account rarer variants of PV positive cells we also included all other reporter positive cells from lines utilizing some form of PV-promoter driven recombination (with the

exception of Htr3a-Cre|Pvalb-T2A-Dre). The SST (n=121) and Htr3a (n= 142) subpopulations were obtained from the Sst-IRES-Cre and Htr3a-Cre\_NO152 reporter positive cells respectively. The Exc were all spiny neurons that did not belong to any transgenic line that contained interneurons.

The training and testing samples were created using the previously described cell types groups. For the training set, an equal number of cells were randomly taken from each cell type (85 cells per cell type, determined from the 70% of the smallest group (SST)). In the testing set, the cell type proportions were determined using an additional factor accounting for the biases in sampling of the patch clamp method in primates (priority to non-pyramidal cells, bias towards cells with big soma, etc.). The testing sample size was 144 cells. The cell type proportions within each group is 15% PV, 12% SST, 8% 5-Htr3a and 65% Exc. These proportions are derived from empirical histological data. The testing set was always formed from cells out of the training set.

- Cross-validation and classifier selection

In order to calculate the global performance of the classifier we run a cross-validation test. In this test the model was trained and tested a specified number of times (1000 times). The resulting correct rate average is 0.96, with a mean sensitivity of 89% and specificity of 97%. The model from the cross-validation test with the closest correct rate to the mean was chosen as the predictive model for FS neurons in primates. This model had a correct rate of 0.96, with a sensitivity of 91% and specificity of 97%.

#### **4.2.3. Classifier performance in various cell type-specific reporter lines**

To better understand the performance of our model and find out which transgenic lines could be the most likely contaminants of our putative FS (pFS) sample, we applied our model to the total mouse population (n= 1895). (See **Figure 13. A**) 14.7% (280 cells) of the cells with reporter status for transgenic lines were classified as pFS neurons. This proportion was bigger than the amount of cells from the *PV-Cre* line (11.5 %, 218 cells) in the mouse dataset; in addition, 7% (18 cells) of the mouse cells known to be from the *PV - Cre* line were not classify as pFS cells by the model. The dendritic type of the pFS cells were mostly aspiny (98.7%), 1% were sparsely spiny and only 0.3% spiny. The pFS cells

were located with the higher proportion in L5, followed by L4, L3 and L6a. These distribution are very similar to observed in the ground truth PV-Cre cells. Comparison of dendritic type and layer distribution between PV-cre and pFS cells can be seen **Figure 13 B and C**. The described results point out to a inclusion of transgenic lines different to PV-Cre in the pFS group. (**Figure 13 B**) However, we observed that most of the included transgenic lines highly mark FS interneurons. This is the case of Chandelier lines such as *Pvalb -FlpO / Vipr2 -Cre*, *Pvalb -CreERT2*, *Slc32a1-FlpO/Vipr2-Cre* and *Nkx2-1-CreERT2*, which represent the 8.2% of the pFS group; transgenic lines with dual recombination with *Pvalb-Dre* (PV promoter) comprise 5% of the pFS cells. Positive cells for *Gad2-Cre* 2.5%, a pan-interneuron line that beside other interneurons could also contains FS cells; *Vipr2-Cre* (1%) and *Chrna2-Cre* (0.7%) which are lines that mark FS cells beside some other excitatory neurons. The majority of the pFS cells belong to the PV-cre line (70.7%). (See **Figure 14**)

The reporter lines in the pFS group with less likelihood to contain FS cells are *Chat-Cre* (0.7%, 2 cells), *Vip-Cre* (0.7%, 2 cells), *Nxtr-Cre* (1.4%), *Htr3a-Cre* (4.3%, 125 cells) and *Sst-Cre* (4.6 %, 13 cells), and lines with only one cell in the pFS group: *Nr5a1-Cre*, *Cux-CreERT2*, *Ndnf-dgCre*. However, Htr3a and especially SST off-target recombination in FS neurons have been reported to occur in 6 to 10% of the cases (Hang Hu, Cavendish, and Agmon 2013).

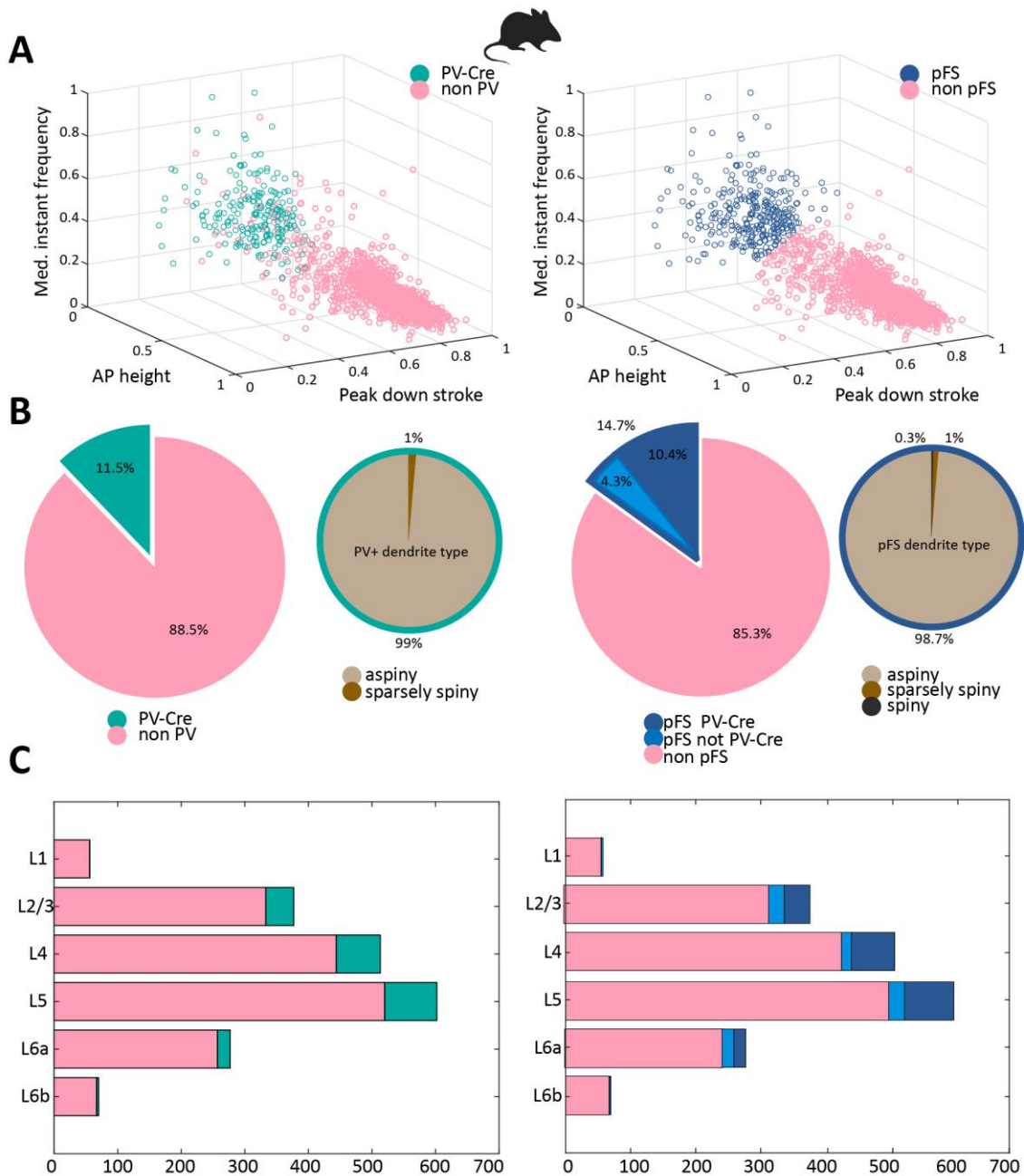


**Figure 13: Comparison between PV+ and pFS cells in the mouse database. A.** Shows the total population of mouse cells clustered according to the median instantaneous frequency (Mdn instant freq), action potential (AP) height and peak down stroke. On the left the PV+ cells (green) and on the right the pFS cells (blue) are assorted from the rest of the cells. Note that both PV+ and pFS cells have smaller AP height amplitude, faster repolarization (low peak down stroke), and higher mdn instant freq. Some non PV cells were identified as pFS neurons by the classifier; keep in mind that other transgenic lines different to PV-cre line also contain FS cells in our database. **B.** Prevalence comparison of PV+ (11.5%) and pFS (14.7%) cells in the mouse database (bigger pie charts), and dendritic type of each group. C. Comparison of distribution across layers of PV+ and pFS cells.

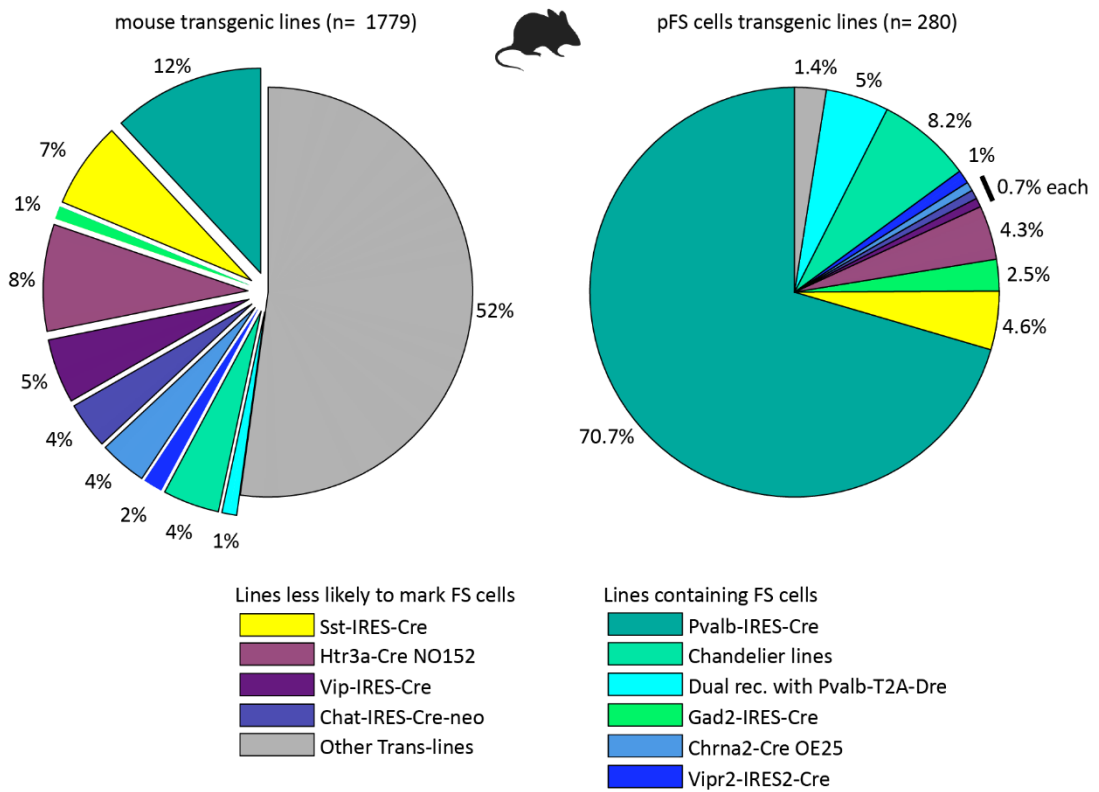


**Figure 14: Prevalence of various transgenic reporter lines in the total mouse dataset and their contribution to the pFS population.**

The right pie chart shows the prevalence of transgenic lines that contributed to the putative FS population in the mouse (n= 280). On the left the prevalence of these same reporter lines are shown in the total mouse population (n= 1779). Observe that lines containing FS PV+ cells increase their proportion considerably in the pFS group (see for example Gad2 and chandelier lines) . Every transgenic line is shown in a different color, and they are listed in groups: lines that contain FS cells and lines that are less likely to mark FS neurons.

In order to better understand the extent of off target expression from the unexpected transgenic lines in the pFS group, we qualitatively compared *Sst-IRES-Cre* , *Htr3a-Cre\_NO152* and *Chat-IRES-Cre-neo* cells to PV-cre neurons and divided them in two different groups. Cells with electrophysiological recordings indistinguishable from FS neurons and cells with at least one ambiguous feature. FS PV-Cre neurons in our mouse database have the classic FS electrophysiological phenotype with a short AP amplitude, low input resistance, fast after hyperpolarization and very little to no adaptation. **Figure 15** shows example traces from Basket (BC) and Chandelier (ChC) cells with positive reporter status for the PV-IRES-cre line. BCs show a dendritic spread more densely near the soma and an axon that extends horizontally (Cells 1, 2 and 3), the ChC instead show the characteristic candlestick-like synaptic terminals of the axon (Cell 4). Observe that even though BC and ChC are morphologically identified as different cell types, the electrophysiological traces are indistinguishable from each other. Three different firing patterns were observed in the PV-Cre neurons. Cells that evoke a single, duplet or triplet action potential at the rheobase current injection, followed by a stuttering firing pattern that at stronger stimulations elicits fast and sustained firing that reaches rates above 200Hz (see **Figure 15 cell 1**). Other cells do not show the stuttering phase and directly respond by a continuous spike train with evenly distributed ISIs (see **Figure 15 cell 2 and 4**). A third group of cells does not have the sustained firing mentioned above and the continuous firing stops abruptly during the stimulus and is preceded by a long delay (see **Figure 15 cell 3**).



When comparing PV-Cre cells with the unexpected reporter lines in the pFS group we find that 69.6% of Sst-IRES-Cre, 41.7% Htr3a-Cre\_NO152 and 100% of Chat-IRES-Cre-neo have indistinguishable recordings to the FS PV-Cre neurons (See **Figure 16**). Given the distinctiveness of the FS phenotype, accurate qualitative classification of 5-HTR3a cells, which do not show intrinsic biophysical properties resembling the PV cells (see introduction), can be done with high confidence and accuracy. On the other hand, SST cells, can show a phenotype that approximates the FS phenotype (also known as quasi fast spiking). Hence, classification was done in a very conservative manner: cells, which showed any feature that raise doubt on the veracity of the classification (spike adaptation, multicomponent afterhyperpolarizations, etc.) were disregarded.

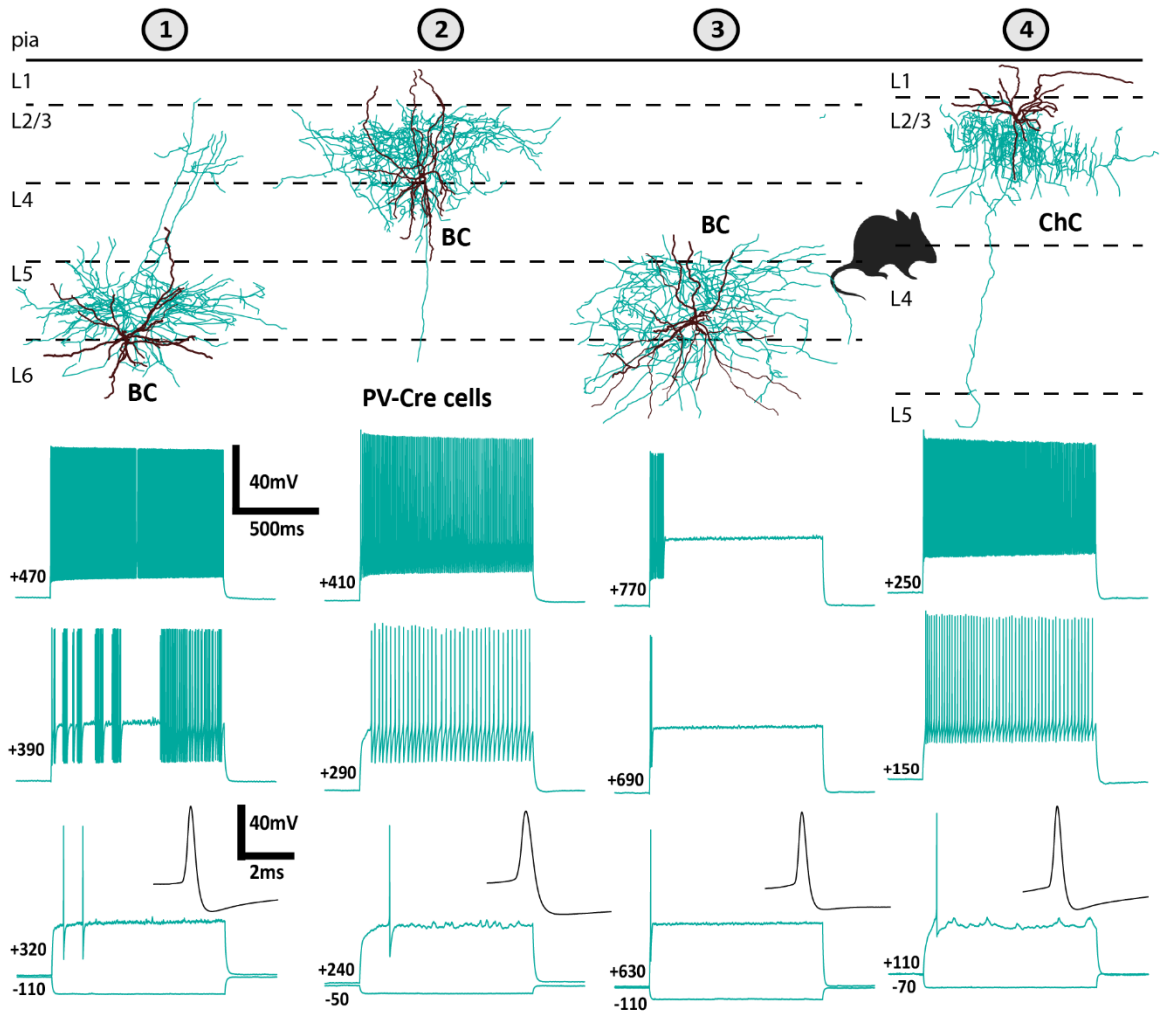
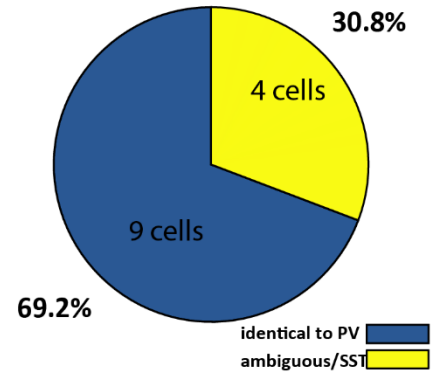
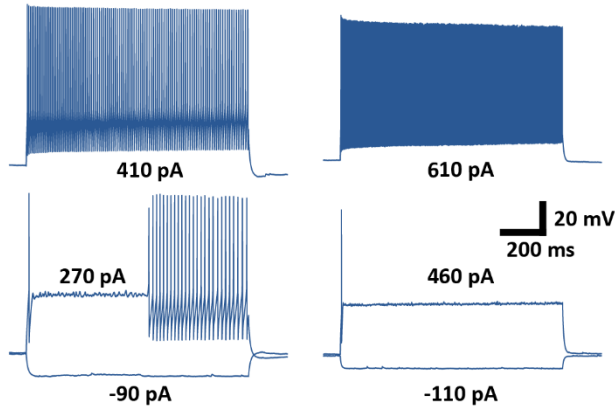


**Figure 15: Intrinsic properties of PV+ cells in the mouse database.**

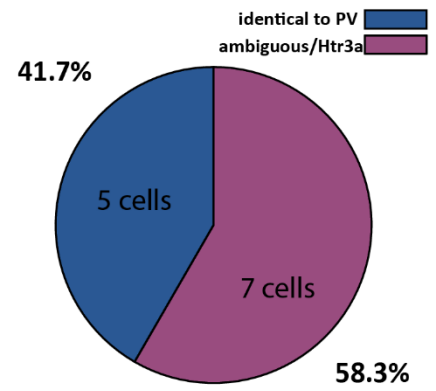
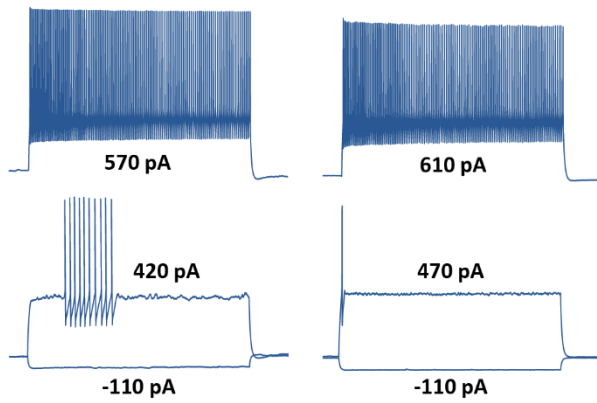
Recording traces exemplifying the PV-cre positive (PV+) cells from the mouse dataset. Cells 1, 2 and 3 are morphologically characterized basket cells (BC), while cell 4 shows the distinct chandelier like axonic arborization (ChC). Despite being morphologically distinct cell types, BCs and ChC show similar electrophysiological features.

In summary, our model correctly classified 92% of reporter positive neurons of the PV-IRES-cre line. However, cells targeted by other transgenic lines are also classified as pFS neurons. Most of these cells belong to transgenic lines that can contain FS PV-positive neurons and therefore do not cast doubt on an accurate classification. That being said, there are several lines which are not suspected to contain the cell type of interest and at first seem to be a serious source of contamination. In particular SST-IRES-Cre and 5-Htr3a-Cre, which are thought to be complementary populations, comprise together almost 9 % of pFS cells. A closer examination on an individual cell level shows that substantial proportion of these cells (69.2% and 41.7% respectively) strongly suggest an off-target expression of the fluorescent reporter induced by the respective Cre lines as reported previously (Hang Hu, Cavendish, and Agmon 2013).

**pFS in SST-IRES-Cre**



**pFS in Htr3a-Cre NO152**



**pFS in Chat-IRES-Cre-neo**

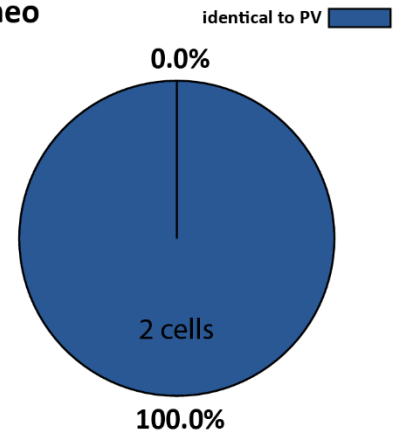
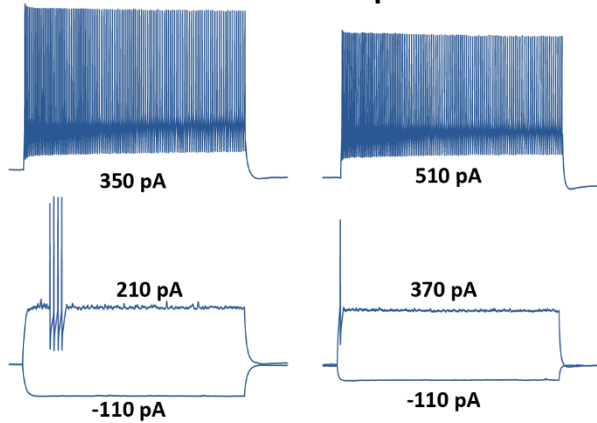


**Figure 16: Non-FS transgenic lines contain cells with a strong FS phenotype.** Example traces of cells from the SST-IRES-Cre, Htr3a-Cre NO152, and Chat-IRES-Cre-neo transgenic lines that were classified as putative FS neurons (pFS). Pie charts on the right show the amount of cells from each line that have undistinguishable electrophysiological properties to the ground truth PV-cre positive cells and therefore do not cast doubt on an accurate classification.

### 4.3. Description of putative cortical FS cells in primates

The previously described model developed from the mouse dataset, was then applied to the primates databases (which do not contain genetic markers) in order to isolate pFS neurons.

As a first step to verify the performance of the classifier when applied to primates we examined morphological features (dendritic type, layer localization, and cell morphology) as well as firing patterns of the resulting pFS cells. As expected, most pFS neurons in the human and NHP databases show an aspiny dendritic type, and were primarily located in L3-L5/6. More detailed information is described in the following sections.

#### 4.3.1. Dendritic type and layer distribution of human pFS cells

From the total human population (n= 393 cells), 11% of the cells (n= 42) were classified as pFS neurons. The dendritic type of 98% of the pFS neurons (41 cells) was aspiny, 1% (1 cell) spiny and no sparsely spiny cells were found. Most pFS neurons are located in L3 (69%, 28 cells) followed by L4 (16.6%, 7 cells) and L5/6 (14.3%, 6 cells). No cells were found in layer 1 which is a good sign for our classifier since FS cells have not been previously described in this layer (See **Figure 17**) (Hestrin and Armstrong 1996; Karube, Kubota, and Kawaguchi 2004).

### 4.3.2. Dendritic type and layer distribution of NHP pFS cells

In the NHP database (n=105 cells), 31% of the cells (n=33) were classified as pFS neurons. This prevalence was almost 3 times higher than the observed in human. All pFS with successful filling for dendritic type and layer localization (n= 6) have an aspiny dendritic type. Most of them were located in L3 (2 cells) an L5/6 (2 cells), followed by L2 (1 cell) and L4 (1 cell). No cells were found in L1 (See **Figure 17**).

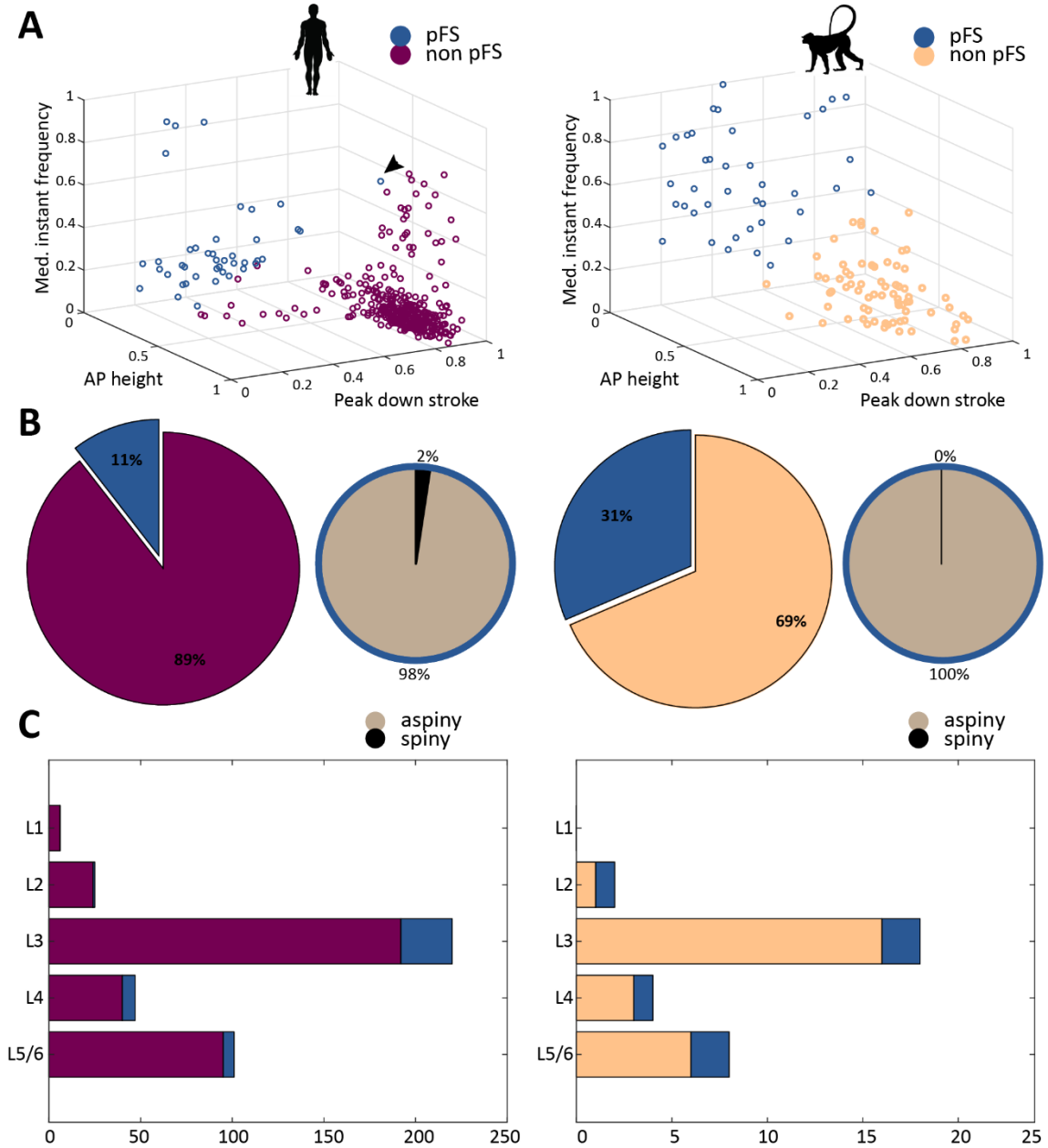


**Figure 17: Classification of pFS primate neurons.**

**A.** 3D scatter plots of normalized predictor variables: Cells classified as pFS are indicated in dark blue. Human data show a concentration of excitatory cells with high APs and lower peak down stroke (close to 1 due to negative sign). The cluster of pFS is strongly segregated, with wider average distances between them. Notably, one pFS (indicated by an arrow head) appears to be closer to the non pFS cluster. In NHP the transition between pFS and non pFS is more fluid. **B.** Incidence of pFS and their respective dendrite types: 11% of human cells are classified as pFS. One cell of these (2% of pFS) has a spiny dendrite. It is the same cell that is marked in subfigure panel A and is the only clear case of a false classification. In NHP the fraction of non pFS cells is with 31% almost 3 times higher. None of these cells show spiny dendrites. **C.** Laminar distribution of pFS cells: In human pFS cells are particularly prevalent in L3 and L4. L1 and L2 are completely devoid of pFS cells. In NHP, on the other hand, no L1 cells have been recorded from and L2 show a high fraction of pFS. However, due to low absolute cell numbers, fractions should be interpreted with caution

#### **4.3.3. Communalities and differences in firing pattern and morphological phenotype**

The human and NHP pFS cells show firing rates that generally go in line with the FS phenotype previously described from mouse (described in section 4.2.3). The pFS neurons in most cases start with continuous spiking at the rheobase, comparable to the activity observed with further current stimulation in mouse. Occasionally, a single action potential is elicited at the rheobase level, but stuttering and bursting firing are also observed. Besides this, some particularities were found in primates. Cells with continuous firing show high frequency firing rates, but do not reach the same frequency levels known from mouse. NHP pFS cells show higher prevalence of rebound spikes in response to a moderate to strong hyperpolarization current injections but this was not observed in non pFS cells. Human instead, show rebound spikes in the non pFS neurons but not in the pFS. Stronger spike adaptation was also observed in human. Prominent difference was observed in the rheobase level which in NHP was lower; around 30-150 pA while in mouse and human is mostly

>100pA and up to 300pA in human and 600pA in mouse. The AP waveform of pFS neurons were characterized by a short height and narrow width when comparing to non pFS cells. However, between primates, NHP cells show wider spikes. Human cells with a fast spiking and bursting firing pattern show an additional hump depolarization at the pre-rheobase level. This hump occurs at the beginning of the stimulus and is followed by a complete lack of APs. In NHP spotting the same hump is difficult due to the low rheobase, high input resistance and the increment of the current stimulation, but they seem similar to what can be observed in human. In comparison to mouse cells, primates also have a more remarkable sag at the hyperpolarizing current steps (See **Figure 18 and 19**).

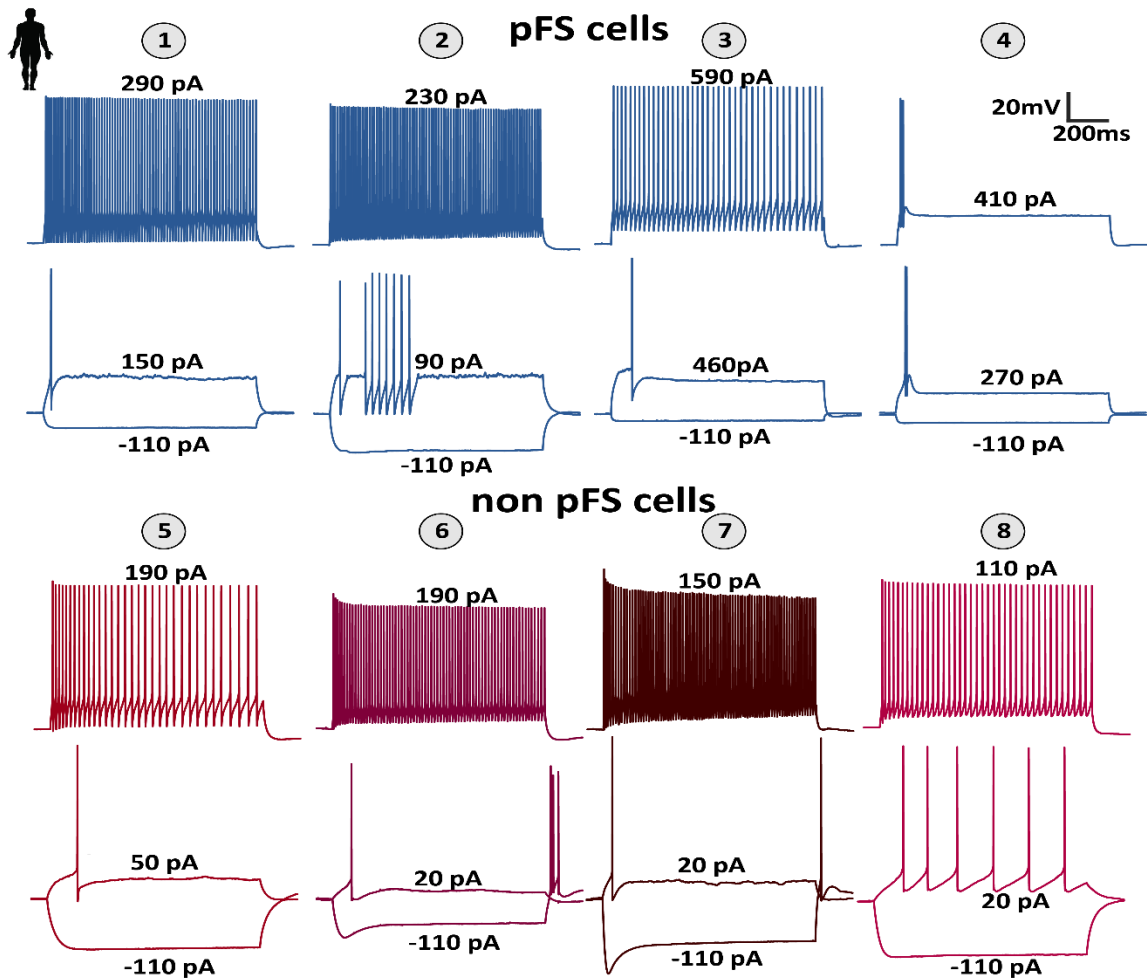


**Figure 18: Intrinsic biophysical properties of human cells.** Example traces from putative fast spiking (pFS) neurons (traces 1-4, shown in dark blue) and non-putative fast spiking (non pFS) cells (traces 5-8, shown in different shades of red) from human. Recordings of pFS cells are generally in line with the FS phenotype, but show a novel variations in their firing pattern: cell 4, for example, shows a mixture of fast spiking and bursting signified by an additional hump depolarization at the beginning of the current injection followed by a complete lack of APs. They show stronger spike adaptation (See cell 1) than mouse PV+ cells. The non pFS cells instead, have hallmarks of other known cell types in particular regular spiking (see cell 8). In addition, occasionally non pFS interneurons show rebound spiking (cell 6 and 7) which is not observed in pFS neurons.

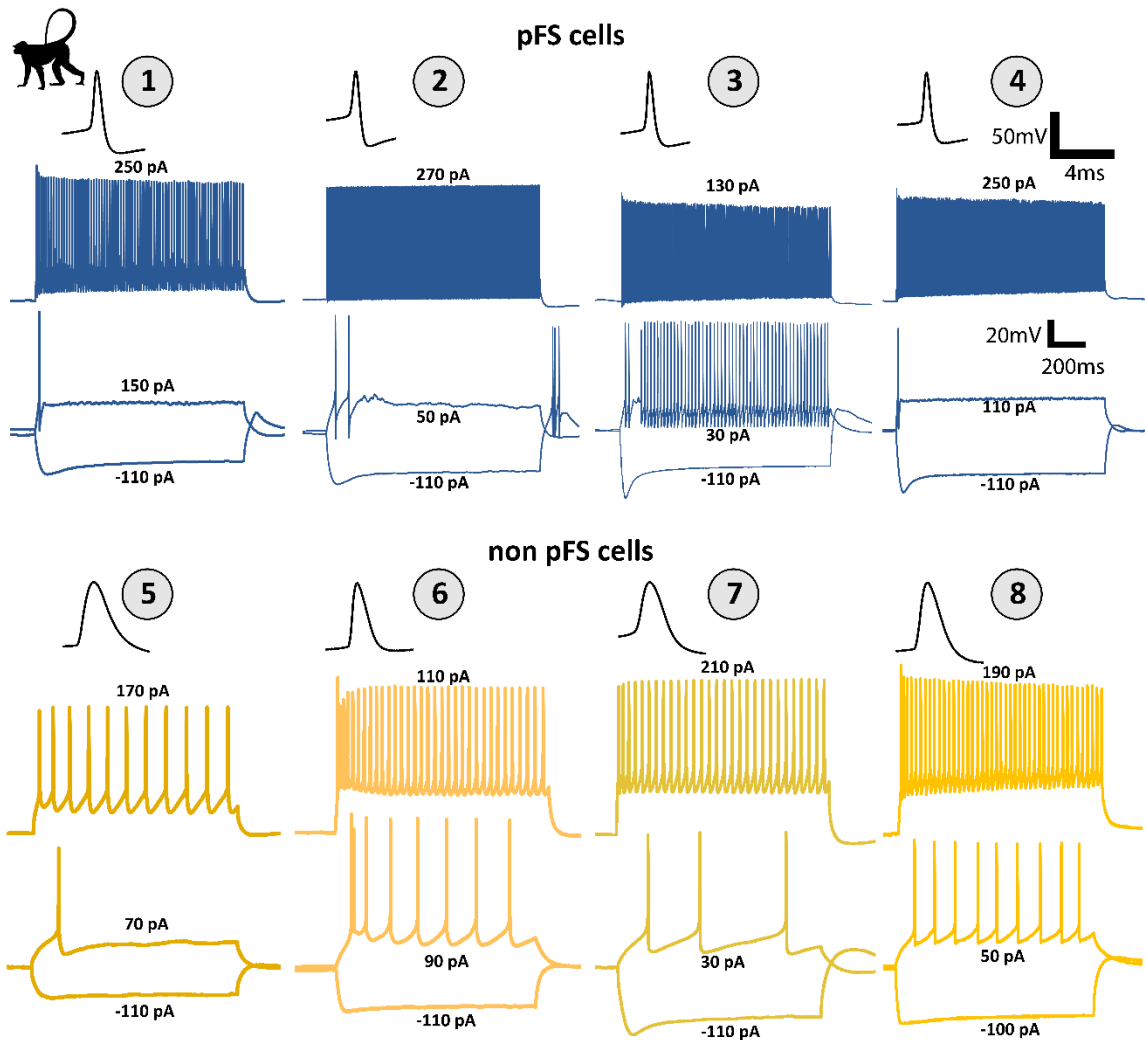




**Figure 18: Intrinsic biophysical properties of NHP cells.**

Example traces from putative fast spiking (pFS) neurons (traces 1-4, shown in dark blue) and non-putative fast spiking (non pFS) cells (traces 5-8, shown in different shades of yellow) from NHP. pFS cells show the characteristic high frequency firing observed in mouse FS PV cells. They have a shorter and narrower AP in comparison with non pFS neurons. Their rheobase can be quite low and is often not determined accurately due to the insufficiently narrow current steps (see cell 3). Some pFS cells have rebound spiking at high to moderate hyperpolarization (as seen in cell 2), but this is not observed in non pFS neurons. pFS cells also have bigger sag in comparison to non pFS cells. The non pFS cells have many different firing patterns but not FS, cell 1 and 8 are examples of regular spiking cells, and cells 6 and 8 show bursting at higher stimulation.

Morphological comparison between human pFS and non pFS cells showed interesting results: Most pFS cells show the typical basket cell morphology with the abundant perisomatic axonal branching (See **Figure 20. Cells 1-4**). In contrast, non pFS neurons, were mostly pyramidal cells (**Figure 20. Cells 8**), although other interneurons (aspiny, sparsely spiny cells) were also found. They show less axonal length, some layer 1 neurons and cells with a bitufted morphology that consist of a stronger vertical orientation spreading up to L1 were found in this class (**Figure 20. Cells 5-7**). No morphological reconstructions were available from NHP pFS. However, non pFS cells show different phenotypes. Some cells were clearly pyramidal (See **Figure 21. Cell 5**), while some others were more difficult to categorized (**Figure 21. Cell 1 and 3**). Vertical oriented cells were also found (**Figure 21. Cell 2 and 4**).

In summary primate pFS cells have electrophysiological features that agree with the FS phenotype previously observed in our mouse PV+ cells. In agreement with this, most human pFS cells have the characteristic BC like morphology. However, some electrophysiological particularities are also observed in primates and could be a result of physiological or stimulation differences across species.

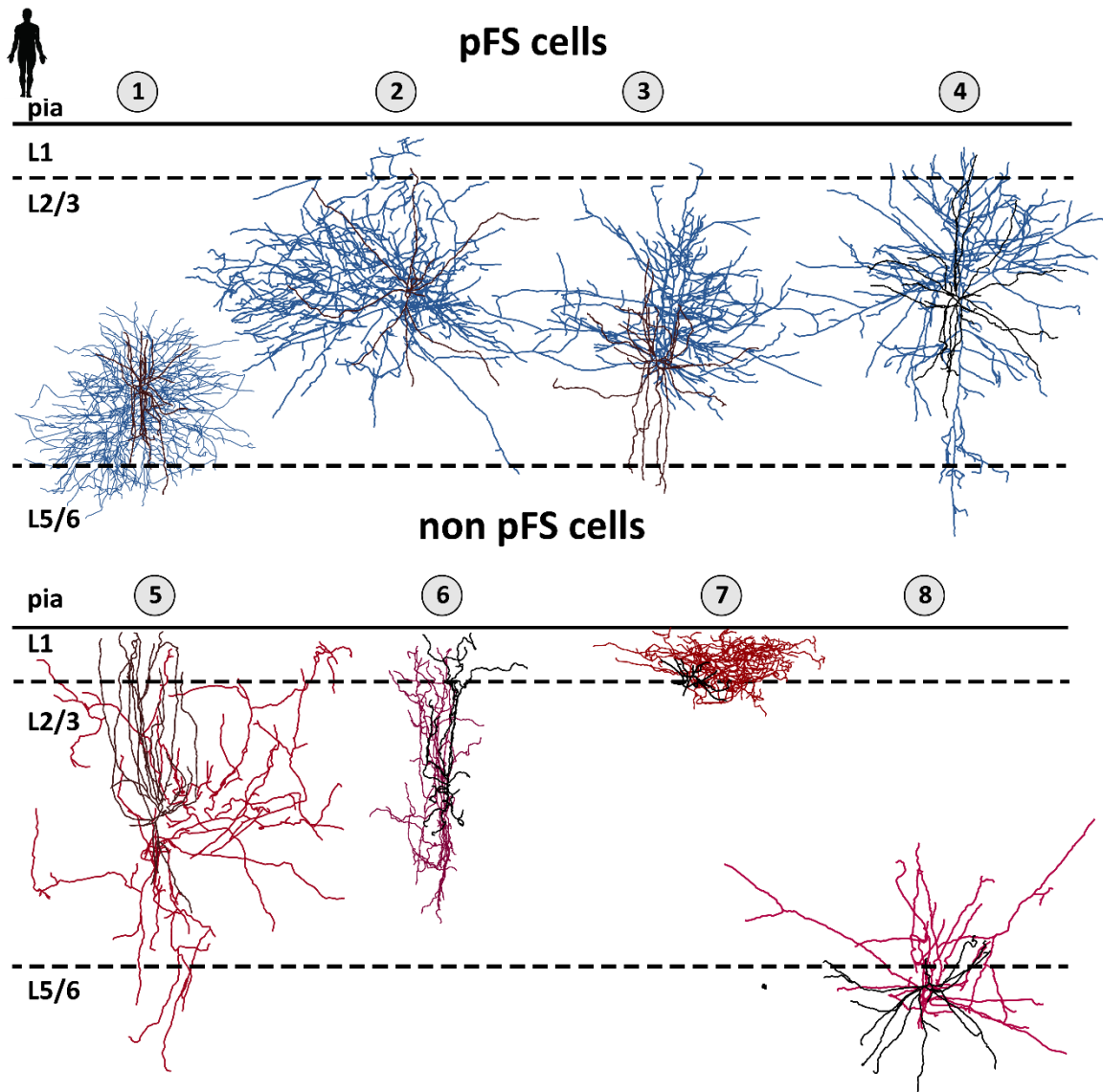


**Figure 20. Morphological characterization of human cells.** Three dimensional reconstructions of putative fast spiking neurons (pFS) are shown at the upper part of the figure (cells 1-4) and non-putative fast spiking (non pFS) cells are showed at the bottom (cells 5-8). The dendritic tree is shown in black, while the axon is shown in blue for the pFS neurons and in red for the non pFS cells. Note that pFS cells show the typical basket cell morphology with the abundant perisomatic axonal branching (cells 1 to 4), whereas non pFS class contains a diverse set of morphologies. The show less axonic length and show a higher proportion of cells that can be described as bitufted (Cell 5 and 6), Cell 7 has the typical morphology of a L1 cell and L8 is a pyramidal cell (cut apical dendrite).

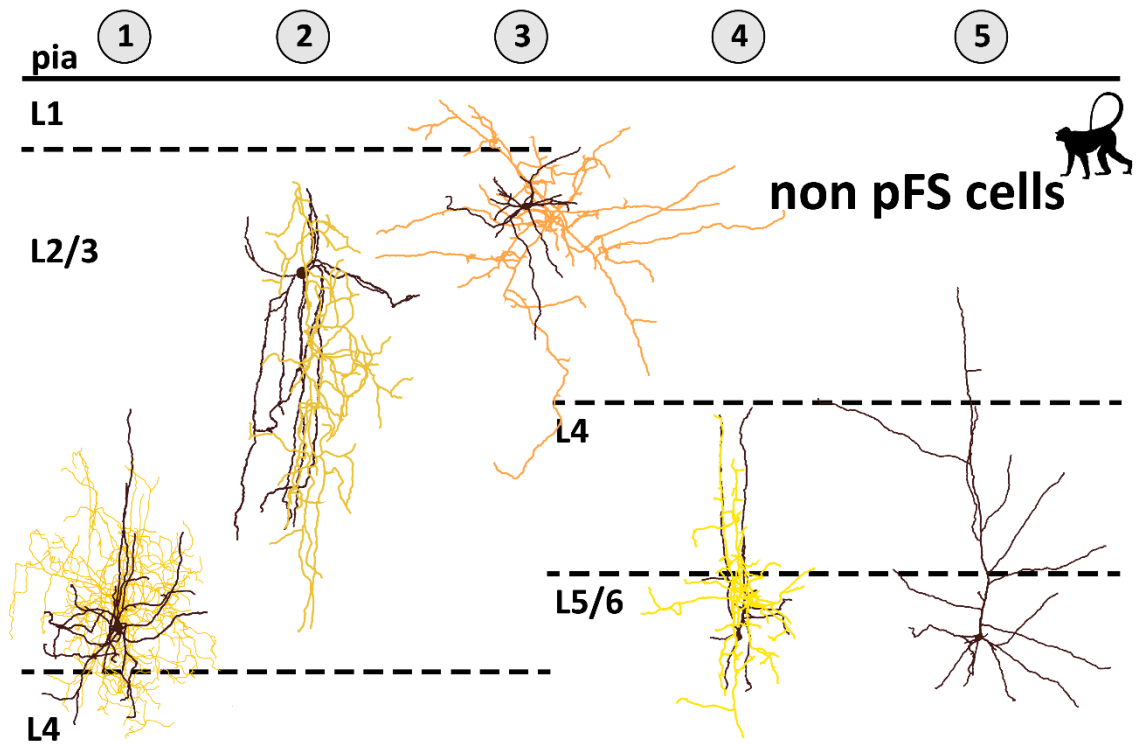


**Figure 21. Morphological characterization of NHP cells.** Three dimensional reconstructions of non-putative fast spiking (non pFS) cells. The dendritic tree is shown in black, while the axon is shown in yellow. NHP non pFS cells contains a diverse set of morphologies. Cell 5, is an example of a pyramidal cell (No axon reconstructed), and some vertical oriented cells can be observed (Cells 2 and 4).

#### 4.4. Comparing FS subthreshold properties across species

Our model shows to successfully isolate pFS neurons in primates and therefore we proceed to compare subthreshold features of pFS neurons across species (These analysed electrophysiological properties are independent from the features used to build the classifier).

##### 4.4.1. Descriptive statistics of subthreshold properties of FS cells

Comparisons between mouse PV+ neurons and primate pFS cells revealed differences across species. All subthreshold parameters (with the exception of rheobase), show

substantially higher values in NHP and smallest in mouse cells. Subthreshold parameters from human are persistently between these two groups. The rheobase instead has a similar pattern but in the opposite direction. Even though strong disparities in the values are observed across species not all parameters had significant differences. The descriptive statistics and p values for each subthreshold parameter are described below (See **Figure 22** and **Table 4.1**):

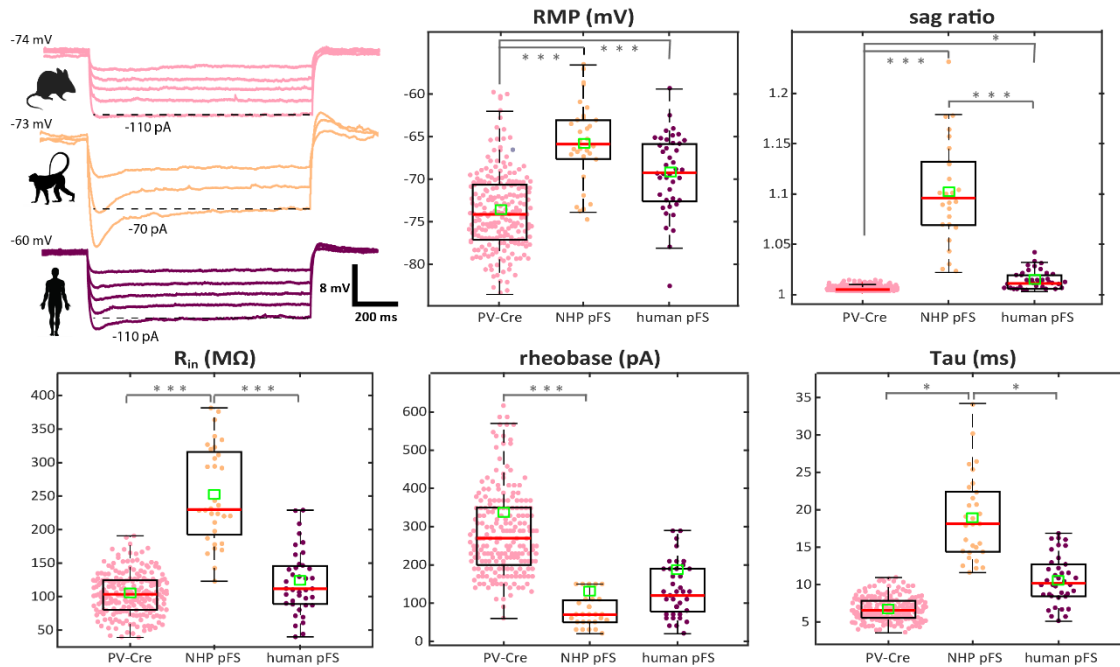


**Figure 22: Subthreshold properties of PV+ and pFS neurons across species.** Example traces and box plots of mouse PV-Cre and pFS neurons from primates comparing subthreshold intrinsic properties across species. The NHP stands out in almost all subthreshold properties having the highest values with exception of the rheobase, while mouse are smallest. Human values are intermediate to these other groups. As can be observed from the example traces, the most predominant differences between NHP and other species is the bigger sag, higher input resistance and higher time constant (Tau), these can be observe in the example traces. On the box plots the mean and median of the distributions are shown with a red line and a green square respectively. \*/\*\*/\*\* show significant differences between groups at different levels (p<0.05/0.01/0.001, respectively).

- Resting membrane potential

Primates show a more depolarized resting membrane potential in comparison to mice (mouse,  $-73.9 \pm 4.6$  mV; human,  $-69.6 \pm 4.7$  mV; NHP,  $-64 \pm 4.7$  mV; mean  $\pm$  S.D.). Significant differences are found between mouse and primates but not within primates ( $p < 0.001$ , Tukey's test).

- Input resistance

Regarding the input resistance, the NHP stands out among other species with values almost twice that observed in the human and more than twice that from the mouse (mouse,  $109.7 \pm 35.5$  M $\Omega$ ; human,  $137.7 \pm 68.9$  M $\Omega$ ; NHP,  $262.5 \pm 86.1$  M $\Omega$ ; mean  $\pm$  S.D.). Significant differences are observed between NHP and the other species ( $p < 0.001$ , Tukey's test).

- Time constant

The NHP shows substantially higher values of Tau followed by human, and mouse with the lower values (mouse,  $6.8 \pm 1.7$  ms; human,  $11.7 \pm 5.4$  ms; NHP,  $20.5 \pm 8.4$  ms; mean  $\pm$  S.D.). Significant differences are observed between NHP and the other two species ( $< 0.05$ , Tukey's test).

- Sag ratio

The sag ratio is the subthreshold parameters with the biggest discrepancies among species. NHP sag ratios are much higher in comparison to human and mouse, however human was also higher than mouse in which almost no sag was observed (mouse,  $1.006 \pm 0.004$ ; human,  $1.019 \pm 0.019$ ; NHP,  $1.102 \pm 0.052$ ; mean  $\pm$  S.D.). Significant differences are found between NHP and other species ( $< 0.001$ , Tukey's test), and between mouse and human ( $< 0.05$ , Tukey's test).

- Rheobase

Mouse FS cells show higher rheobase values, whereas primate cells have the lowest (mouse,  $293.8 \pm 126.7$  pA; human,  $140.7 \pm 85.2$  pA; NHP,  $88.2 \pm 50.4$  pA; mean  $\pm$  S.D.). A significant difference was only observed between mouse and NHP.

**Table 3. Subthreshold properties of FS cells across species**

	Mouse	NHP	human
	<b>PV</b>	<b>pFS</b>	<b>pFS</b>
	<b>(n=218)</b>	<b>(n=33)</b>	<b>(n=42)</b>
<b>RMP</b>	-73.9±4.6	-64±4.7	-69.6±4.7
<b>Sag ratio</b>	1.006±0.004	1.102±0.052	1.019±0.019
<b>R<sub>in</sub></b>	109.7±35.5	262.5±86.1	137.7±68.9
<b>Rheobase</b>	293.8±126.7	88.2±50.4	140.7±85.2
<b>Tau</b>	6.8±1.7	20.5±8.4	11.7±5.4

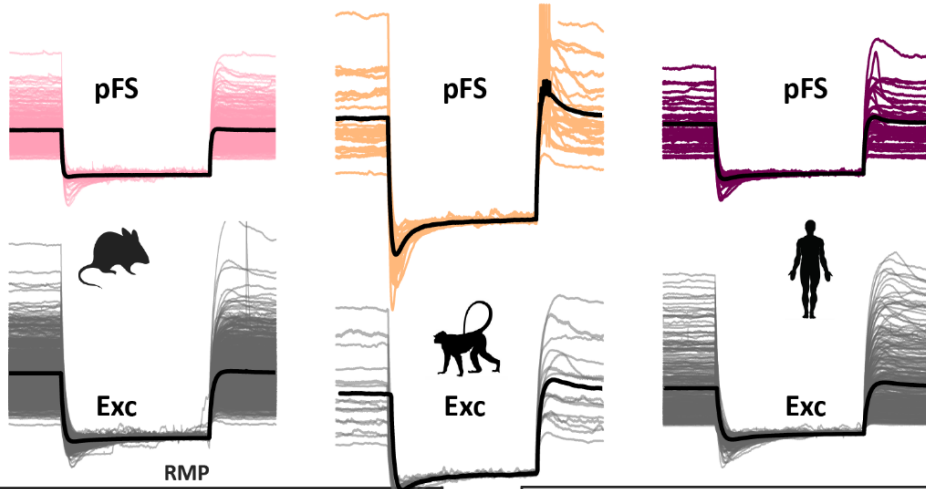
Mean and standard deviation of subthreshold parameters of PV-Cre and pFS cells across species. Abbreviation: RMP, resting membrane potential; R<sub>in</sub>, input resistance; Tau, time constant.

In summary, neurons from different primate species show similar tendencies compared to the mouse. The more depolarized resting membrane potential, stronger effect on the membrane voltage by current stimulus, and lower rheobase level demonstrate higher excitability of the primate cells. Bigger sag and higher time constant were also observed. Surprisingly, the hypothesized pattern of mouse<NHP<human did not manifest due to high NHP values.

#### **4.5. Revealing cell type and species dependent effects by comparing FS with excitatory cells**

In order to better understand if the pattern observed in FS interneurons across species are cell type specific features or if they are dependent on unique properties of each species we performed a two-way ANOVA with factors cell type and species. Interestingly, almost all subthreshold parameters show a significant modulation by both cell type and species with exception of R<sub>in</sub> which is only modulated by species. Furthermore, the two factors have a very consistent interaction effect across all subthreshold features (See **Table 4, Figure 23**). Descriptive statistics and significant findings are described below:

A



B

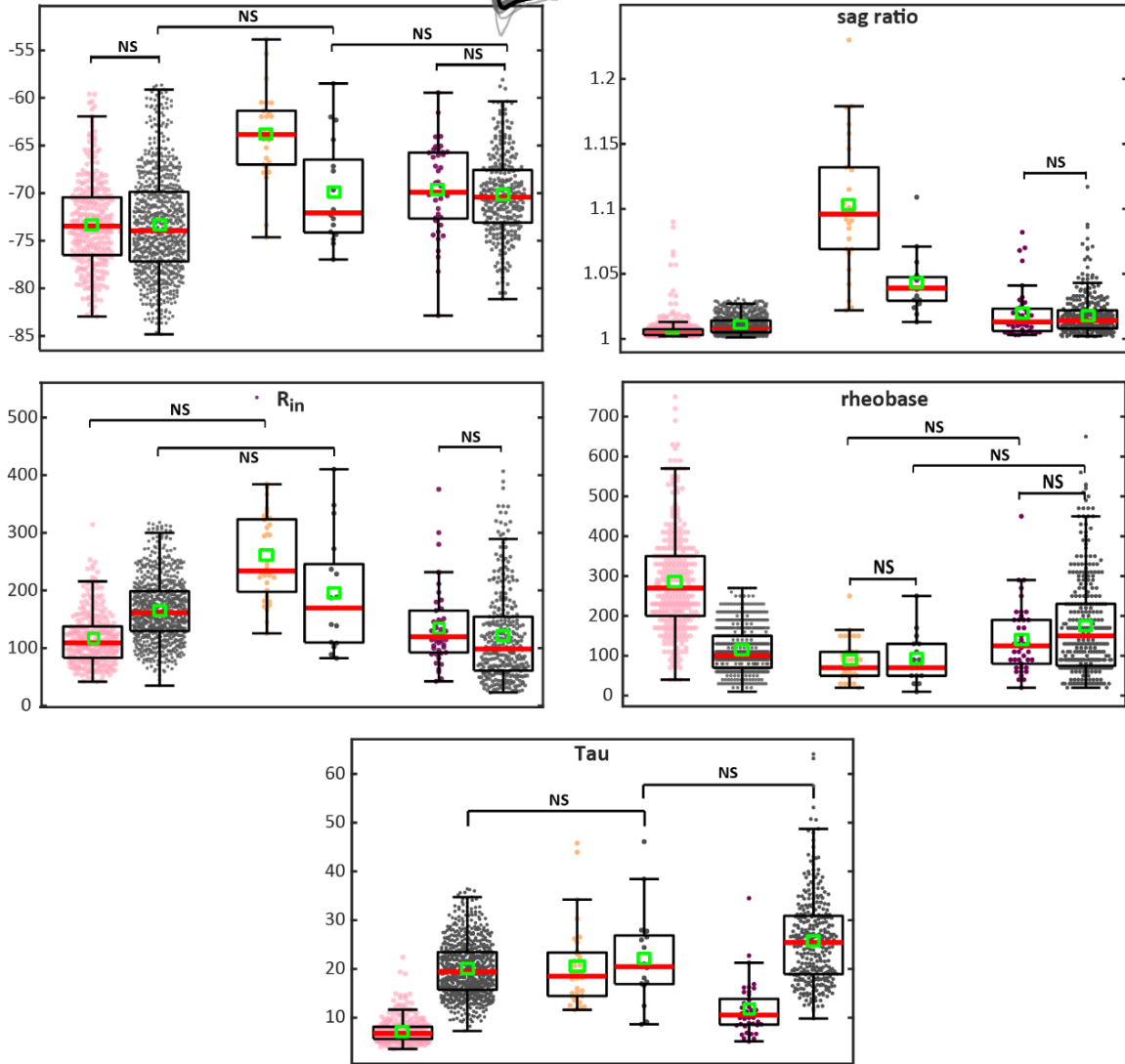


**Figure 23: Comparison of subthreshold properties of FS and Exc cells across species.**

Comparison of subthreshold intrinsic properties of FS and Exc neurons across species. A. Overlapped traces from putative fast spiking cells (pFS) and excitatory cells (Exc) from different species. B. The mean and median of the distributions are shown with a red line and a green square respectively. Traces on top show all available responses to the current stimulations that were used to determine the sag ratio according to cell type (top row: pFS, bottom row: Exc) and species (columns from left to right: mouse, NHP, human). All features show a significant interaction effect, which is the most salient in case of Vest, time constant and sag ratio when comparing differences between cell types in NHP vs the other two. Whereas input resistance and rheobase show the highest differences between cell types in mouse, but not in the other species. Groups with no significant differences are shown as “NS” ( $p > 0.05$ ), all remaining groups show significant differences with each other ( $p < 0.05$  /  $< 0.01$  /  $< 0.001$ ).

- Resting membrane potential

In the mouse, RMPs show little difference between FS PV-Cre ( $-73.9 \pm 4.6$ ) and Exc cells ( $-73.3 \pm 5.4$ ), while in primates this difference increases with more depolarized values in the pFS cells, especially in NHPs. The mean and standard deviation of the RMP in pFS cells from humans is  $-69.6 \pm 4.7$  mV and for Exc cells  $-70.2 \pm 4.3$  mV. In NHP pFS cells have a mean RMP of  $-64 \pm 4.7$  mV while for the Exc cells is  $-70 \pm 5.4$  mV. The RMP show modulation by species and cell type, as well as interaction between them ( $p < 0.001$ ). However, only the cell type comparison within NHP is significant ( $p < 0.01$ , post-hoc test).

- Sag ratio

The sag ratio shows the biggest differences across species. In the NHP, a remarkable disparity is found, while in mouse and human, lesser differences are observed between FS and Exc cells (with the latter having the bigger sag). Furthermore, the relationship of the sag ratio with cell type inverts in the NHP with FS cells having a bigger sag. When



comparing across species, primate cells have generally more sag than mouse. There is a significant effect of both species and cell type, as well as interaction between them ( $p < 0.001$ ). The sag ratio mean and standard deviation in mouse PV-Cre cells is  $1.006 \pm 0.004$  and in Exc is  $1.010 \pm 0.007$ ; in NHP pFS cells is  $1.102 \pm 0.052$  and in Exc  $1.042 \pm 0.022$ ; in human pFS cells is  $1.019 \pm 0.019$  and in Exc is  $1.018 \pm 0.016$ . Significant differences are found across all groups ( $p < 0.001$ , post-hoc test) with the exception of human FS and Exc cells.

- Input resistance

$R_{in}$  values are generally higher in primates than in mouse. Moreover, the NHP distribution of values start at a higher level of the spectrum observed in human and mouse.  $R_{in}$  is significantly modulated by species but not cell type, nevertheless, there is a significant effect of the interaction between them ( $p < 0.001$ ). Mean and standard deviation in mouse PV-Cre cells are  $109.7 \pm 35.5 M\Omega$  and in Exc cells,  $166.2 \pm 61.5 M\Omega$ ; in human pFS cells,  $137.7 \pm 68.9 M\Omega$  and in human Exc cells,  $119.6 \pm 78.9 M\Omega$ ; in NHP pFS cells,  $262.5 \pm 86.1 M\Omega$  and in NHP Exc cells,  $195.1 \pm 97.6 M\Omega$ . Comparisons within the species show a very interesting pattern: first,  $R_{in}$  in pFS cells is significantly lower than in Exc cells in mouse ( $p < 0.001$ , post-hoc test),  $R_{in}$  is not dependent on the cell type in humans ( $p=1$ , post-hoc test), but significantly higher in pFS cells NHPs ( $p < 0.01$ , post-hoc test). Interestingly, Exc cells in humans have a significantly lower  $R_{in}$  compared to both species (mouse:  $p < 0.001$ , NHP:  $p < 0.001$ ). However, there is no significant difference between mouse and NHP Exc ( $p=0.75$ , post-hoc test).

- Rheobase

The rheobase in FS PV-Cre cells from mouse stands out completely, whereas differences between other groups are comparatively subtle. That being said, rheobase values for NHP cells are consistently lower than humans. The mean and standard deviation of PV-Cre cells from mouse is  $293.8 \pm 126.7 pA$ , and in Exc cells is  $112.0 \pm 52.3 pA$ ; in NHP the mean is  $88.2 \pm 50.4 pA$  in pFS cells and  $91.2 \pm 55.6 pA$  in the Exc cells; human pFS cells have a mean rheobase of  $140.7 \pm 85.2 pA$  and Exc cells,  $174.9 \pm 123.4 pA$ . Rheobase values show significant modulation by both species and cell type, as well as interaction between them ( $p < 0.001$ ). Except in the mouse ( $p < 0.001$ , post-hoc test), there were no significant

differences across cell types within species (human:  $p=0.29$ , NHP:  $p=1$ ). Considering the comparison between NHPs and humans within the same cell type, we find a significant effect in Exc ( $p < 0.001$ , post-hoc test), but not in pFS cells ( $p=0.16$ , post-hoc test; but note the small sample: 33 pFS, 17 Exc).

- Time constant

Differences in tau between FS and Exc cells in mice and humans are similarly large. In NHPs, this difference between groups seems reduced, but this could be due to the small number of Exc cells in the NHP sample. Mean and standard deviation of tau in mouse PV-Cre cells were  $6.8 \pm 1.7$ ms, in Exc  $20.0 \pm 5.6$ ms, in human pFS cells  $11.7 \pm 5.4$ ms and human Exc  $25.9 \pm 9.0$ ms; in NHP pFS cells,  $20.5 \pm 8.4$ ms and NHP Exc cells  $22.2 \pm 9.7$ ms. The time constant shows a significant modulation by both species and cell type, as well as an interaction between them ( $p < 0.001$ ). Within species, significant differences are observed between FS and Exc in mouse and human (both:  $p < 0.001$ , post-hoc test) but not in the NHP ( $p=1$ , post-hoc test). Across cell types all groups show significant differences in tau with the exception of Exc cells from mice and NHPs, and for the comparison between Exc cells from NHPs and humans.

**Table 4: Two-way ANOVA and descriptive statistics comparing FS and Exc cells across species.**

	Mean $\pm$ std						Two-way ANOVA		
	Mouse		NHP		human		Species	Cell type	Specie*cell type
	PV (n=218)	Exc cells (n=772)	pFS (n=33)	Exc cells (n=17)	pFS (n=42)	Exc cells (n=303)	p	p	p
<b>RMP</b>	-73.9 ( $\pm$ 4.6)	-73.3 ( $\pm$ 5.4)	-64.0 ( $\pm$ 4.7)	-70 ( $\pm$ 5.4)	-69.6 ( $\pm$ 4.7)	-70.2 ( $\pm$ 4.3)	8.1 e- 26***	8.3 e- 04***	1.5 e-04***
<b>Sag ratio</b>	1.006 ( $\pm$ 0.004)	1.010 ( $\pm$ 0.007)	1.102 ( $\pm$ 0.052)	1.042 ( $\pm$ 0.022)	1.019 ( $\pm$ 0.019)	1.018 ( $\pm$ 0.016)	8.0 e- 169***	5.1 e- 33***	2.2e-51***
<b>R<sub>in</sub></b>	109.7 ( $\pm$ 35.5)	166.2 ( $\pm$ 61.5)	262.5 ( $\pm$ 86.1)	195.1 ( $\pm$ 97.6)	137.7 ( $\pm$ 68.9)	119.6 ( $\pm$ 78.9)	2.0e-22***	0.1691	3.7 e-18***
<b>Rheobase</b>	293.8 ( $\pm$ 126.7)	112.0 ( $\pm$ 52.3)	88.2 ( $\pm$ 50.4)	91.2 ( $\pm$ 55.6)	140.7 ( $\pm$ 85.2)	174.9 ( $\pm$ 123.4)	6.1e-20***	3.4e- 06***	0.6e-43***
<b>Tau</b>	6.8 ( $\pm$ 1.7)	20.0 ( $\pm$ 5.6)	20.5 ( $\pm$ 8.4)	22.2 ( $\pm$ 9.7)	11.7 ( $\pm$ 5.4)	25.9 ( $\pm$ 9.0)	6.3e-30***	7.6e- 37***	1.7e-08***

\*\*\* Significant difference ( $p < 0.001$ ). Abbreviations, RMP, resting membrane potential;

R<sub>in</sub>, input resistance; Tau, time constant.

## 5. Discussion

### 5.1. Summary of results

To classify FS interneurons in primates we developed a model based on recordings from parvalbumin specific mouse lines. Our model, successfully classifies pFS neurons in primates. Ultimately, we compared the subthreshold intrinsic properties of FS cells across species. In order to understand if our observations were given by a cell type or species modulation, we performed a two way ANOVA. The following paragraphs summarize the most pertinent results.

We trained and validated a linear classifier to identify FS cells using the PV-Cre reporter line as ground truth label. To have a representative sample of the entire spectrum of non FS cells in a non-overlapping manner, we used the SST-Cre and 5-HTR3a-Cre line as well as spiny cells from all known excitatory reporter lines available to train the classifier. Applying the classifier to the mouse data showed mostly expected results. pFS cells can be predominantly found in lines known to include PV cells (but not necessarily in an exclusive manner, see **Figure 14**). Intriguingly, the classifier also shines light on known and unreported issues of off target expression in PV cells (see **Figure 16**) (Hang Hu, Cavendish, and Agmon 2013). Data used for training and testing future models should exclude these cells. Falsely labeled pFS cells can mainly be attributed to two groups of cells: firstly, bursting cells with non-continuous firing and slightly lower AP height (in the mouse particular VIP and some 5-HTR3a lines); secondly SST cells with the quasi FS phenotype (which includes L4 MCs and NMCs). In summary, the classifier is highly specific for true murine FS neurons (at least 94.1 % specificity, see **Figure 14, 16**).

Due to the lack of markers, results from applying the same model to primate cells are more difficult to evaluate. In order to gain some insights into the performance of the classifier we considered dendrite type, laminar distribution, morphological class and firing pattern. Human pFS cells show the expected dendrite type and firing patterns with one notable exception (see **Figure 17**). They were most prevalent in layer 3 and 4, which is also in line with the literature on PV cell distribution in human cortex (Avoli et al. 1994). Firing patterns (see **Figure 18**) and morphology (see **Figure 19**) of human pFS suggest a

classification with comparable specificity to the mouse data. Similar inferences with NHP data set can be made on the basis of firing patterns (see **Figure 20**). Morphological fillings, however, provided only sparse information on morphological parameters like laminar position or dendrite type (see **Subfigure 17C**). That being said, all pFS that could be assessed have aspiny dendrites and the previous examination of pFS in human shows that cross species application of the model leads to reasonable results.

After classification and verification based solely on suprathreshold parameters, subthreshold parameters of pFS are compared across species. Interestingly, most parameters do not follow the expected gradient of Mouse<NHP<Human (see **Figure 20**). NHP pFS cells show on average highest values in time constant, input resistance and sag ratio, while being the most depolarized. To further clarify, which differences have to be attributed to general differences between species and which are specific to pFS cells, we performed a 2-way ANOVA with species and cell identity (pFS/Exc) as factors. Interestingly, all features showed a significant interaction effect, with NHP cells usually being the exception from the expected pattern (see RMP, sag ratio and time constant). pFS cells in NHP show considerable disparities to their excitatory equivalents having a more depolarized membrane potential and a higher input resistance. In conclusion, features of the classic FS cell known from rodents (like low input resistance and time constant, high rheobase) are not present in primates.

The three datasets used in this study have different compositions in dendritic type. The mouse and NHP dataset are richer in interneurons based on the prevalence of aspiny cells (47.8% and 61.4% respectively, see **Figure 4 and 6**), exceeding the proportion known for their respective area by about 2-3 times (Condé et al. 1994; Pfeffer et al. 2013). The human dataset on the other hand seem to be rather balanced with 22% aspiny or sparsely spiny (see **Figure 5**). The NHP and human datasets are dominated by cells recorded from supra-granular layers, which to some extent is expected due to the expansion of late born layers in primates (Dehay, Kennedy, and Kosik 2015; Hutsler, Lee, and Porter 2005). In terms of laminar distributions the mouse dataset seems to be more evenly sampled (**Figure 4B**). The diverse mouse dataset also contains the widest distribution of intrinsic biophysical properties followed by the NHP (see **Table 2**). The overall distribution of waveform

parameters within each species suggests that they contain a considerable amount of FS cells (see for example human AP through in **Figure 7**, that suggests a high fAHP amplitude or human AP width in **Figure 8**).

## 5.2. Methodological considerations

- Cross-species application of the classifier

How valid is the application of a classifier that was trained by data from different species? Results observed in human tissue is encouraging in terms of both specificity and flexibility. On one hand, from the 393 human cells only one cell is obviously mislabeled due to a high median instantaneous frequency; on the other hand, the classifier showed a good performance even when recordings included novel or unusual phenomena. The choice of a robust set of features that are independent of other unforeseen conductances is key here. Due to the all-or-nothing nature of the action potential, waveform parameters of the rheobase sweep are especially suited for this purpose. Choosing the median instantaneous frequency over the maximum firing rate was done with the same reasoning in mind. It is a much more robust readout of high firing rates and not biased against bursts and non-persistent spiking. Interestingly, state of the art analysis done by researchers at the Allen institute itself shows that a set of very similar features, namely the AP width and instantaneous firing rate, were the most informative in replicating results of unsupervised interneuron type classification (Gouwens et al. 2019).

It is a good sign that potential sources of contaminations seem to be rather consistent across species, since in mouse bursting and non-persistent firing of VIP and 5-HTR3a also lead to a few wrong classifications. Consequentially, it is reasonable to assume that there are also some human equivalents of QFS SST cells within the human pFS population. However, since the field of primate GABAergic interneurons is not as well developed as in the mouse, the literature does not offer much information on important characteristics of these cells like prevalence and hallmarks. From the mouse we know that QFS cells are associated with a stronger spike adaptation and the non MC morphology (but see L4 MCs in visual cortex) (Scala et al. 2019). Adaption is generally much higher in human due to a commonly observed depolarization hump that leads to more spikes at the initial part of the long pulse

stimulus and inflates the adaption index (see descriptions of spike train features in chapter 1 and human pFS in chapter 3), using the firing pattern as a heuristic or indicator of contamination is not viable. A look at (qualitative) morphological identification also does not offer much, because unlike BCs crucial portions of the ascending axon of SST cells are cut comparatively often. Of 46 full reconstructions of human interneurons only 4 cells had axonal arborizations that strongly suggest that they belong to a population equivalent to murine SST cells. None of them were classified as pFS. Best indicator of checking contaminations would be immunohistochemistry, which can also be done with intracellularly labeled cells (Kawaguchi et al. 1987). Additional antigen of choice in this context should be either SST or calbindin (CB), which is known to stain MCs in rats and primates (Wang et al. 2004; Aleksey V. Zaitsev, Povysheva, Gonzalez-Burgos, Guillermo Rotaru, et al. 2009). It was shown to be an inadequate marker for MCs in mouse due to a subpopulation expressing calretinin instead, but is still widely used as a marker in primate and thought to be the “equivalent” of the murine SST population (Xu, Roby, and Callaway 2006). Interestingly, a recent immunohistochemical study by Constantinople et al. examines the co-expression of CB, PV and the fast potassium channel subunits of the Kv3 family, which are associated with the FS phenotype, in macaque primary visual cortex (Constantinople et al. 2009). They report that 40-50% of CB cells, express at least one of Kv3.1b or Kv3.2, which is considerably higher than in mouse. However, since then studies combining immunohistochemistry and intracellular recordings in L2 and L3 of the macaque dIPFC reported minimal overlap (A. V. Zaitsev et al. 2005; Aleksey V. Zaitsev, Povysheva, Gonzalez-Burgos, et al. 2009). In summary, co-stainings with PV and CB (or perhaps SST) would be a valuable control for the current classification.

- Experimental Procedures

Given that, in many ways the NHP dataset stands out to the other species, a thorough discussion on possible effects by differences in methodology is warranted. The NHP data set has been acquired by a different institution without direct involvement of the Allen Institute. Many aspects of the pipeline may have been developed in inspiration of the Allen Cell Type Database, but it was developed in a basically independent approach. **Appendix A** gives a comprehensive account of differences in the methodology. Indeed, there are some

minor differences in solutions used. Probably the most straightforward and eminent issue is the ion composition of intracellular and extracellular solutions. In this matter the NHP protocols follow the Allen ones with the notable exception of a higher chloride concentration in the intracellular solution (16 vs 4 mMol). The mechanism in which chloride ions could impact biophysical intrinsic properties are not really clear. It is safe to assume, however, that they have a rather weak direct influence compared to sodium and potassium. That being said, a higher chloride concentration could contribute to a more depolarized membrane potential due to background/leak conductances. Calculating the resting membrane potentials via the Goldman equation (assuming a relative membrane permeability of 0.45) with both protocols, results in cells being 10 mV more depolarized with our protocols. Hence, the more depolarized NHP RMPs could be at least partially explained by this difference.

Another noteworthy difference in materials used are the solution used for tissue extraction and slicing. The Allen institute uses an NMDG-based solution, whereas we use a choline-based one, which is only recommended as method of last resort (see <https://www.brainslicemethods.com>) (Ting et al. 2014). The literature strongly suggests that neuronal stressors like trauma, changes in the osmotic and ionic environment or an insufficient recovery lead to hyper-excitability (Baltan et al. 2008; Vezzani and Viviani 2015). The tissue extraction itself poses to be an extremely invasive and traumatic procedure. Many additional factors like age of the individual and area of interest of this process determine the eventual health and resilience of the obtained tissue and cells. Unfortunately, these issues are hard to quantify and standardize. Elevated values in most if not all subthreshold features would be in agreement with a more traumatic extraction of the tissue of interest (higher intracellular calcium-> higher cAMP-> stronger sag). Furthermore it is reasonable to expect that GABAergic cells and in particular the metabolically challenged FS cells are more affected by this (Tanaka et al. 2008). There are several possibilities to improve our current tissue extraction method, which would aid in the clarification of the issue of tissue/cell health: First, there is the switch to NMDG-based solution (a step we are already determined to take for future experiments); second, a transcardiac perfusion ensures the best transition from in-vivo to ex-vivo and has become the gold standard to obtain tissue including for the purpose of making acute brain slices.



Implementing this technique for macaques involves a considerable additional effort, but is commonly used in laboratories field (Gonzalez-Burgos et al. 2009; González-Burgos et al. 2019).

Differences in cortical areas sampled in the datasets could have potentially an effect beyond tissue viability. NHP cells are primarily obtained from high-order associative areas (in particular PFC), whereas mouse cells are obtained from primarily primary visual cortex and human cells primarily from the temporal lobe due to clinical reasons. Hence, the used datasets span the entire spectrum of cortical areas and hierarchies, which could have an effect on cell type compositions and intrinsic biophysical properties. Transcriptional single cell profiling across cortical areas in mouse suggests that excitatory cells show far more area dependent diversity, which seems reasonable considering their output connectivity extends beyond the local network and has area-specific targets. Interneurons, on the other hand, seem to be comparatively homogeneous across areas (Yao et al. 2020). Actual studies comparing intrinsic properties of specific cell types across areas are relatively scarce. However, there are some systematic comparisons of NHP pyramidal cells of PFC with other cortical areas (including V1), which could give a hint at a possible influence: differences in input resistance across areas are subtle and do not match with the observed effect sizes in this study (Amatrudo et al. 2012; González-Burgos et al. 2019). However, NHP PFC is marked by having a comparatively high fraction of neuropil and low cell density. Furthermore, PFC pyramidal cells have more elaborate dendrites, which makes them well suited as integrative hubs of associative inputs. It is very reasonable to assume that the excitatory drive of PFC cells relies on cross-cortical inputs more than in other cortical areas. This could have far-reaching demands on intrinsic properties and circuitry of local GABAergic neurons, which are supposed to keep excitation at bay. A higher excitability of PV cells would be in agreement with this theory. However, longer time constants are somewhat puzzling in that context, since they are thought to be one of the requirements to mediate the fast feed-forward inhibition basket cells are known for in sensory areas and the hippocampus. To sum up, differences in cortical areas might compound on the disparity of the NHP data, but is unlikely to be the top contributor. Future studies will be carried out in our group including recordings in the primary visual cortex. Then, the issue can and will be addressed conclusively.

## 6. Conclusion

To the knowledge of the author this project is the first successful attempt of applying a classifier derived from supervised learning via Cre line labels as ground truth data across species. Due to their distinct biophysical properties and comparatively high homogeneity the PV/FS cells are an ideal candidate for such an approach. Convincing further differentiation of their electrophysiological phenotype (strongly suggested by the distinction of BCs and ChCs) has not been achieved yet. In the previously mentioned study by Gouwens et al. published in concert with the mouse data set used here, 6 clusters associated with the FS phenotype are reported (Gouwens et al. 2019). However, these labels cannot be tied to any morphological labels that were obtained in a similar manner.

Correct classifications of pFS cells in the two primate data sets are in overwhelming majority credible. However, the amount of homology between the populations is unclear. Firing patterns observed in human show interesting divergence with a so far undescribed type: a blend of bursting and fast spiking. Furthermore, both human and NHP show the same tendencies when compared to mouse, suggesting that subthreshold parameters could be influenced by a novel repertoire of conductances that have been introduced with the evolution of primates. The mechanisms and the functional necessity of these changes are at times puzzling and poorly understood: cell bodies of primate cells, for example, are known to be considerable larger (which correlates very well with the inverse of the total resistivity of cell membrane within the species; see for example values for big L5 pyramidal, large basket and Purkinje cells). The input resistance of primate cells, however, is considerably higher. So if the surface of the neuron is not the main determinant, it has to be the so called leak or background conductances. These are mediated by channels that are spontaneously open at rest. Their permeability, which is usually dominated by  $K^+$  determines the voltage of the resting membrane potential. Consequently, primate pFS cells (in particular in our NHP dataset) have to have a considerable lesser amount of these channels. Since primates show a wider range in active conductances (see for example sag-

ratio or depolarization hump) they might have simply be partially displaced by voltage-gated channels (like HCN1 or low-threshold calcium channels). Close to certainty is that these differences in subthreshold properties will lead to a substantial change in integrative properties of the cell: For one, basic mechanism like temporal and spatial summation are highly dependent on membrane resistivity and time constant; second, voltage-gated subthreshold conductances increase non-linear response profiles. Particularly interesting in this context is that for some reason particularly the pFS cells in the NHP are eminent in all discussed features. This is in line with several studies, that compared morphologically defined populations of FS in NHP and rodents (N. V. Povysheva et al. 2008; Nadezhda V. Povysheva et al. 2013). However, none of them include a reference population of non FS cells. Hence, the already known effects could be considerably higher than previously thought.

Unfortunately, we can only speculate on what necessitates such a particular changes in cell type specific manner. PV cells of the dIPFC have gained prominence in regard of the pathophysiological mechanisms of various psychiatric disorders. It seems reasonable to assume that these cells serve a specific function in cortical processing that makes them particularly vulnerable for degeneration or malfunction. Interneurons of associative areas are usually dominated by cells derived from the CGE (equivalent to the 5-HTR3a population), which are thought to promote activity by selectively inhibiting other GABAergic cells (Pi et al. 2013; Staiger et al. 2004). Consequently, the delicate equilibrium of excitation and inhibition has to be kept in check by smaller number of other interneurons. The intrinsic gain of PV cell activity could be scaled up by a higher demand of the local network, since they are particular required for delivering fast feed-forward inhibition accompanying external excitatory input. Unlike waveform parameters, subthreshold properties seem to be rather heterogeneous within the same cell type. Therefore, they must rather set by the environment they find themselves in, than by genetically determined programs. Further studies illuminating the interaction between cell type and their diverse environments assessed by cortical area or even more local activity patterns of their respective cell ensemble will be key in understanding cortical organization and function.

## 7. References

- Amatrudo, Joseph M. et al. 2012. "Influence of Highly Distinctive Structural Properties on the Excitability of Pyramidal Neurons in Monkey Visual and Prefrontal Cortices." *Journal of Neuroscience* 32(40): 13644–60.
- Ascoli, Giorgio A. et al. 2008. "Petilla Terminology: Nomenclature of Features of GABAergic Interneurons of the Cerebral Cortex." *Nature Reviews Neuroscience* 9(7): 557–68.
- Avoli, Massimo et al. 1994. "Electrophysiological and Repetitive Firing Properties of Neurons in the Superficial/Middle Layers of the Human Neocortex Maintained in Vitro." *Experimental Brain Research* 98(1): 135–44.
- Baltan, Selva et al. 2008. "White Matter Vulnerability to Ischemic Injury Increases with Age Because of Enhanced Excitotoxicity." *Journal of Neuroscience* 28(6): 1479–89.
- Bienvenu, Thomas C.M. et al. 2012. "Cell-Type-Specific Recruitment of Amygdala Interneurons to Hippocampal Theta Rhythm and Noxious Stimuli In Vivo." *Neuron* 74(6): 1059–74. <http://dx.doi.org/10.1016/j.neuron.2012.04.022>.
- Bissonette, Gregory B. et al. 2014. "Prefrontal Cognitive Deficits in Mice with Altered Cerebral Cortical GABAergic Interneurons." *Behavioural Brain Research* 259: 143–51.
- Buhl, E H, V V Stezhka, and P Somogyi. 1994. "Physiological Properties of Anatomically Identified Axo-Axonic in the Rat Hippocampus." *Journal of Neurophysiology* 71(4): 1289–1307.
- Castner, Stacy A, Patricia S Goldman-rakic, and Graham V Williams. 2004. "Animal Models of Working Memory: Insights for Targeting Cognitive Dysfunction in Schizophrenia." *Psychopharmacology* 174: 111–25.
- Condé, Françoise et al. 1994. "Local Circuit Neurons Immunoreactive for Calretinin, Calbindin D-28k or Parvalbumin in Monkey Prefrontal Cortex: Distribution and Morphology." *Journal of Comparative Neurology* 341(1): 95–116.
- Constantinidis, Christos, and Patricia S. Goldman-Rakic. 2002. "Correlated Discharges among Putative Pyramidal Neurons and Interneurons in the Primate Prefrontal Cortex." *Journal of Neurophysiology* 88(6): 3487–97.
- Constantinople, Christine M. et al. 2009. "Quantitative Analysis of Neurons with Kv3 Potassium Channel Subunits, Kv3.1b and Kv3.2, in Macaque Primary Visual Cortex." *The Journal of Comparative Neurology* 516(4): 291–311.
- Di Cristo, Graziella, and B Chattopadhyaya. 2012. "GABAergic Circuit Dysfunctions in Neurodevelopmental Disorders." 3(May): 1–9.
- Dehay, Colette, Henry Kennedy, and Kenneth S. Kosik. 2015. "The Outer Subventricular Zone and Primate-Specific Cortical Complexification." *Neuron* 85(4): 683–94.
- Dehorter, Nathalie et al. 2015. "Tuning of Fast-Spiking Interneuron Properties by an Activity-Dependent Transcriptional Switch." *Science* 349(6253): 1216–20.
- Doty, H. U., A Frick, K. Kampe, and W. Zieglgänsberger. 1998. "NMDA and AMPA Receptors on Neocortical Neurons Are Differentially Distributed." *European Journal of Neuroscience* 10(11): 3351–57.
- Emmenegger, Vishalini, Guanxiao Qi, Haijun Wang, and Dirk Feldmeyer. 2018. "Morphological and Functional Characterization of Non-Fast-Spiking GABAergic Interneurons in Layer 4 Microcircuitry of Rat Barrel Cortex." *Cerebral Cortex* (April): 1439–57. <http://academic.oup.com/cercor/advance->

article/doi/10.1093/cercor/bhx352/4796916.

- Enwright, J. F. et al. 2018. "Transcriptome Alterations of Prefrontal Cortical Parvalbumin Neurons in Schizophrenia." *Molecular Psychiatry* 23(7): 1606–13.
- Enwright, John F. et al. 2016. "Reduced Labeling of Parvalbumin Neurons and Perineuronal Nets in the Dorsolateral Prefrontal Cortex of Subjects with Schizophrenia." *Neuropsychopharmacology* 41(9): 2206–14.
- Eyal, Guy, Huibert D. Mansvelter, Christiaan P.J. de Kock, and Idan Segev. 2014. "Dendrites Impact the Encoding Capabilities of the Axon." *Journal of Neuroscience* 34(24): 8063–71.
- Fenko, Lief E et al. 2014. "Targeting Cells with Single Vectors Using Multiple-Feature Boolean Logic." *Nature Methods* 11(7): 763–772.
- Ferguson, Brielle R., and Wen-Jun Gao. 2018. "PV Interneurons: Critical Regulators of E/I Balance for Prefrontal Cortex-Dependent Behavior and Psychiatric Disorders." *Frontiers in Neural Circuits* 12(May): 1–13.
- Friedman, H. R., and Patricia S Goldman-Rakic. 1994. "Coactivation of Prefrontal Cortex and Inferior Parietal Cortex in Working Memory Tasks Revealed by 2DG Functional Mapping in the Rhesus Monkey." *The journal of neuroscience* 14(5): 2775–88.
- Fung, Samantha J. et al. 2010. "Expression of Interneuron Markers in the Dorsolateral Prefrontal Cortex of the Developing Human and in Schizophrenia." *American Journal of Psychiatry* 167(12): 1479–88.
- Gao, R., and P Penzes. 2015. "Common Mechanisms of Excitatory and Inhibitory Imbalance in Schizophrenia and Autism Spectrum Disorders." *Curr Mol Med.* 15(2): 146–67.
- Glausier, Jill R., Sohei Kimoto, Kenneth N. Fish, and David A. Lewis. 2015. "Lower Glutamic Acid Decarboxylase 65-Kda Isoform Messenger RNA and Protein Levels in the Prefrontal Cortex in Schizoaffective Disorder but Not Schizophrenia." *Biological Psychiatry* 77(2): 167–76. <http://dx.doi.org/10.1016/j.biopsych.2014.05.010>.
- Goldberg, Ethan M. et al. 2005. "Specific Functions of Synaptically Localized Potassium Channels in Synaptic Transmission at the Neocortical GABAergic Fast-Spiking Cell Synapse." *Journal of Neuroscience* 25(21): 5230–35.
- Gonzalez-Burgos, Guillermo et al. 2009. "GABA Transporter GAT1 Prevents Spillover at Proximal and Distal GABA Synapses onto Primate Prefrontal Cortex Neurons." *Journal of Neurophysiology* 101(2): 533–47.
- González-Burgos, Guillermo et al. 2019. "Distinct Properties of Layer 3 Pyramidal Neurons from Prefrontal and Parietal Areas of the Monkey Neocortex." *The Journal of neuroscience : the official journal of the Society for Neuroscience* 39(37): 7277–90.
- Gouwens, Nathan W. et al. 2019. "Classification of Electrophysiological and Morphological Neuron Types in the Mouse Visual Cortex." *Nature Neuroscience* 22(7): 1182–95.
- Gouwens, Nathan W et al. 2018. "Classification of Electrophysiological and Morphological Types in Mouse Visual Cortex." *bioRxiv*. <http://dx.doi.org/10.1101/368456>.
- Hamill, O. P. et al. 1981. "Improved Patch-Clamp Techniques for High-Resolution Current Recording from Cells and Cell-Free Membrane Patches." *Pflügers Archiv European Journal of Physiology* 391(2): 85–100.
- Hashimoto, Takanori et al. 2003. "Gene Expression Deficits in a Subclass of GABA Neurons in the Prefrontal Cortex of Subjects with Schizophrenia." *Journal of Neuroscience* 23(15): 6315–26.
- He, Miao et al. 2016. "Strategies and Tools for Combinatorial Targeting of GABAergic Neurons in Mouse Cerebral Cortex NeuroResource Strategies and Tools for Combinatorial Targeting of GABAergic

- Neurons in Mouse Cerebral Cortex.” *Neuron* 91(6): 1228–43.
- Hendry, SHC et al. 1984. “Neuropeptide-Containing Neurons of the Cerebral Cortex Are Also GABAergic.” *Proceedings of the National Academy of Sciences* 81(October): 6526–30.
- . 1989. “Two Classes of Cortical GABA Neurons Defined by Differential Calcium Binding Protein Immunoreactivities.” *Exp Brain Res* 76: 467–72.
- Hendry, S H C, and E G Jonest. 2000. “By Immunoreactivity Monkey.” *Neurobiology* 86(March 1989): 2093–97.  
<http://www.pubmedcentral.nih.gov/articlerender.fcgi?artid=286854&tool=pmcentrez&rendertype=abstract>.
- Herculano-Houzel, Suzana. 2009. “The Human Brain in Numbers: A Linearly Scaled-up Primate Brain.” *Frontiers in Human Neuroscience* 3(NOV): 1–11.
- Hestrin, Shaul, and William E. Armstrong. 1996. “Morphology and Physiology of Cortical Neurons in Layer I.” *Journal of Neuroscience* 16(17): 5290–5300.
- Hu, Hang, John Z. Cavendish, and Ariel Agmon. 2013. “Not All That Glitters Is Gold: Off-Target Recombination in the Somatostatin-IRES-Cre Mouse Line Labels a Subset of Fast-Spiking Interneurons.” *Frontiers in neural circuits* 7(December): 195.
- Hu, Hua, Jian Gan, and Peter Jonas. 2014. “Fast-Spiking, Parvalbumin+ GABAergic Interneurons: From Cellular Design to Microcircuit Function.” *Science* 345(6196).
- Hu, Hua, and Peter Jonas. 2014. “A Supercritical Density of Na<sup>+</sup> Channels Ensures Fast Signaling in GABAergic Interneuron Axons.” *Nature Neuroscience* 17(5): 686–93.
- Hu, Jia Sheng, Daniel Vogt, Magnus Sandberg, and John L. Rubenstein. 2017. “Cortical Interneuron Development: A Tale of Time and Space.” *Development* 144(21): 3867–78.
- Hutsler, Jeffrey J., Dong-Geun Lee, and Kristin K. Porter. 2005. “Comparative Analysis of Cortical Layering and Supragranular Layer Enlargement in Rodent Carnivore and Primate Species.” *Brain Research* 1052(1): 71–81.
- Jensen, Ole, Jochen Kaiser, and Jean Philippe Lachaux. 2007. “Human Gamma-Frequency Oscillations Associated with Attention and Memory.” *Trends in Neurosciences* 30(7): 317–24.
- Jones, Edward G., and Stewart H.C. Hendry. 1986. “Co-Localization of GABA and Neuropeptides in Neocortical Neurons.” *Trends in Neurosciences* 9(C): 71–76.
- Jung, Min W., Yulin Qin, Bruce L. McNaughton, and Carol A. Barnes. 1998. “Firing Characteristics of Deep Layer Neurons in Prefrontal Cortex in Rats Performing Spatial Working Memory Tasks.” *Cerebral Cortex* 8(5): 437–50.
- Kalmbach, Brian E. et al. 2018. “H-Channels Contribute to Divergent Intrinsic Membrane Properties of Supragranular Pyramidal Neurons in Human versus Mouse Cerebral Cortex.” *Neuron* 100(5): 1194–1208.e5. <https://doi.org/10.1016/j.neuron.2018.10.012>.
- Karube, Fuyuki, Yoshiyuki Kubota, and Yasuo Kawaguchi. 2004. “Axon Branching and Synaptic Bouton Phenotypes in GABAergic Nonpyramidal Cell Subtypes.” *Journal of Neuroscience* 24(12): 2853–65.
- Kawaguchi, Yasuo et al. 1987. “Fast Spiking Cells in Rat Hippocampus (CA1 Region) Contain the Calcium-Binding Protein Parvalbumin.” *Brain Research* 416(2): 369–74.
- Kuang, H, Philip L. Wang, and Joe Z. Tsien. 2009. “Towards Transgenic Primates: What Can We Learn from Mouse Genetics?” *Sci China C Life Sci* 52(6): 506–14.
- Leutgeb, Jill K., Stefan Leutgeb, May Britt Moser, and Edvard I. Moser. 2007. “Pattern Separation in the Dentate Gyrus and CA3 of the Hippocampus.” *Science* 315(5814): 961–66.

- Lim, Lynette, Da Mi, Alfredo Llorca, and Oscar Marín. 2018. "Development and Functional Diversification of Cortical Interneurons." *Neuron* 100(2): 294–313.
- Madisen, Linda et al. 2015. "Transgenic Mice for Intersectional Targeting of Neural Sensors and Effectors with High Specificity and Performance NeuroResource Transgenic Mice for Intersectional Targeting of Neural Sensors and Effectors with High Specificity and Performance." *Neuron* 85(5): 942–58.
- McCormick, D. A., B. W. Connors, J. W. Lighthall, and D. A. Prince. 1985. "Comparative Electrophysiology of Pyramidal and Sparsely Spiny Stellate Neurons of the Neocortex." *Journal of Neurophysiology* 54(4): 782–806.
- Miller, Earl K., Cynthia A. Erickson, and Robert Desimone. 2018. "Neural Mechanisms of Visual Working Memory in Prefrontal Cortex of the Macaque." *The Journal of Neuroscience* 16(16): 5154–67.
- Miyoshi, Goichi et al. 2010. "Genetic Fate Mapping Reveals That the Caudal Ganglionic Eminence Produces a Large and Diverse Population of Superficial Cortical Interneurons." *Journal of Neuroscience* 30(5): 1582–94.
- Miyoshi, Goichi, S. J. B. Butt, Hirohide Takebayashi, and Gord Fishell. 2007. "Physiologically Distinct Temporal Cohorts of Cortical Interneurons Arise from Telencephalic Olig2-Expressing Precursors." *Journal of Neuroscience* 27(29): 7786–98.
- Mountcastle, V. B., W. H. Talbot, H. Sakata, and J. Hyvärinen. 1969. "Cortical Neuronal Mechanisms in Flutter-Vibration Studied in Unanesthetized Monkeys. Neuronal Periodicity and Frequency Discrimination." *Journal of neurophysiology* 32(3): 452–84.
- Ongur, D., and J.L. Price. 2000. "The Organization of Networks within the Orbital and Medial Prefrontal Cortex of Rats, Monkeys and Humans." *Cerebral Cortex* 10: 206–19.
- Paul, Anirban et al. 2017. "Transcriptional Architecture of Synaptic Communication Delineates GABAergic Neuron Article Transcriptional Architecture of Synaptic Communication Delineates GABAergic Neuron Identity." *Cell* 171(3): 522-525.e20.
- Pfeffer, Carsten K. et al. 2013. "Inhibition of Inhibition in Visual Cortex: The Logic of Connections between Molecularly Distinct Interneurons." *Nature Neuroscience* 16(8): 1068–76.
- Pi, Hyun-Jae et al. 2013. "Cortical Interneurons That Specialize in Disinhibitory Control." *Nature* 503(7477): 521–24.
- Pouille, F., and M. Scanziani. 2001. "Enforcement of Temporal Fidelity in Pyramidal Cells by Somatic Feed-Forward Inhibition." *Science* 293(5532): 1159–63.
- Povysheva, N. V. et al. 2008. "Parvalbumin-Positive Basket Interneurons in Monkey and Rat Prefrontal Cortex." *Journal of Neurophysiology* 100(4): 2348–60.
- Povysheva, Nadezhda V., Aleksey V. Zaitsev, Guillermo Gonzalez-Burgos, and David A. Lewis. 2013. "Electrophysiological Heterogeneity of Fast-Spiking Interneurons: Chandelier versus Basket Cells." *PLoS ONE* 8(8).
- Rossignol, E et al. 2013. "CaV2.1 Ablation in Cortical Interneurons Selectively Impairs Fast-Spiking Basket Cells and Causes Generalized Seizures." *Bone* 74(2): 209–22. <https://www.ncbi.nlm.nih.gov/pmc/articles/PMC3624763/pdf/nihms412728.pdf>.
- Rudy, Bernardo, Fishell Gordon, Lee SooHyun, and Hjerling-Leffler Jens. 2011. "Three Groups of Interneurons Account for Nearly 100% of Neocortical GABAergic Neurons." *Dev Neurobiol* 71(1): 45–61.
- Scala, Federico et al. 2019. "Layer 4 of Mouse Neocortex Differs in Cell Types and Circuit Organization between Sensory Areas." *Nature Communications* 10(1): 4174.
- Staiger, Jochen F., Alexandre J.C. Loucif, Dirk Schubert, and Martin Möck. 2016. "Morphological

- Characteristics of Electrophysiologically Characterized Layer Vb Pyramidal Cells in Rat Barrel Cortex.” *PLoS ONE* 11(10): 1–21.
- Staiger, Jochen F., Carmen Masannek, Axel Schleicher, and Werner Zuschratter. 2004. “Calbindin-Containing Interneurons Are a Target for VIP-Immunoreactive Synapses in Rat Primary Somatosensory Cortex.” *The Journal of Comparative Neurology* 468(2): 179–89.
- Tanaka, Yasuyo et al. 2008. “The Effects of Cutting Solutions on the Viability of GABAergic Interneurons in Cerebral Cortical Slices of Adult Mice.” *Journal of Neuroscience Methods* 171(1): 118–25.
- Taniguchi, Hiroki. 2014. “Genetic Dissection of GABAergic Neural Circuits in Mouse Neocortex.” *Frontiers in Cellular Neuroscience* 8(JAN): 1–22.
- Tasic, Bosiljka et al. 2018. “Shared and Distinct Transcriptomic Cell Types across Neocortical Areas.” *Nature* 563(7729): 72–78. <http://dx.doi.org/10.1038/s41586-018-0654-5>.
- Teeters, Jeffery L et al. 2015. “NeuroView Neurodata Without Borders : Creating a Common Data Format for Neurophysiology NeuroView.” : 629–34.
- Ting, Jonathan T., Tanya L. Daigle, Qian Chen, and Guoping Feng. 2014. “Acute Brain Slice Methods for Adult and Aging Animals: Application of Targeted Patch Clamp Analysis and Optogenetics.” In *Methods in Molecular Biology*, , 221–42.
- Tremblay, Robin, Soohyun Lee, and Bernardo Rudy. 2016. “GABAergic Interneurons in the Neocortex: From Cellular Properties to Circuits.” *Neuron* 91(2): 260–92. <http://dx.doi.org/10.1016/j.neuron.2016.06.033>.
- Tsutsui, Ken Ichiro, Kei Oyama, Shinya Nakamura, and Toshio Iijima. 2016. “Comparative Overview of Visuospatial Working Memory in Monkeys and Rats.” *Frontiers in Systems Neuroscience* 10(DEC): 1–12.
- Vezzani, Annamaria, and Barbara Viviani. 2015. “Neuromodulatory Properties of Inflammatory Cytokines and Their Impact on Neuronal Excitability.” *Neuropharmacology* 96(PA): 70–82.
- Wang, Yun et al. 2004. “Anatomical, Physiological and Molecular Properties of Martinotti Cells in the Somatosensory Cortex of the Juvenile Rat.” *Journal of Physiology* 561(1): 65–90.
- Watson, Karli K., and Michael L. Platt. 2012. “Of Mice and Monkeys: Using Non-Human Primate Models to Bridge Mouse- and Human-Based Investigations of Autism Spectrum Disorders.” *Journal of Neurodevelopmental Disorders* 4(1): 1–10. *Journal of Neurodevelopmental Disorders*.
- Wilson, Fraser A.W., Seamas P.Ó Scalaidhe, and Patricia S. Goldman-Rakic. 1994. “Functional Synergism between Putative  $\gamma$ -Aminobutyrate-Containing Neurons and Pyramidal Neurons in Prefrontal Cortex.” *Proceedings of the National Academy of Sciences of the United States of America* 91(9): 4009–13.
- Wonders, Carl P., and Stewart A. Anderson. 2006. “The Origin and Specification of Cortical Interneurons.” *Nature Reviews Neuroscience* 7(9): 687–96.
- Woodruff, Alan R. et al. 2011. “State-Dependent Function of Neocortical Chandelier Cells.” *Journal of Neuroscience* 31(49): 17872–86.
- Xu, Xiangmin, Keith D. Roby, and Edward M. Callaway. 2006. “Mouse Cortical Inhibitory Neuron Type That Coexpresses Somatostatin and Calretinin.” *The Journal of Comparative Neurology* 499(1): 144–60.
- Yao, Zizhen et al. 2020. “A Taxonomy of Transcriptomic Cell Types across the Isocortex and Hippocampal Formation.” *bioRxiv*: 2020.03.30.015214.
- Zaitsev, A. V., N. V. Povysheva, G. Gonzalez-Burgos, and D. A. Lewis. 2012. “Electrophysiological Classes of Layer 2/3 Pyramidal Cells in Monkey Prefrontal Cortex.” *Journal of Neurophysiology* 108(2): 595–609. <http://jn.physiology.org/cgi/doi/10.1152/jn.00859.2011>.



- Zaitsev, A.V. et al. 2005. "Localization of Calcium-Binding Proteins in Physiologically and Morphologically Characterized Interneurons of Monkey Dorsolateral Prefrontal Cortex." *Cerebral Cortex* 15(8): 1178–86.
- Zaitsev, Aleksey V., Nadezhda V. Povysheva, Guillermo Gonzalez-Burgos, et al. 2009. "Interneuron Diversity in Layers 2-3 of Monkey Prefrontal Cortex." *Cerebral Cortex* 19(7): 1597–1615.
- Zaitsev, Aleksey V., Nadezhda Povysheva, Diana Gonzalez-Burgos, Guillermo Rotaru, et al. 2009. "Interneuron Diversity in Layers 2–3 of Monkey Prefrontal Cortex." *Cerebral Cortex* 19(7): 1597–1615.

## 8. Appendix

### Appendix A. Methodology comparison table

METHODOLOGY	MOUSE & HUMAN	NON-HUMAN PRIMATE
<i>electrophysiology</i>		
<b>Brain area</b>	<p>Mouse: AUDp, AUDpo, RSPagl, RSPd, RSPPv, SSp-bfd, SSp-n, SSp-tr, SSp-un, VISa, VISal, VISam, VISI, VISp, VISpl, VISpm.</p> <p>Human: AnG, FroL, IFG, ITG, MFG, MTG, PLP, SFG, TemL</p>	DLPFC
<b>Slicing Solution</b>	<p>Mouse slicing solution: 2.5 mM KCl, 1.2 mM NaH<sub>2</sub>PO<sub>4</sub>, 25 mM NaHCO<sub>3</sub>, 25 mM D-glucose, 0.5 mM CaCl<sub>2</sub>, 5.0 mM Na-L-ascorbate, 3.0 mM Na-pyruvate, 10 mM MgSO<sub>4</sub>, 20 mM HEPES, 3.0 mM myoinositol, 12 mM NALC, 96 mM NMDG-Cl, 1.01 mM taurine, 2 mM thiourea. 295-305 mOsm/kg, pH 7.3. Human slicing solution: 2.5 mM KCl, 1.2 mM NaH<sub>2</sub>PO<sub>4</sub>, 30 mM NaHCO<sub>3</sub>, 25 mM D-glucose, 0.5 mM CaCl<sub>2</sub>, 5.0 mM Na L-ascorbate, 3.0 mM Na pyruvate, 10 mM MgSO<sub>4</sub>, 20 mM HEPES, 92 mM NMDG-Cl, 2 mM thiourea. 295-305 mOsm/kg, pH 7.3</p>	<p>Slicing solution. 2.5 mM KCl, 1.2 mM NaH<sub>2</sub>PO<sub>4</sub>, 25 mM NaHCO<sub>3</sub>, 20 mM D-glucose, 0.5 mM CaCl<sub>2</sub>, 1.3 mM Ascorbate, 2.4 mM Na-Pyruvate, 7.0 mM MgCl<sub>2</sub></p> <p>110 mM choline chloride, 300-305 mOSM, pH 7.3-7.4</p>

(modified to contain a decreased Na concentration substituted with NMDG)

<b>Maintenance solution</b>	<p>Mouse maintenance solution: 2.5 mM KCl, 1.2 mM NaH<sub>2</sub>PO<sub>4</sub>, 25 mM NaHCO<sub>3</sub>, 25 mM D-glucose, 2.0 mM CaCl<sub>2</sub>, 5.0 mM Ascorbate, 3.0 mM Na-Pyruvate, 2.0 mM MgSO<sub>4</sub>, 94 mM NaCl, 20mM HEPES, 3.0 mM myoinositol, 12.3 mM NALC, 2.0 mM thiourea, 0.01mM taurine. 295-305 mOsm/kg, pH 7.3.</p> <p>Human maintenance solution: 2.5 mM KCl, 1.2 mM NaH<sub>2</sub>PO<sub>4</sub>, 30 mM NaHCO<sub>3</sub>, 25 mM D-glucose, 2.0 mM CaCl<sub>2</sub>, 5.0 mM Ascorbate, 3.0 mM Na-Pyruvate, 2.0 mM MgSO<sub>4</sub>, 92 mM NaCl, 20 mM HEPES, 2.0 mM thiourea. 295-305 mOsm/kg, pH 7.3</p>	<p>Maintenance solution: 2.5 mM KCl, 1.2 mM NaH<sub>2</sub>PO<sub>4</sub>, 25, 2.4 mM NaHCO<sub>3</sub>, 25 mM D-glucose, 2.0 mM CaCl<sub>2</sub>, 5.0 mM Ascorbate, 3.0 mM Na-Pyruvate, 2.0 mM MgCl<sub>2</sub>, 92 mM NaCl, 20mM HEPES, 2.0 mM thiourea. 300-350 mOSM, pH 7.3-7.4</p>
<b>Bathing solution</b>	<p>bathing aCSF: 2.5 mM KCl, 1.25 mM NaH<sub>2</sub>PO<sub>4</sub>, 26 mM NaHCO<sub>3</sub>, 12.5 mM D-glucose, 2.0 mM CaCl<sub>2</sub>, 1.0 mM MgSO<sub>4</sub>, 126 mM NaCl. 295-305 mOsm/kg, pH 7.3. Synaptic blockers, 1 mM kynurenic acid and 0.1 mM picrotoxin were added (<math>V_K</math>, -94.36; <math>V_{Na}</math>, 64.53; <math>V_{Cl}</math>, -82.86; <math>V_m</math>, -65.80)</p>	<p>bathing aCSF: 2.5 mM KCl, 1.2 mM NaH<sub>2</sub>PO<sub>4</sub>, 26 mM NaHCO<sub>3</sub>, 10 mM D-glucose, 2.0 mM CaCl<sub>2</sub>, 2.0 mM MgCl<sub>2</sub>, 126 mM NaCl. 300-305 mOSM/kg, pH 7.3-7.4. To block fast glutamatergic and GABAergic synaptic transmission, 2 mM of Kynurenic and 100 uM of picrotoxin were added, respectively. (<math>V_K</math>, -94.18; <math>V_{Na}</math>, 60.23; <math>V_{Cl}</math>, -57.36; <math>V_m</math>, -59.66)</p>

<b>Internal solution with Biocytin</b>	4.0 mM KCl, 10.0 mM HEPES, 126 mM K-gluconate, 0.3 mM EGTA, 0.3 mM Na3GTP, 10 mM PCr2Na, 4 mM ATP, 0.5% biocytin. 285-295 mOsm/kg. pH 7.3. Internal solution batches used within 60 days	8.0 mM KCl, 2.0 mM CaCl <sub>2</sub> , 2.0 mM MgCl <sub>2</sub> , 10 mM HEPES, 116 mM K- gluconate, 12 mM Na-gluconate, 1.0 mM K2EGTA, , 0.3 mM Na3GTP, 4.0 mM K2ATP, biocytin 0.5-1%. 290-295 mOsm/kg, pH 7.2-7.4
--	--	--

<b>Target cells</b>	Mouse: Fluorescence guided targeting for Cre-positive and Cre-negative neurons in all cortical layers. Human: Pyramidal neurons were targeted for the initial dataset by focusing on larger cells with clear apical dendrites. Interneurons were targeted based on their usual smaller, more round or elongated soma shape	The neurons were target at all cortical layers with preference to interneurons, identified based on their small soma size, with round or oval shape and the absence of an apical dendrite
---------------------	--	---

<b>Electrophysiological conditions</b>	Target temperature of 34 ± 1 °C  Signals recorded using ITC-18 Data Acquisition Interface (HEKA), were process and amplified using the Wavemetrics (Igor Pro) software program, filtered at 10kHz, and digitized at 200KHz (befor2016) and 50 KHz (2016 and later)	Target temperature of 34 ± 1 °C  Experiment time up to 17hrs  Recordings were process using a MultiClamp 700B amplifier(Axon) operating in bridge-balance mode, filtered on line at 10 kHz, digitized with an Axon Digidata 1440A and acquired on a personal computer at sampling rate of 20 kHz using pClamp software (Axon)
--	--	---

<b>Long Square pulse</b>	1s current injections from -110 pA (or -190 for some Pvalb neurons) to rheobase + 160 pA, in 20 pA increments. For some human neurons	1s current injection from -110pA to rheobase + 270pA, in 20pA increments
--------------------------	---	--

with low IR, steps were from -220 pA in 40 pA increments

<b>Quality control</b>	<p>Cell level: Pipette offset adjusted to 0 pA before recording, GΩ seal, initial access resistance &lt;20 MΩ and &lt; 15% (mouse) or 20% (human) of the R<sub>in</sub>, electrode drift within 1mV of the original pipette offset</p> <p>Sweep level: R<sub>a</sub> &lt; 20 MΩ and &lt;15% of the R<sub>in</sub> (mouse) or 20% (human, high frequency noise (&lt;0.07mV), patch instability (0.5mV), voltage stability across the sweep</p>	<p>Cell level: Pipette offset adjusted to 0 pA before recording, GΩ seal, initial access resistance &lt;20 MΩ and or 20% of the R<sub>in</sub>, electrode drift within 1mV of the original pipette offset</p> <p>Sweep level: high frequency noise (&lt;0.07mV), patch instability (0.5mV), voltage stability across the sweep</p>
<i>morphology</i>		
<b>Slice thickness</b>	350μm	300μm
<b>IHC staining</b>	DAB staining, DAPI	Immunofluorescence staining (Biocytin-streptavidin, DAPI, CBP: PV, CR)
<b>Mounting media</b>	Glycerol-based Mowiol	Water-soluble Aqua-Poly Mount
<b>Fixation method</b>	4% paraformaldehyde (+/- PFA 2.5% glutaraldehyde) at 4°C for 40-95hrs	Fixated and storage in 4% paraformaldehyde at 4°C
<b>Microscope</b>	Brightfield and fluorescence images obtained with an AxioImager Z2 microscope (Zeiss, Germany) equipped with an AxioCam 506	Fluorescence images were acquired with a Zeiss LSM800 confocal microscope with Airyscan, and epifluorescence images with an Olympus BX51

	monochrome camera (6 megapixels with a 4.54 $\mu\text{m}$ per pixel size) and 0.63x magnifying camera mount adapter	microscope equipped with a Teledyne Photometrics CoolSNAP camera (6.45 x 6.45 microns per pixel)
<b>Imaging acquisition</b>	2D images captured with a 20x objective lens (Zeiss Plan-NEOFLUAR 20x/0.5, 12.6x total magnification yielding (0.360 x 0.360 $\mu\text{m}$ pixel size)	2D epifluorescence images: captured with 10x/0.30air, 20x/0.50air and 60x/1.25 oil objective lens (Olympus UPlanFl)
	z-stack images 63X objective lens (Zeiss Plan APOCHROMAT 63X/1.4 oil, 39.69x total magnification. X-Y effective pixel size of 0.114 micron x 0.114 micron and step size of 0.28 $\mu\text{m}$ along the Z-axis	Confocal images: z-stacks overview images (2-3 planes, 1.0 $\mu\text{m}$ step size) obtained under 10x/0.2 and 20x/0.4 objectives from the complete x-y axis of the slice. High-resolution z-stack images at 63x/1.4 oil magnification from the entire thickness of the slice in z-axis, and the visual extension of the neuron in x-y-axis (0.0706 x 0.0706 $\mu\text{m}$ pixel size)
<b>Layer localization of soma</b>	20x brightfield and/or fluorescent images of DAPI. Mouse: Individual cells were manually placed by matching the 20x slice image with a virtual brain slice to calculate soma depth relative to pia and white matter. Human: individual cells manually assigned to a corresponding anatomical area in the (MNI-ICBM152-T1 template)	Overview z-stack (2-3 z-planes) at 10 or 20x air magnification with DAPI channel for layer delimitation and green channel for neuron localization. The images were used to overlap and orient the 3D reconstructions in the slice, according to its position relative to the Pia and white matter

<b>3D reconstruction</b>	Automatic reconstruction with manual correction of biocytin-filled neurons using Vaa3D software (Mozak extension) from 63x z-stacks. Cut and truncated dendrites were marked	Manual reconstruction of biocytin-filled neurons, using NeuroLucida (MBF Bioscience). Incomplete dendritic branches were marked to provide perspective on the completeness of the cell
--------------------------	--	--

<b>Dendritic type</b>	Brightfield-Identification under microscope as sparsely spiny or spiny at 20x or 63x magnification. (Spines not reconstructed or quantified)	DAB. under microscope as aspiny, spiny at 20x or 63x magnification. (Spines not reconstructed or quantified)	Fluorescence imaging. Identification under microscope as aspiny or spiny at 63x oil magnification. (Spines not reconstructed or quantified)
-----------------------	--	--	---

**Abbreviations:** Ra, access resistance; Rin, input resistance;  $V_K$ , equilibrium potential for potassium;  $V_{Na}$ , equilibrium potential for sodium;  $V_{Cl}$ , equilibrium potential for chloride and  $V_m$ , resting membrane potential according to the Goldman-Hodgkin-Katz equation ;IHC staining, immunohistochemical staining; AUDp, primary auditory area; AUDpo, posterior auditory area; RSPagl, retrosplenial area, lateral agranular part; RSPd, retrosplenial area, dorsal part; RSPv, retrosplenial area, ventral part; SSp-bfd, primary somatosensory area, barrel field; SSp-n, primary somatosensory area, nose; SSp-tr, primary somatosensory area, trunk; SSp-un, primary somatosensory area, unassigned; VISa, anterior visual area; VISal, anterolateral visual area; VISam, anteriomedial visual area; VISl, lateral visual area; VISp, primary visual area; VISpl, posterolateral visual area; VISpm, posteromedial visual area; AnG, angular gyrus; FroL, frontal lobe; IFG, inferior frontal gyrus; ITG, inferior temporal gyrus; MFG, middle frontal gyrus; MTG, middle temporal gyrus; PLP, planum polare; SFG, superior frontal gyrus; TemL, temporal lobe; DLPFC, dorso-lateral prefrontal cortex; DAPI, 4',6-diamidino-2-phenylindole; CBP, calcium binding proteins; PV, parvalbumin; CR, calretinin.

# Curriculum Vitae

**Name:** Michelle Stephanie Jimenez-Sosa

**Post-secondary** Universidad Autónoma de Nuevo León

**Education and** Monterrey, Nuevo Leon, Mexico

**Degrees:** 2010-2017 Medical degree.

**Honours and** National Council for Science and Technology (CONACYT)

**Awards:** Scholarship

2018-2020

National Council for Science and Technology (CONACYT)

IV Meeting of Young Researches of Nuevo Leon

1<sup>st</sup> place in health science research

2016

## **Publications:**

Jimenez-Sosa et al. (2017). Anatomical Variants of Anterior Cerebral Arterial Circle: A Study by Multidetector Computerized 3D Tomographic Angiography. *Int. J. Morphol.*, 35(5):1121-1128, 2017.